EFFECT OF PERIPHERAL WALL CONDUCTION ON HEAT TRANSFER FROM A CYLINDER IN CROSS FLOW

by

Subhash Govind Kakade

A thesis submitted in partial fulfillment of
the requirements for the degree of
MASTER OF APPLIED SCIENCE
in the
DEPARTMENT OF MECHANICAL ENGINEERING
UNIVERSITY OF OTTAWA

Ottawa, Canada

November, 1972

ABSTRACT

This thesis describes a study made on the effect of peripheral wall conduction on convection heat transfer from a cylinder with a non-isothermal surface placed in an asymmetric fluid flow.

With constant heat flux generation, temperature gradients are developed around the periphery due to variation in surface heat transfer coefficient around the circumference of a cylinder with the result that heat flows by conduction in the peripheral direction. It is probable that this peripheral heat flow is significant and could be an important factor in engineering design.

Experiments with air were conducted on the test tubes with materials of different conductivity and of different areas of cross-section over a range of Reynolds number ranging 1,000 and 100,000. The range of non-dimensional peripheral wall conduction parameter, K^*, defined as $\frac{K_\infty R}{K_t b}$ was between 0.00164 and 0.0289. All test tubes were electrically heated to provide uniform heat flux generation throughout the test section. The local heat transfer coefficients were determined by measuring the electric heat input and surface temperature variation around the circumference of the test tube.

The effect of peripheral wall conduction on wall temperature distribution, local and average heat transfer

coefficient has been noted. To determine the effect of K^* qualitatively, a theoretical analysis for the wall temperature distribution is obtained from an idealized model and experimental results are compared with the predictions. The large values of peripheral wall conduction parameter, K^*, (corresponding to poor thermal conductors; either wall thickness is too small or the conductivity of the wall is too low) were associated with large variation of wall temperature distribution, local heat transfer coefficient, around the circumference of cylinder with the result that the average heat transfer coefficients were found to increase slightly with K^* over the range of Reynolds number 30,000 to 100,000. At Reynolds number 80,000, less than 15 percent increase in the average Nusselt number was observed when K^* was increased from 0.00164 to 0.0289. In addition, the peak wall temperature was observed to decrease with increased rate of peripheral wall conduction in the tubes having low values of K^* which greatly reduces the danger of hot spot formation on the cylinder surface. The present results are also compared with the results obtained by previous investigators using isothermal and non-isothermal cylinder surfaces.

It can be concluded that the effect of K^* on heat transfer coefficient is less when the separation of boundary layer takes place. This is deduced by the comparison of the present results with those which were obtained in an asymmetric flow where there was no boundary layer separation.

ACKNOWLEDGEMENT

The author wishes to express his sincere gratitude to Dr. Y. Lee who initiated and supervised the present project. The guidance, encouragement and invaluable help provided by him during the course of this project are particularly appreciated.

Sincere thanks are also due to Mr. George Toth and Mr. Paul Inderbitzin for their technical assistance.

The author also wishes to extend his sincere thanks to his colleague Mr. K. C. Goel and Mr. D. A. Seaman, Administrative Officer, Department of Mechanical Engineering, for their kind assistance from time to time.

TABLE OF CONTENTS

LIST OF TABLES

LIST OF FIGURES

NOMENCLATURE

A	Surface area, ft^2
b	Thickness of the cylinder wall, ft
C_p	Specific heat of fluid, Btu/lb ^oF
D	Outside diameter of the cylinder, ft
E	Voltage drop, volt
h	Local heat transfer coefficient, Btu/hr ft^2 ^oF
I	Current flow, amp
K	Thermal conductivity, Btu/hr ft^2 (^oF/ft)
K*	Dimensionless peripheral wall conduction parameter $\frac{K_\infty R}{K_t b}$
L	Length of test section, ft
NU	Local Nusselt number, hD/K_f
Pr	Prandtl number, $\mu C_p/K$
P_{atm}	Atmospheric pressure, lb/ft^2
q	Local heat flux, Btu/hr ft^2
$\dot{q}$	Heat generation per unit volume, Btu/hr ft^3
Re	Reynolds number, $\rho D\bar{U}_\infty/\mu$
R	Outside radius of the cylinder, ft
t	Temperature in ^oF
Δt	Temperature difference, $t_w - t_\infty$ in ^oF
T	Temperature in ^oR
TU	Turbulence intensity, $\sqrt{\overline{U'^2}}/U_\infty$
U	Velocity, ft/sec
w	Width of wind tunnel, ft

Greek Symbols

ε Emissivity

ρ Density, lbm/ft^3

μ Dynamic viscosity, lbm/sec ft

ν Kinematic viscosity, ft^2/sec

θ Angle in degrees

η Dimensionless temperature, $\frac{t_w - t_\infty}{t_{st} - t_\infty}$

ψ Dimensionless temperature, $\frac{t_w - t_\infty}{\bar{t} - t_\infty}$

Superscripts

' = Fluctuating component

- = Mean

Subscripts

b = Bulk of fluid

f = Arithmetic average (film)

st = Front stagnation point

t = Tube material

∞ = Free stream

1 = Pertaining to inner cylinder

CHAPTER 1

INTRODUCTION

A circular duct is one of the most common geometry employed for a number of engineering applications and the problem of heat transfer from a cylinder has been studied extensively by numerous investigators in the past.

The problem of constant heat generation arises in many situations as in electric resistance heating, radiant heating, nuclear heating, etc. With constant heat generation, the variations in heat transfer rate due to the asymmetric nature of fluid flow around the periphery of the cylinder appears as variations in surface temperature with the result that the temperature gradients developed and cause heat flow by conduction in the peripheral direction. It is probable that the peripheral heat flow in the cylinder wall could influence the wall temperature distribution. This fact is of considerable practical importance in engineering design. For the study of this effect, the non-dimensional peripheral wall conduction parameter, K^*, should be varied independently of cylinder diameter by employing tubes of different materials and with different wall thicknesses, if a quantitative investigation of the effect is to be pursued.

The aims of the present study, therefore, are to investigate the effect of peripheral wall conduction on, wall

temperature distribution, local and average heat transfer coefficients, when a cylinder with uniform heat flux generation is placed normal to an air stream.

Experiments have been conducted on five test tubes with non-dimensional peripheral wall conduction parameter, K^*, ranging from 0.00164 to 0.0289, over the range of Reynolds number 1,000 to 100,000. All the test tubes were electrically heated to provide uniform heat flux generation throughout the test section. Local heat transfer coefficients around the circumference of cylinder were determined by measuring the electrical energy consumed and rise in surface temperature over that of free air stream temperature at different angles. In order to show the influence of peripheral wall conduction parameter, K^*, on non-dimensional wall temperature distribution, a theoretical equation was derived from an idealized model and is solved by assuming a hypothetical heat flux distribution.

CHAPTER 2

PREVIOUS STUDIES

A great amount of work has been done on convective heat transfer from a cylinder to a gas stream in cross-flow.

The experimental data on the overall heat transfer coefficients have been summarized and correlated by several authors. McAdams (1) correlated Hilperts data for a cylinder with a constant surface temperature by the equation:

$$\overline{Nu}_f = C\ Re_f^n \qquad (2.1)$$

where the constants C and n are given in the Table 2.1. Richardson (2) proposed the following relation for flows accompanying separation,

$$\overline{Nu}_f = C_1 Re_f^{1/2} + C_2\ Re_f^{2/3} \qquad (2.2)$$

The first term on the right-hand side of Eq. (2.2) represents the heat transfer from the front surface of a cylinder to a laminar boundary layer. The second term expresses the contribution of the separated region on the rear surface of the cylinder. The value of 0.37 is given to C_1 and it is reported that if a significant turbulence intensity is present it should be increased to about 0.55 for a 10 percent free-stream turbulence intensity. The value of C_2 ranges from 0.057 to 0.084. From a similar consideration, Douglas and

Churchill (3) obtained a correlation, having the form

$$\overline{Nu}_f = 0.46\ Re_f^{1/2} + 0.00128\ Re_f \qquad (2.3)$$

Zijnen (4) obtained good results with the following correlation formula:

$$\overline{Nu}_f = 0.35 + 0.5\ Re_f^{0.5} + 0.001\ Re_f \qquad (2.4)$$

Fand and Keswani (5) developed a single, continuous, algebraic correlation equation in the range

$$10^{-2} < Re_f < 2 \times 10^5$$

$$\overline{Nu}_f\tau = 0.184 + 0.324\ Re_f^{0.5} + 0.291\ Re_f^{\gamma} \qquad (2.5)$$

where $\tau = (T_f/T_\infty)^{-0.17}$ and

$$\gamma = 0.247 + 0.0407\ Re_f^{0.168}$$

Otatake (6) proposed the following relation for air flow,

$$\overline{Nu}_f = 0.5 + 0.563[Pr_f F(Re_f)\ Re_f]^{1/2} + 0.31\ Pr_f^{1/3}\ Re_f^{1/2} \qquad (2.6a)$$

$$10^2 < Re_f < 5 \times 10^3$$

$$\overline{Nu}_f = 0.5 + 0.253\ Pr_f^{1/2}\ Re_f^{1/2} + 0.0214\ Pr_f^{1/3}\ Re_f^{0.8} \qquad (2.6b)$$

$$5 \times 10^3 < Re_f < 5 \times 10^5$$

$F(Re_f)$ in Eq. (2.6a) is given by

$$F(Re_f) = 0.198\ (1 - 19.4/Re_f)$$

$$50 < Re_f < 4 \times 10^3$$

The physical properties of the air are to be taken at the film temperature. Churchill and Brier (7) correlated the experimental data obtained at large temperature differences between the gas and cylinder surface by an equation:

$$\overline{Nu}_b = 0.60\ Pr_b^{1/3}\ Re_b^{1/2}\ (T_b/T_w)^{0.12} \qquad (2.7)$$

(where T_b is bulk-gas temperature in ^oR).
The outer tube surface temperature was maintained at 100^oF by internal cooling water circulation and the gas stream temperatures were between 580^oF and 1800^oF.

Giedt (8) investigated the variation of local heat transfer coefficient around a cylinder with non-isothermal surface in cross-flow. At Reynolds numbers up to 10^5, he reported that, a maximum heat transfer rate was observed at the forward stagnation point at 0^o and on the rear side at 180^o, minimum values at around 80^o from the forward stagnation point. Similar results were obtained by Schmidt and Wenner (9) with an isothermal cylinder surface. They kept the cylinder surface at constant temperature by the condensation of vapor. They also determined the effect of an interference wire on the surface of the cylinder at 77.5^o from forward stagnation point. They found that the transition from laminar to turbulent flow takes place due to the wire and the heat transfer coefficient increases slightly.

Comings, Clapp and Taylor (10) studied the effect of the intensity of free-stream turbulence on heat transfer

from a cylinder. They reported 25% increase in the average Nusselt number when the turbulence intensity was increased from 1 to 7% at constant Reynolds number. They found that the effect of a change in turbulence level on the Nusselt number is greater at larger Reynolds numbers and less at smaller. Giedt (11) also reported that the increase turbulence level causes the average heat transfer coefficient to increase between 10 and 20 percent over the low turbulence level values. Kestin and Maeder (12) stated that the measured increase in the heat transfer rate is due to the effect of turbulence on local rates of heat transfer. Zapp (13) reported that the increase turbulence intensity causes transition from a laminar to a turbulent boundary layer at much lower Reynolds numbers. Zijnen (14) showed how, Nu^*, the ratio between Nusselt number in turbulent flow and the Nusselt number in smooth flow varies as a function of the Reynolds number, of the intensity of turbulence and of the ratio between the scale of turbulence and cylinder diameter. Like Zijnen, Dyban and Epik (15) also showed that Nu^* is a function of Reynolds number and turbulent intensity and correlated the experimental data on the forward surface of cylinder by an equation:

$$\varepsilon = 1 + 0.01 \, (Re_f \, Tu)^{0.5}$$

where $$\varepsilon = \frac{Nu_{Tu \neq 0}}{Nu_{Tu = 0}}$$

(where $Nu_{Tu=0}$ - Nusselt number at a given perimeter point for "zero" turbulence of the external flow;

$Nu_{Tu\neq 0}$ - Nusselt number at a given perimeter point for a given turbulence level).

Petrie and Simpson (16) expressed the Nusselt number at the rear stagnation point by the following correlation formula:

$$Nu = 0.0065(Re_f)^{0.89} + [1+6.3\times10^3 \left(\frac{Tu}{Re_f}\right)^{0.74}]^{1.1} \qquad (2.8)$$

Their results show that in the Reynolds number range 5,000-35,000 increases in the free-stream turbulence intensity of 10 percent result in improvements of heat transfer at the rear of the cylinder of up to 100 percent.

A marked difference in the distribution of the heat flow rate at inner and outer surfaces of the cylinder, was observed by Thomson, Scott, Laird and Holden (17). They accounted this difference to the conduction taking place around the tube due to the circumferential temperature variation. They found that as the tube thickness decreases, the disparity between outside and inside heat transfer rates tends to disappear. Although the flow situations are not the same, Deissler and Taylor (18) analyzed the fully turbulent heat transfer and flow in annulus with various eccentricities. They found that the average Nusselt number is a function of peripheral wall temperature distribution and suggested a wall conduction parameter, $K_\infty R_1/K_t b_1$. Reynolds (19) defined the wall conduction parameter as $K_t b/K_\infty R$ and showed that the

temperature distribution in a circular tube with variable circumferential heat flux is a function of wall conduction parameter $K_t b/K_\infty R$. Lee (20) and Leung (21) were among the earlier workers who mentioned the significance of wall conduction effect on h. Like Deissler, Lee also suggested the wall conduction parameter as $K_\infty R_1/K_t b_1$. The systematic study of the effect of the peripheral wall conduction on turbulent heat transfer in eccentric annular ducts was first done by Lee (22). He has shown that the wall temperature distribution is greatly affected by wall conduction parameter, $K_\infty R_1/K_t b_1$. Grewal (23) studied the effect of wall conduction on overall heat transfer rate from a cylinder in cross-flow. He defined the wall conduction parameter, K^*, and attempted to modify McAdams' correlation to include the wall conduction effect.

However, no detailed information is available in the published literature on the influence of peripheral wall conduction, on local and overall heat transfer rate, on wall temperature distribution when a cylinder is placed normal to an air stream which is sought in the present investigation.

CHAPTER 3

EXPERIMENTAL STUDIES

3.1 Apparatus

A schematic diagram of the apparatus used in the present study is shown in Fig. 3.1 and a general view of the apparatus in Fig. 3.2. The experiments were made with the test pipes made of different materials and of different areas of cross-section, the details being included in Fig. 3.3 and Table 3.1. The test pipes were placed normal to the air-stream in the rectangular wind tunnel. The wind tunnel was of rectangular section 10" x 6" and was about 29" in length, the details are shown in Fig. 3.5a. It was connected to a rectangular box of dimension 36" x 30" x 44" which was in turn connected to the blower of 6000 cfm capacity at 14" of water. The blower was driven by a 20 HP, 1800 rpm electric motor and was capable of generating air speeds up to 190 ft/sec at the test section. A flow control valve, located at the inlet of the blower, was used for changing air speeds in the rectangular channel by controlling the inlet air flow. Two side-ports of 6" diameter were also provided to make fine adjustments in conjunction with the flow control valve to obtain the desired air speed in the channel while the blower was running. Two static pressure taps were located at the bottom of the rectangular channel and a

provision was also made in the channel to hold a thermometer and pitot tube.

3.2 Test Tubes

Five test tubes, made of different materials and with different wall thicknesses, were used (Table 3.1). Outside diameters of the test tubes were kept nearly close to 1 inch to maintain the hydrodynamic part or flow pattern around the tubes to be the same for each test tube. All the five test tubes were about 9-1/2" in length. The temperature distribution on the surface of the cylinder was measured at sixteen points with copper and constanton thermocouples (24 B&S Gauge.) embedded in the cylinder wall. The locations of the thermocouples are shown in Fig. 3.3b. The thermocouple junctions 1 to 13 (Fig. 3.3b) measured the surface wall temperatures at the interval of 15^{o} in the upper portion of the cylinder and the thermocouple junctions 14, 15, and 16 located at the interval of 45^{o} were used to check the symmetry in the temperature distribution on the upper and lower portions of the cylinder. All the thermocouple junctions on the periphery of the cylinder were made by using the "split hot junction" method which is illustrated in Fig. 3.4a. This method, devised by Lee (28), prevents the shorting of the two thermocouple wires in the tube. The voltage drop in a 5.00" length of test tube was measured with two copper wires (24B&S Gauge) embedded in the cylinder wall 5.00" apart. For heating the

test tube electrically, two copper conductors were shrink fitted into the test tube as shown in Fig. 3.3a. The surface of the test tube was polished on a lathe and a mirror like finish was obtained. The polished test cylinders are shown in Fig. 3.6. Great care was taken to have each tube with the same surface finish.

The test tube was placed horizontally in the central portion of the rectangular channel. Teflon fixed into the walls of the channel, were used for insulating and supporting electrically heated test tube in the channel as shown in Fig. 3.5b.

3.3 Instrumentation

3.3.1 Air Velocity Measurement

The air velocity in the channel was measured by means of a pitot-tube and manometer. The details of the pitot tube are shown in Fig. 3.7a. The pitot tube was supported in the channel with the help of a threaded teflon shown in Fig. 3.7b. The air velocity was measured in the channel at different points 1/4" apart vertically in the planes 2-2', 3-3' and horizontally in the plane 1-1' as shown in Fig. 3.4b. It was observed that the air velocity measured at a distance 7.49" from the side ab of the rectangular channel was nearly the same as the velocity at the test section. Hence, free-stream air velocity in the channel was measured with pitot head situated at point P,

at a distance of 7.49" from the side ab of the channel as shown in Fig. 3.4b, a few inches in front of the test cylinder under test. In Fig. 3.8 the free-stream velocity, U_∞, is plotted against the distance from the left side, ab, of the channel. Fig. 3.8 shows that the free-stream velocity over the test section, located in the central portion of the channel, is almost uniform.

The pressure was read on either a differential micro-manometer or a long alcohol manometer depending on the pressure heads. The micro-manometer used was a DISA 55 D 41/42 and was rated to be accurate within about 0.001" of the manometer fluid, the specific gravity being 0.80 in the present study. The long alcohol manometer used was Casella 326 type which read to 0.001" with the help of a vernier.

3.3.2 Temperature - Measurement

The surface temperature around the circumference of the cylinder was measured at 16 points by means of copper constantan thermocouple wires of B & S Gauge 24 (Fig. 3.3b). The calibration of the thermocouples was carried out against a standard thermometer, Fisher 15-043B which read to $0.1^{\circ}C$, by measuring the temperature of an oil bath maintained at a constant temperature. A typical calibration curve of the thermocouple is shown in Fig. 3.9. The common cold junction of the thermocoupleswas kept at the melting point of ice. A 16 point Leeds and Northrup rotary thermocouple switch was

used for convenience and rapidity of temperature measurement. The output of these thermocouples were recorded on a Hewlett and Packard Model 17501A strip chart recorder and after reaching the steady state, by a Leeds and Northrup No. 8686 potentiometer. The accuracy of the potentiometer was rated as ±0.03% of the reading for 100 mV range with a resolution of 3 μV. The air temperature was measured upstream of the test tube by means of copper constantan thermocouples GA 24 and also with the help of a thermometer which could read up to 0.1°C.

3.3.3 Power Measurement

The test tubes were heated electrically and the power was delivered to the test tubes through a powerstat (a variable transformer 13.4 KVA Super Electric Co.) and a step down transformer (Dry Type 15 KVA Marcus Co.) to obtain a high current. The power supply and measuring circuit are shown in Fig. 3.10. The power dissipated in the test tube was determined by measuring the voltage drop across 5" length along the test tube and current through it. The voltage drops were read by a Hewlett and Packard 427A precision voltmeter with full scale sensitivities ranging from 0.1 V to 300 V A.C. which was rated with a measuring accuracy of ±2% of the full scale. The electric current through the test tube was measured with an Ammeter (Bepco Canada Ltd.) in conjunction with a current transformer (General Electric Co. JP-1) because of a high current flow through the tube.

3.3.4 Measurement of Turbulence Intensity

A DISA 55 D00 series hot-wire anemometer system along with a miniature hot-wire probe (DISA 55 F31) was used to measure the turbulence intensity in the channel. Details of operation of this equipment are given in the DISA service manual (24). The hot-wire probe was calibrated as described in the reference (25). The mean velocity and R.M.S. values of the axial components of the velocity fluctuations were measured after reaching the steady state condition with the help of a hot-wire anemometer and are tabulated in Table 3.2. The calibration of the hot-wire anemometer and measurement of turbulence intensity are explained in detail in the reference (26). The turbulence intensity in the channel was found to be about 4% and was almost constant throughout the present study.

3.4 Experimental Procedure

The experiments were carried out in the following manner.

The blower was started by switching on the electric motor. The flow control valve and side port openings were adjusted to obtain the desired air velocity in the channel. The power was switched on and the hand wheel of the powerstat was rotated slowly until the desired power was supplied to the test cylinder so that the difference between the cylinder surface temperature and the free stream air

temperature was between 20 and 70°F. The Thermocouple output was recorded on a strip chart recorder. The steady state was observed by noting that the manometer reading was unchanged and that the strip chart recorder was showing constant reading. A duration of 1 to 1-1/2 hours was normally required to reach the steady state condition. The manometer readings were taken and recorded. The initial free-stream air temperature was recorded with the help of a potentiometer as well as by mercury-in-glass thermometer. Simultaneously voltage drop across the test-section and current flow through it were recorded with the help of voltmeter and ammeter, respectively. The surface temperature at 16 points around the circumference of the cylinder as shown in Fig. 3.3b was measured by recording the output of the copper constantan thermocouples by means of the potentiometer in conjunction with the rotary switch. A representative curve is drawn in Fig. 3.11 which shows Δt vs. θ at Re = 70,000 and $\bar{q}$ = 904.7 $\frac{\text{Btu}}{\text{hr ft}^2}$. There are no significant differences between measurements at symmetric angles on the upper and lower portions of the cylinder as seen from Fig. 3.11. Therefore, measurements were generally limited to the top half of the cylinder circumference; however, as a check on the symmetry, measurements were also taken on the bottom portion of the cylinder circumference from time to time. The free-stream air temperature and manometer readings were again recorded at the end of the run. The power input to the test tube was varied by operating

the hand wheel of the powerstat and the above procedure was repeated, keeping the air velocity constant. Thus, 3 to 4 readings were taken in one run, then the air flow was changed again and the above procedure was repeated for different runs.

The tests were carried out over the range of Reynolds numbers from 10^3 to 10^5 and Δt between 20 to $70^{\circ}F$. The test tubes of different K^* were changed and tests were repeated as explained above for each test tube. The reproducibility of the experimental results was checked by carrying out a number of test runs.

3.5 Data Reduction

The local Nusselt number was calculated from the definition

$$Nu_f = hD/K_f \qquad (3.1)$$

K_f, the thermal conductivity of air was calculated from the equation as given in the reference (26) at the film temperature t_f.

$$K_f = 0.13168 \times 10^{-1} + 0.25432 \times t_f \times 10^{-4} - 0.52249 \times t_f^2 \times 10^{-8}$$

$$\text{Btu/hr ft}^2 - {}^{\circ}\text{F/ft} \qquad (3.2)$$

The equation defining the local heat transfer coefficient, h, in terms of the experimental measurements is as follows,

$$h = \frac{3.414\ E \times I}{\pi DL(t_w - t_\infty)} \quad Btu/hr\ ft^2\ ^oF \qquad (3.3)$$

The average Nusselt number, $\overline{Nu}_f$, for $\theta = 0$ to 180^o was calculated by numerical integration using Simpson's rule with double precision.

The average Reynolds number is defined by the equation

$$Re_f = \frac{\rho D \overline{U}_\infty}{\mu}$$

The dynamic viscosity was calculated from the equation, given in the reference (26), at the average film temperature.

$$\mu = 0.11005 \times 10^{-4} + 0.18071 \times \overline{t_f} \times 10^{-7} - 0.51587 \times \overline{t_f} \times 10^{-11} \qquad (3.5)$$

$lb_m/sec\ ft$

ρ_∞, the density of air is given by

$$\rho_\infty = \frac{0.07647 \times P_{atm} \times 518.7}{29.92 \times (460 + \overline{t}_f)} \quad lb_m/ft^3 \qquad (3.6)$$

The velocity of air is evaluated from

$$U_\infty = \left[\frac{(\rho_{water} - \rho_\infty) \times 2.0 \times 32.2 \times \text{constant} \times \text{manometer reading}}{\rho_\infty}\right]^{1/2}$$

ft/sec

The radiation correction can be obtained from

$$\frac{Q_{rad}}{A} = \varepsilon\sigma[(T_w/100)^4 - (T_\infty/100)^4] \quad Btu/hr\ ft^2 \qquad (3.7)$$

where Stephan Boltzmann constant $\sigma = 0.1714 \times 10^{-8}$ Btu/hr-ft^2-$^oR^4$, emissivity $\epsilon \approx 0.074$ for polished stainless steel surface and $A = \pi LD$ the surface area.

The difference between t_w and t_∞ was less than 70^oF throughout the study. Hence, the radiation corrections obtained from Eq. (3.7) were calculated to be less than $1.5 \times 10^{-8}\%$ which is very negligible.

CHAPTER 4

RESULTS AND DISCUSSION

The local temperature distribution is plotted as Δt versus θ in Figs. 4.1 to 4.3 at constant Reynolds number, where Δt is the difference between the local surface temperature of the cylinder and the free air stream temperature in ^{o}F. The non-dimensional temperatures, ψ, are plotted against θ in Figs. 4.4, 4.5 and 4.6. Figs. 4.1 to 4.6 show that the Δt and dimensionless temperature, ψ, have a minimum value at the forward stagnation point and the maximum value of Δt and ψ occur in the range of angles 70^{o} and 135^{o} from the forward stagnation point depending on the value of Reynolds number. The present results show that the temperature distributions, Δt and ψ, around the surface of the cylinder are greatly influenced by the dimensionless peripheral wall conduction parameter K^{*}. The vertical shifts in the curves of Figs. 4.1 to 4.3 are partially caused due to differences in the heat flux. However, the discrepancy in the curves of Figs. 4.4 to 4.6 at constant Reynolds number could be attributed to the peripheral conduction in the cylinder wall. The slope of the curves in Figs. 4.1 to 4.6 decreases with K^{*} due to increased rate of peripheral wall conduction. It is observed that as the peripheral wall conduction parameter, K^{*}, increases (large values of K^{*} corresponds to poor thermal conductors), the

variation of Δt and dimensionless temperature, ψ, around the cylinder surface also increases. The temperature distributions, Δt and ψ, become more and more uniform with respect to θ with increased rate of peripheral conduction in the cylinder wall. The increased rate of peripheral conduction in the cylinder wall at lower K^* was also found to augment the mean temperature level of the cylinder surface slightly. The difference between the stagnation temperature and peak temperature on the cylinder surface was found to increase with K^* due to a decreased rate of peripheral wall conduction. For constant heat flux condition, at constant Reynolds number, the peak temperature on the cylinder surface is greatly influenced by K^* and this fact is of great practical importance. As K^* increases (such as heat exchanger tube with low thermal conductivity thin wall), the peak temperature on the cylinder surface also increases and there is a possibility of forming a <u>hot spot</u> at the point of maximum temperature which will eventually damage the tube material and may cause fluid leakage. The formation of hot spot on the tube surface can arise in a constant heat flux generation problem which arise in a number of situations like, electric resistance heating, radiant heating and nuclear heating, etc. and can be avoided by increasing the peripheral heat conduction in the cylinder wall by employing tubes made of good thermal conductivity material and having more wall thickness resulting in lower values for K^*.

In Figs. 4.4a and 4.4b, Re = 15,700, the non-dimensional temperature, ψ, increases with θ, reaches a maximum value at about 135^{o}, and in the range of angles 135^{o} to 180^{o} the change in ψ was less sudden. At low values of K^{*}, 1.64×10^{-3} and 7.1×10^{-3}, the slope of the curves (Fig. 4.4a) in the range of angles 135^{o} to 180^{o} was almost zero which indicates that the surface temperature at lower K^{*} in this range of angles was nearly constant. At Re = 15,700, the ψ reached the maximum value at about 135^{o} from the forward stagnation point and the point of maximum ψ shifted toward the side of the cylinder as Reynolds number increased. At Re = 54,500 and 70,500 (Figs. 4.5 and 4.6), the maximum value of ψ occurred at about 105^{o} from the forward stagnation point. Figs. 4.5 and 4.6 show that the ψ increases with θ, reaches to maximum value at about $\theta = 105^{o}$ and then decreases with θ in the range of angles 105^{o} to 180^{o}. The drop in ψ with θ in the range of angles 105^{o} to 180^{o} is more at Re = 70,500 as compared with the one at Re = 54,500. The non-dimensional temperature, ψ, is plotted vs. K^{*} in Figs. 4.7, 4.8 and 4.9. From Figs. 4.7, 4.8 and 4.9 it is observed that the high values of ψ_{max} are associated with the large values of K^{*}. Likewise, $\Delta\psi_{max}$, the difference between the minimum and maximum values of ψ increases with K^{*}, reaches certain maximum and after that increases in K^{*} have no significant influence on $\Delta\psi_{max}$.

To show the effect of K^* qualitatively, the non-dimensional temperature distribution is plotted as η vs. the angle θ for constant K^* in Fig. 4.10. These curves are obtained by solving differential equation (A2.5) numerically based on the hypothetical heat flux distribution by employing CSMP** technique, the details are given in Appendix 2. These curves indicate that dimensionless temperature increases with K^* and θ. These curves give a qualitatively general pattern of change in η with respect to K^* and more meaningful results could be obtained by using the realistic function $q/\bar{q}$ in Eq. (A2.5). The experimental results are compared with the analytical results obtained by solving Eq. (A2.5) in Fig. 4.11, at Re = 19,800 and average heat flux = 783.2 Btu/hr ft^2.

The dimensionless temperature, η, is given as

$$\eta = \frac{t_w - t_\infty}{t_{st} - t_\infty}$$

The thermal boundary layer thickness is minimum at the forward stagnation point. Hence, at $\theta = 0$, the heat transfer rate is maximum which results in the minimum surface temperature at the front stagnation point. As θ increases, the boundary layer thickness increases and the resistance to heat transfer between the hot cylinder surface and free air

---

** Continuous System Modeling Program

stream also increases and causes a decrease in the heat transfer rate. Hence, the surface temperature increases with θ until the boundary layer separates from the cylinder surface. In the separated region on the rear of the cylinder, the turbulent eddies in the wake increase the heat transfer rate which subsequently reduce the surface temperature of the cylinder in the rear. The present experimental results (Fig. 4.11) show that η increases with θ, reaches a maximum value at about 135^{o} from the forward stagnation point and onward in the range of angles 135^{o} and 180^{o} decreases for $K^{*} = 9.45 \times 10^{-3}$, remains constant at low K^{*} value = 1.64×10^{-3} due to an increased rate of peripheral conduction in the cylinder wall. It can be concluded that the results obtained by solving differential Eq. (A2.5) are in fair agreement with the experimental results for $0 < \theta^{o} < 120$ whereas in the range of angles 120^{o} and 180^{o} the analytical results based on no separation give much higher values than the experimental one as expected. This deviation could be mainly attributed to inaccuracy in the assumption of function for $q/\bar{q}$ in Eq. (A2.5). Besides the heat transfer on the rear side of the cylinder occurs in the wake and our knowledge of this mode of heat transfer is still very limited.

The local heat transfer distribution is plotted non-dimensionally as Nusselt number vs. θ in Figs. 4.12 to 4.14. Figs. 4.15 to 4.17 show the plots of local Nusselt number vs. K^{*}, at constant Reynolds number. There was a

continuous fall in the local Nusselt number from front to rear in Figs. 4.12a and 4.12b at Re = 15,700 and the point of minimum Nusselt number shifted from the rear towards the side of the cylinder near the separation point in Figs. 4.13 and 4.14, respectively, at Reynolds number 54,500 and 70,500. Beyond the separation point the turbulent eddies developed in the wake cause intense mixing of the fluid portion and an increase in the local heat transfer coefficient in the rear of the cylinder. However, the conductance over the rear was lesser than over the front in Figs. 4.13 and 4.14, because the eddies recirculate part of the free stream air and the kinetic energy of eddies dissipates in the wake in the form of heat energy.

For conditions of constant heat flux generation; variations in the surface heat transfer appears as variations in the surface temperature and temperature gradients are developed around the cylinder. Peripheral wall conduction results due to these temperature gradients and further changes the temperature field around the cylinder which influences the local heat transfer distribution. The curves in Figs. 4.12 to 4.17 show the large variation in the local heat transfer distribution with peripheral wall conduction parameter K^*. The variation in the heat transfer rate with θ and temperature gradients are larger over the front protion of the cylinder than over the rear. Hence, the effect of a peripheral wall conduction parameter, K^*, was found to be

more pronounced over the front portion of the cylinder. The local heat transfer rate increases on the rear of the cylinder as Reynolds number increases. This further increases the temperature gradients on the rear. Hence, the rear portion of the cylinder becomes more responsive to the effect of peripheral wall conduction parameter, K^*, as Reynolds number increases from 15,700 to 54,500 and 70,500 (Figs. 4.12 to 4.17).

From Figs. 4.12 to 4.17 it is seen that at constant Reynolds number, as K^* increases, the local Nusselt number increases in the front portion of the cylinder due to a decreased rate of peripheral wall conduction until the separation of the boundary layer occurs. After the separation point, the local Nusselt number fluctuates as vortices are shed into the wake. As K^* decreases (the small values of K^* are associated with good conductors), the peripheral conduction in the cylinder wall increases and distribution of the heat transfer coefficient with θ becomes more and more uniform with θ. The influence of K^* on the local Nusselt number at the front stagnation point was found to be prominent. In Fig. 4.17a at Re = 70,500, the local Nusselt number at the front stagnation point increased up to 20 percent when K^* was increased from 1.64×10^{-3} to 28.9×10^{-3}.

The present results are compared in Figs. 4.18 to 4.23 with those of previous investigators (8,9,15,16,27) to verify the effect of peripheral wall conduction on the local

heat transfer coefficient observed in the present study. The Figs. 4.18, 4.19 and 4.20 show the plots of the local Nusselt number vs. θ at constant Reynolds number and Figs. 4.21, 4.22 and 4.23 show the plots of the local Nusselt number against K^*. Schmidt and Wenner (9) measured the local heat transfer coefficient around the cylinder with an isothermal surface. Their data were taken in a narrow jet of air and with a minimum of turbulence, but the value of the turbulence intensity was not mentioned. The cylinder surface temperature was constant in their case with the result that the peripheral wall conduction was absent and K^* can be considered as infinite.

Giedt (8), Dyban and Epick(15) and Petrie and Simpson (16) obtained their data for constant heat flux condition. From Figs. 4.18, 4.19 and 4.20 it can be seen that up to 60^o from the forward stagnation point the local heat transfer coefficient increases with K^*. After that, the local heat transfer coefficient decreases as K^* increases and again starts increasing in the rear portion of the cylinder. In Fig. 4.18, the vertical downward shift of the curve of Petrie and Simpson (16) at $K^* = 354.6 \times 10^{-3}$, $T_u = 5.78\%$ and the vertical upward shift of the curve of Dyban and Epick(15) at $K^* = 140.5 \times 10^{-3}$, Tu = 5% could be attributed to the influence of many factors such as cylinder diameter, the turbulence scale, the turbulence intensity, etc. The influence of these factors on the heat transfer

rate from a cylinder in the cross-flow has been demonstrated by Zijnen (14) and Dyban and Epick(15). From Figs. 4.18, 4.19 and 4.20 it can be seen that the general shape of the curves determined in the present experiments agree in shape with those determined by the previous investigators (8,9,15, 16,27), but that quantitatively there is considerable deviation. This deviation could mainly be attributed to the influence of peripheral heat conduction in the cylinder wall. It is observed that as the peripheral wall conduction parameter, K^*, increases, the variation in the heat transfer coefficient around the cylinder also increases and the data reported by previous investigators (8,9,15,16,27) agree with this conclusion. From Fig. 4.18 it is observed that at Re = 15,700, the variation in the heat transfer coefficient in the range of angle 60 to 180^o reported by Dyban and Epic (15) corresponding to $K^* = 140.5 \times 10^{-3}$ and Tu = 5% is not as great as reported by Schmidt and Wenner (9) at $K^* = \infty$. From Fig. 4.19 it is seen that at Re = 39,800, the results of Small (27) obtained at $K^* = \infty$ are in close agreement with the results of Schmidt and Wenner also obtained at $K^* = \infty$. The curves of Small and Schmidt and Wenner also agree very closely in shape. At Re = 39,800, Fig. 4.22, the local heat transfer coefficient given by Schmidt and Wenner (9), at the front stagnation point is 46.5 percent higher than in the present experiments at $K^* = 1.64 \times 10^{-3}$, on the side of the cylinder was much lower than in the present results. From

Figs. 4.21, 4.22 and 4.23 it is observed that the difference between the local heat transfer coefficient at the front stagnation point and on the side of the cylinder increases with K^*. The difference between the local Nusselt number at $\theta = 0^o$ and the one at $\theta = 90^o$ from the forward stagnation point is approximately, 9.8 percent at $K^* = 1.64 \times 10^{-3}$ (Fig. 4.22), 86.5 percent in the case of Schmidt and Wenner's results obtained at $K^* = \infty$.

Hence it can be concluded that the local heat transfer coefficient is very sensitive to the influence of peripheral wall conduction parameter, K^*, and the large values of K^* are associated with a large variation of the local heat transfer coefficient around the cylinder in the cross-flow.

Squire (28) solved the equations of motion and energy for a cylinder at 'constant temperature' in the cross-flow over that portion of the surface to which a laminar boundary layer adheres. He showed that at the front stagnation point the local heat transfer coefficient is given by

$$Nu_{st} = 1.01 \sqrt{Re} \qquad (4.3)$$

and is plotted in Fig. 4.24. The local Nusselt number at the forward stagnation point obtained at different K^* in the present experimental study at 'constant heat flux' are compared with the Squire's curve in Fig. 4.24. Schmidt and Wenner (9) reported that their data at $K^* = \infty$ under constant surface temperature condition agreed exceptionally well with

the Squire's curve. Giedt (8) obtained his data at $K^* = 2029 \times 10^{-3}$, $T_u = 2.25\%$ at constant heat flux condition. He also reported excellent agreement at Reynolds number less than 10^5 with the Squire's curve and at Reynolds numbers, greater than 10^5 Giedt's experimental points obtained at $K^* = 2029 \times 10^{-3}$, $T_u = 2.25\%$ were about 10 percent above Squire's curve. In Fig. 4.24 coordinates are plotted on a logarithmic scale and a large difference between the present results at $K^* = 1.64 \times 10^{-3}$ and Squire's curve can be noticed. Squire's results are given by $Nu = 1.01 \sqrt{Re}$ were found to be 40 to 90 percent higher than the present results at $K^* = 1.64 \times 10^{-3}$. At Re = 2000 and 6000, Squire's curve is respectively 83 percent and 47 percent higher than the experimental results obtained at $K^* = 1.64 \times 10^{-3}$, at constant heat flux. At Re = 70,500, the present results obtained at $K^* = 28.9 \times 10^{-3}$ were about 20 percent higher than the results obtained at $K^* = 1.64 \times 10^{-3}$. Hence, from the above discussion it can be concluded that as K^* increases, the peripheral wall conduction decreases and the heat transfer coefficients at the front stagnation point at large values of K^* are approaching towards the Squire's line given by equation $Nu_{st} = 1.01 \sqrt{Re}$, but not necessarily lie on the line.

The average Nusselt numbers are compared with those obtained by McAdams (1), Schmidt and Wenner (9), Coming, Clapp and Taylor (10), Gibson (29) and Hughes (30) in Fig. 4.25

which contains the plots of the average Nusselt number against the Reynolds number at different K^*. The data of Hughes (30) are found to be in fair agreement with McAdams' curve. Wide discrepancies among the results of previous investigators observed in Fig. 4.25 may be attributable to the influence of many factors such as, different flow characteristics, different boundary conditions, width of free air stream, channel blockage ratio (viz. D/W; in the present study D and W were kept constant), temperature gradient in the cylinder wall, turbulence intensity, cylinder diameter, peripheral wall conduction, etc. The influence of turbulence intensity on the average heat transfer coefficient is found to be important by many investigators. In most of the previous work the intensity of turbulence has not been given clearly. Coming, Clapp and Taylor (10) found that the rate of transfer of heat increases with turbulence intensity; this increase being relatively the largest in the region of turbulence intensity, 1.8 to 4 percent. A deviation of up to 20 percent in the present results from McAdams' curve (Fig. 4 .25) is observed. The experimental data in the present study were obtained at 4 percent turbulence intensity and at constant heat flux generation. Whereas, McAdams' correlation is based on Hilpert's data obtained at relatively low turbulence level, 1 to 2 percent, and for constant surface temperature condition. Along with turbulence intensity and different boundary conditions, the peripheral wall conduction was also found to be a major factor which also could

have contributed to this deviation.

The experimental data of other workers (8,9,15,16) are plotted in Fig. 4.26 along with the present data. Fig. 4.26 contains the plots of the mean Nusselt number vs. K^* at constant Reynolds number and the values of Nu^* are plotted against K^* in Fig. 4.27. Nu^* is the ratio of the mean Nusselt number at certain K^* to the mean Nusselt number obtained by extrapolation of the data at zero K^*. From Figs. 4.26 and 4.27 it is observed that the mean Nusselt number increases slightly with K^* and this variation is more at the higher Reynolds number. At Re = 80,000, the mean Nusselt number increases by 20.6 percent for the variation in K^* from 0 to ∞ and at Re = 8,200, the variation in the mean Nusselt number is of the order of 0.8 percent. Initially, the slope of the curves plotted in Figs. 4.26 and 4.27 are more but as K^* increases the slope of these curves almost becomes zero. Hence, it can be concluded that at low Reynolds number the mean heat transfer coefficient is not so sensitive to the influence of peripheral wall conduction parameter, K^*, and the measured increase in the mean heat transfer coefficient observed at high Reynolds number is due to the influence of K^* on the local heat transfer coefficient.

CHAPTER 5

CONCLUSIONS

The following conclusions can be drawn from the present study:

(1) At constant Reynolds number, the large values of peripherhal wall conduction parameter, K^*, are associated with the large variation of the local heat transfer coefficient around the cylinder.

(2) At constant Reynolds number, the local heat transfer coefficient increases with K^* in the front portion of the cylinder until the boundary layer separates from the cylinder surface. After the point of separation, the local heat transfer coefficient changes at random with K^*.

(3) The local heat transfer coefficient at the front stagnation point is substantially influenced by peripheral conduction in the cylinder wall and increases with K^*.

(4) The local Nusselt numbers at the front stagnation point given by Squire's equation, $Nu_{st} = 1.01 \sqrt{Re}$ were much higher than the present results obtained at low values of K^*. A 40 to 90 percent deviation from the Squire's curve was observed at $K^* = 1.64 \times 10^{-3}$.

However, the heat transfer coefficients at the front stagnation point at large values of K^* approach towards the Squire's line given by equation, $Nu_{st} = 1.01 \sqrt{Re}$, but not necessarily lie on the line.

(5) At low Reynolds numbers (Re < 30,000), no appreciable effect of K^* on the average heat transfer coefficient was observed but in the range of Reynolds numbers 30,000 and 80,000, the average heat transfer coefficient was found to be a function of peripheral wall conduction parameter K^*. At Re = 80,000, less than 15% increase in the average Nusselt number was observed when K^* was increased from 1.64×10^{-3} to 28.9×10^{-3}.

(6) Increase in the non-dimensional peripheral wall conduction parameter, K^*, (large values of K^* are associated with bad conductors and thin wall tubes) causes,

a) the large variation in dimensionless temperature around the cylinder surface,

b) increase in the temperature gradients along the circumference of the cylinder,

c) increase in the peak temperature on the cylinder surface. There is a danger of the formation of a hot spot at the point of maximum temperature and it can be avoided by increasing the peripheral heat conduction in the cylinder wall by employing the tubes with lower K^*,

d) increase in $\Delta\psi_{max}$, the difference between the minimum and maximum values of dimensionless temperature ψ. $\Delta\psi_{max}$ reaches to maximum value at certain K^* and after that increase in K^* have no significant influence on $\Delta\psi_{max}$.

(7) As K^* decreases, (the small values of K^* are associated with good conductors and thick wall tube) the rate of peripheral heat conduction in the cylinder wall increases and the mean temperature level of the cylinder surface is slightly augmented.

(8) The results obtained by solving the differential Eq. (A2.5) were in good agreement with the experimental results for $0^o < \theta^o < 120^o$ whereas in the range $120^o < \theta^o < 180^o$ the analytical results were much higher than the present results.

More accurate results can be obtained by predicting the function for $q/\bar{q}$ in Eq. (A2.5). For more meaningful results it is recommended that further investigation is to be carried out on a number of cylinders with a wide range of K^* at Reynolds number $>10^5$.

APPENDIX 1

ESTIMATION OF EXPERIMENTAL UNCERTAINTIES

The experimental uncertainty is estimated by employing the method of Kline and McClintock (31). Their method is as follows,

Let the result R be a function of n independent variables, v_1, v_2, ..., v_n

$$R = R(v_1, v_2, \ldots\ldots, v_n) \tag{A1.1}$$

Let W_R be the uncertainty in the result and w_1, w_2, ..., w_n be the uncertainties in the independent variables, then the uncertainty, W_R, in the result is given by

$$W_R = \left[\left(\frac{\partial R}{\partial v_1} w_1\right)^2 + \left(\frac{\partial R}{\partial v_2} w_2\right)^2 + \ldots\ldots + \left(\frac{\partial R}{\partial v_n} w_n\right)^2\right]^{1/2} \tag{A1.2}$$

The uncertainties in the Re, Nu, Tu, etc. are evaluated by using Eq. (A1.2)

a) $Re_f = \dfrac{D\overline{U}_\infty}{\nu}$

where the estimated uncertainties in each term are:

$D = \pm 0.1\%$, $\overline{U}_\infty = \pm 1.8\%$ and $\nu = \pm 1.5\%$

Then

$$\left[\frac{W_R}{R}\right]_{Re_f} \quad \pm 2.35\%$$

b) $Nu_f = \frac{hD}{K_f} = \frac{3.414\ E\ I}{\pi\ L\ K_f\ \Delta t}$

where the estimated uncertainties in each term are:

$E = \pm 4.1\%$, $I = \pm 0.65\ \%$, $\Delta t = 1.03\ \%$ and $L = \pm 0.02\%$.

Then

$$\left[\frac{W_R}{R}\right]_{Re_f} = \left[\left(\frac{W_E}{E}\right)^2 + \left(\frac{W_I}{I}\right)^2 + \left(\frac{W_L}{L}\right)^2 + \left(\frac{W_{\Delta t}}{\Delta t}\right)^2\right]^{1/2}$$

$$= \left[\left(\frac{4.1}{100}\right)^2 + \left(\frac{0.65}{100}\right)^2 + \left(\frac{0.02}{100}\right)^2 + \left(\frac{1.03}{100}\right)^2\right]^{1/2}$$

$$= \pm 4.3\ \%$$

c) Turbulence Intensity $= \frac{\sqrt{\overline{U'^2}}}{\overline{U}_\infty}$

$$\left(\frac{W_R}{R}\right)_{Tu} = \pm 2.06\%$$

APPENDIX 2

ANALYSTICAL CONSIDERATION

Consider a test tube of radius R and thickness b as shown in Fig. A2.1.

Then for unit length of test tube,

$$Q_1 = -K_t \, b \, \frac{dt_w}{Rd\theta}$$

$$Q_2 = -\left[K_t \, b \, \frac{dt_w}{Rd\theta} + \frac{d}{Rd\theta}\left(K_t \, b \, \frac{dt_w}{Rd\theta}\right) Rd\theta\right]$$

$$= - K_t \, b \, \frac{1}{R} \frac{dt_w}{d\theta} - K_t \, b \, \frac{1}{R} \frac{d^2 t_w}{d\theta^2} \, d\theta$$

$$Q_c = q \, R \, d\theta$$

$$Q_i = \dot{q} \, b \, R \, d\theta$$

From energy balance,

$$Q_1 + Q_i = Q_2 + Q_c$$

Hence

$$-K_t \frac{b}{R} \frac{dt_w}{d\theta} + \dot{q} b R d\theta = -K_t \frac{b}{R} \frac{dt_w}{d\theta} - K_t \frac{b d^2 t_w}{Rd\theta^2} d\theta + qRd\theta \qquad (A2.1)$$

which can be simplified as

$$\frac{d^2 t_w}{d\theta^2} - \frac{qR^2}{K_t b} + \frac{\dot{q} R^2}{K_t} = 0 \qquad (A2.2)$$

Non-dimensional temperatures η and $\bar{\eta}$ are defined as,

$$\eta = \frac{t_w - t_\infty}{t_{st} - t_\infty} \qquad \text{and} \qquad \bar{\eta} = \frac{\bar{t}_w - t_\infty}{t_{st} - t_\infty}$$

Replacing t_w by η in Eq. (A2.2) gives

$$\frac{d^2\eta}{d\theta^2} - \frac{q}{(t_{st} - t_\infty)} \frac{R^2}{K_t b} + \frac{\dot{q} R^2}{(t_{st} - t_\infty) K_t} = 0 \qquad \text{(A2.3)}$$

Now from energy balance,

$$\bar{q} \times 2\pi R \times 1 = \dot{q}\, 2\pi R \times b \times 1$$

Hence $$\dot{q} = \frac{\bar{q}}{b}$$

Then Eq. (A2.3) reduces to

$$\frac{d^2\eta}{d\theta^2} - \frac{R^2}{K_t b (t_{st} - t_\infty)} \times \bar{q} \left[\frac{q}{\bar{q}} - 1\right] = 0 \qquad \text{(A2.4)}$$

With the definition of $\bar{h}$, given as

$$\bar{q} = \bar{h} \, (\bar{t}_w - t_\infty)$$

and from Eq. (A2.4), we now obtain

$$\frac{d^2\eta}{d\theta^2} - \frac{K^*}{2} \overline{Nu_f} \, \bar{\eta} \left[\frac{q}{\bar{q}} - 1\right] = 0 \qquad \text{(A2.5)}$$

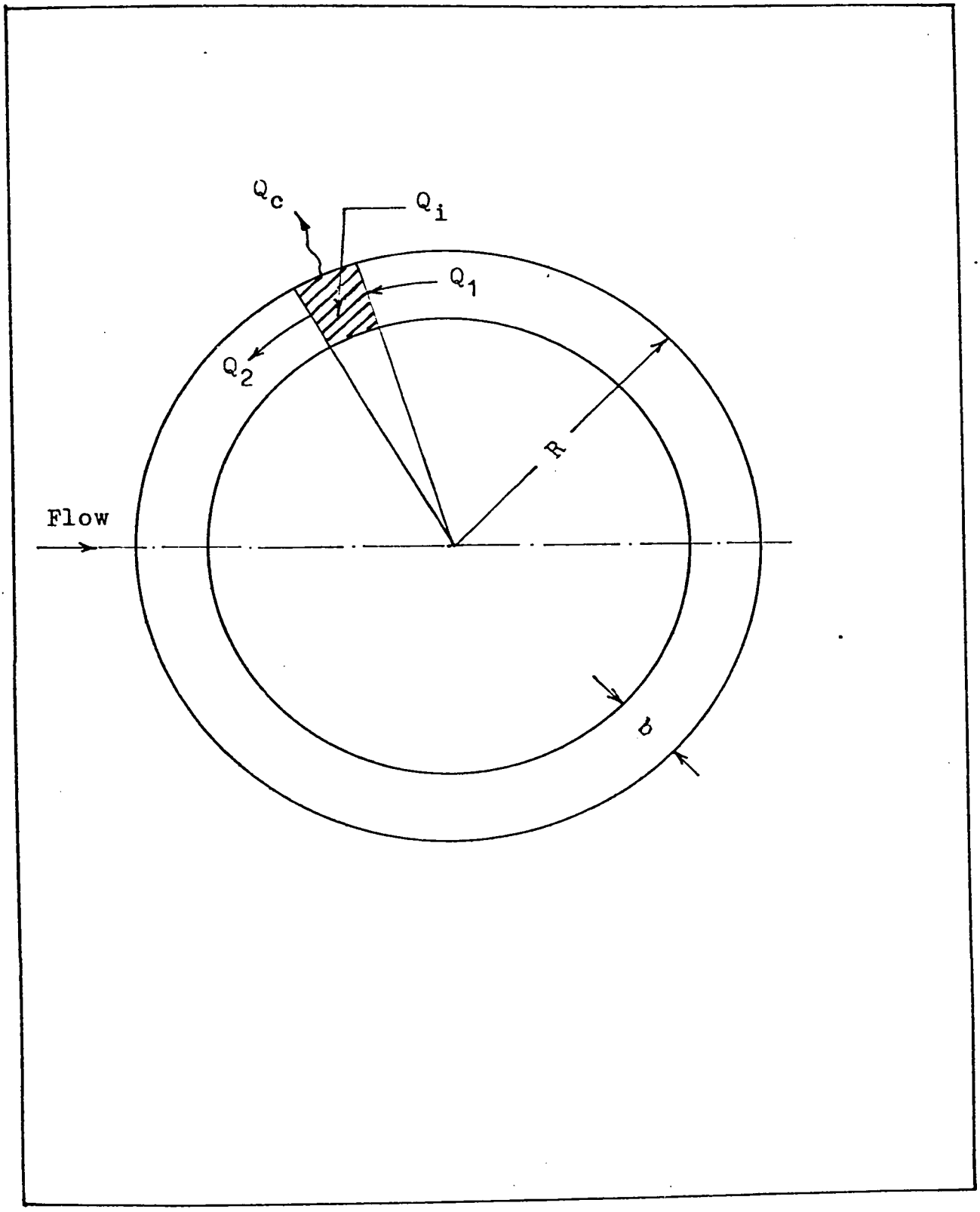

Fig. A2.1 Idealized Model

The differential Eq. (A2.5) is solved numerically based on the hypothetical heat flux distribution by employing CSMP (vis. Continuous System Modeling Program) method with double precision

The Eq. (A2.5), is given as

$$\eta'' - \frac{K^*}{2} \overline{Nu_f} \; \bar{\eta} \; [q/\bar{q} - 1] = 0$$

The circumferential heat flux distribution is assumed, for an example here, as

$$q = \bar{q}(1 + 0.5 \cos \theta)$$

in Eq. (A2.5) which then reduces to

$$\eta'' - \frac{K^*}{4} \overline{Nu_f} \; \bar{\eta} \cos\theta = 0 \qquad \text{(A2.6)}$$

and the boundary conditions are

1) $\eta' = 0$

2) $\eta = 1$

at $\theta = 0$

The flow diagram of calculation of non-dimensional temperature distribution, η, from Eq. (A2.6) is given in Fig. A2.2.

At Re = 19,800 the approximate value of Nusselt number is 87.00 which is taken as a constant in Eq. (A2.6) and values of η with respect to θ at different values of K^* are obtained.

```
****CONTINUOUS SYSTEM MODELING PROGRAM****

***PROBLEM INPUT STATEMENTS***

TITLE          NON  DIMENTIONAL  TEMP  DISTRIBUTION
CONSTANT       NU=87.0, KSTAR=(0.001645,0.0071,0.009454,0.01912,0.02395)
DYNAMIC
               Y=INTGRL(1.0,YDOT)
               YDOT=INTGRL(0.0,YDDOT)
               YDDOT=Y
               ETAD=INTGRL(0.0,ETADD)
               ETA=INTGRL(1.0,ETAD)
               ETAG=INTGRL(0.0,ETA)
               ETAB=ETAG/3.1416
               ETADD=0.25*KSTAR*NU*ETAB*Y
TIMER          FINTIM=3.1416,DELT=0.01,OUTDEL=0.08725
METHOD         RKSTY
PRTPLT         ETA
LABEL          ETA PLOTTED WITH THETA
END
STOP
```

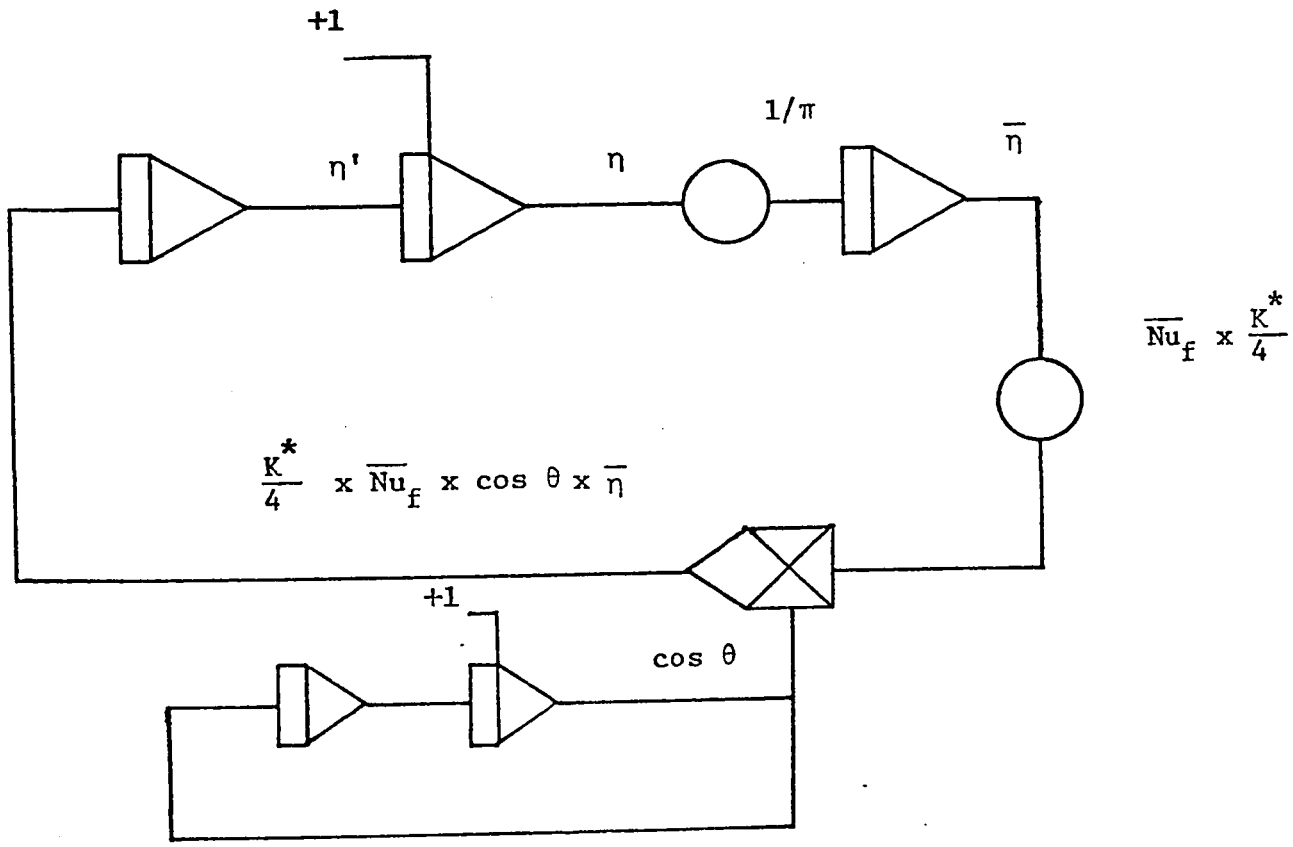

Fig. A 2.2

REFERENCES

1) W. H. McAdams:
"Heat Transmission," 3rd ed., McGraw-Hill Book Co., New York, 1954.

2) P. D. Richardson:
"Heat and Mass Transfer in Turbulent Separated Flows," Chem. Eng. Science, Vol. 18, pp.149-155, 1953.

3) W. J. M. Douglas and S. W. Churchill:
"Recorrelation of Data for Convective Heat Transfer for Gases and Single Cylinders with Large Temperature Differences," Chem. Eng. Prog. Symp. Series No. 18, Vol. 52, pp.23-28, 1956.

4) B. G. Van Der Hegge Zijnen:
"Modified Correlation Formulae for Heat Transfer by Natural and Forced Convection from Horizontal Cylinders," Applied Sci. Research Sec. A, Vol. 5, pp.129-40, 1956.

5) R. M. Fand and K. K. Keswani:
"A Continuous Correlation Equation for Heat Transfer from Cylinders to Air in Cross-Flow for Reynolds Numbers from 10^{-2} to 2×10^{5}," Int. J. Heat Mass Transfer, Vol. 15, pp.559-562, 1972.

6) N. Ototake:
"Forced Convection Heat Transfer from a Uniformly Concentrated Cylinder," Int. Chem. Eng., Vol. No. 3, pp.545-551, July 1968.

7) S. W. Churchill and J. C. Brier:
"Convective Heat Transfer for a Gas Stream at High Temperature to a Circular Cylinder normal to the Flow," Chem. Eng. Prog. Symp. Series No. 17, Vol. 51, pp.57-66, 1955.

8) W. H. Giedt:
"Investigation of Variation of Point Unit Heat Transfer Coefficient Around a Cylinder Normal to an Air Stream," Trans. A.S.M.E. Vol. 71, pp.375-381, 1949.

9) E. Schmidt and K. Wenner:
"Heat Transfer over the Circumference of a Heated Cylinder in Transverse Flow," NACA Technical Memorandum No. 1050, October 1943.

10) E. W. Coming, J. T. Clap and J. F. Taylor:
"Air Turbulence and Transfer Process; Flow Normal to Cylinders," Ind. and Eng. Chem. Vol. 40, No. 6, pp.1076-1082, June 1948.

11) W. H. Giedt:
"Effect of Turbulence Level of Incident Air Stream on Local Heat Transfer and Skin Friction on a Cylinder," J. of the Aeronautical (Aero/Space) Sciences 18, pp.725-30, 766, 1951.

12) J. Kestin and P. Maeder:
"Influence of Turbulence on Transfer of Heat from Cylinders," NACA T.N. 4018, 1957.

13) G. M. Zapp:
"The Effect of Turbulence on Local Heat Transfer Coefficient around a Cylinder Normal to an Air Stream," M.S. Thesis, Oregon State College, 1950.

14) B. G. Van Der Hegge Zijnen:
"Heat Transfer from Horizontal Cylinders to a Turbulent Airflow," Appl. Sci. Res. Section A, Vol. 7, pp.205-223, 1957.

15) E. P. Dyban and E. Y. Epick:
"Some Heat Transfer Features in the Airflows of Intensified Turbulence," FC 5.7, 4th Int. Nat. Heat Trans. Con., Paris, 1970.

16) A. M. Petrie and H. C. Simpson:
"An Experimental Study of the Sensitivity to Freestream Turbulence of Heat Transfer in Wakes of Cylinders in Crossflow," Int. J. Heat Mass Transfer, Vol. 15, pp.1497-1513, 1972.

17) A. S. T. Thomson, A. W. Scott, A. McK. Laird and H. S. Holden:
"Variation in Heat Transfer Rates Around Tubes in Crossflow," Proceeding of the General Discussion on Heat Transfer," pp.177-180, A.S.M.E., 1951.

18) R. G. Deissler and M. F. Taylor:
"Analysis of Fully Developed Turbulent Heat Transfer and Flow in an Annulus with Various Eccentricities," NACA TN 3451, 1955.

19) W. C. Reynolds:
"Effect of Wall Heat Conduction on Convection in a Circular Tube with Arbitrary Circumferential Heat Input," Int. J. Heat Mass Transfer, Vol. 6, pp.925-930, 1963.

20) Y. Lee and H. Barrow:
"Turbulent Flow and Heat Transfer in Concentric and Eccentric Annuli," Proceedings, Vol. 178, pt. 3I4, pp.1-16, 1963-64, Thermodynamics and Fluid Mechanics Conv., I. Mech. E., Cambridge, U.K. April 1964.

21) E. Y. Leung, W. M. Kays and W. C. Reynolds:
"Heat Transfer with Turbulent Flow in Concentric and Eccentric Annuli with Constant and Variable Heat Flux," Report AHT-4, Stanford University, 1962 (cited on Ref. (22)).

22) Y. Lee:
"The Effect of the Peripheral Wall Conduction on Turbulent Heat Transfer in Eccentric Annular Ducts," Unpublished May 21, 1969.

23) R. S. Grewal:
"Effect of Peripheral Wall Conduction on Forced Convection from a Cylinder Normal to the Gas Flow," B.Sc. Thesis, Department of Mechanical Engineering, University of Ottawa, March 1969.

24) DISA Elecktronics A/S, Herlev, Denmark, "Instruction Manual for Type D 41/42 Calibration Equipment," 1970.

25) K. C. Goel:
"Effect of Free Stream Turbulence on Fluid Flow and Heat Transfer," M.A.Sc. Thesis, University of Ottawa, April 1972.

26) S. D. Park:
"Developing Turbulent Flow and Heat Transfer in Concentric Annuli; an Analytical and Experimental Study," Ph.D. Thesis, University of Ottawa, March 1971.

27) J. Small:
"The Average and Local Rates of Heat Transfer from the Surface of a Hot Cylinder in a Transverse Stream of Fluid," Philosophical Magazine, Ser. 7, Vol. 49, pp.251-260, 1935.

28) H. B. Squire:
"Modern Developments in Fluid Dynamics," Vol. 2, Oxford, p.531, 1938.

29) A. M. Gibson:
"Heat Dissipation from the Surfaces of Pipes and Cylinders in an Air Current," Phil. Mag., Ser. 6, Vol. 47, pp.324-336, 1924.

30) J. A. Hughes:
"On the Cooling of Cylinders in a Stream of Air," Phil. Mag., Vol. 31, pp.118-127, 1915.

31) S. J. Kline and F. A. McClintock:
"The Description of Uncertainties in Single Sample Experiments," Mech. Eng., 3, 1953.

Table 2.1

$\overline{Re}_f$	C (Gases)	n
0.4 - 4	0.891	0.330
4 - 40	0.821	0.385
40 - 4,000	0.615	0.466
4,000 - 40,000	0.174	0.618
40,000 - 400,000	0.0239	0.805

Table 3.1

No.	Material	O.D. in inches	I.D. in inches	b in inches	$K_t^{\dagger}$ Btu/hr ft^2 $^oF/ft$	K^*
1	Monel 400	1.016	0.738	0.139	33.33	1.645×10^{-3}
2	Stainless Steel T304	0.995	0.735	0.13	8.08	7.1×10^{-3}
3	Inconel 600	1.017	0.829	0.094	8.58	9.45×10^{-3}
4	Stainless Steel T304	0.999	0.903	0.048	8.08	19.16×10^{-3}
5	Stainless Steel T304	0.998	0.934	0.032	8.08	28.9×10^{-3}

†Ref. Standard Handbook for Mechanical Engineers by Marks McGraw-Hill, 7th ed. 1967

Note: Physical properties of air were taken from Table 16, p.274. E.R.G. Eckert and R.M. Drake, Jr., McGraw-Hill, N.Y., Appendix of property values, 1959.

Table 3.2

No.	Voltmeter reading x 10 = U ft/sec	R.M.S. volts x 10 = $\sqrt{\overline{U'^2}}$ ft/sec	Turbulence Intensity = $\frac{\sqrt{\overline{U'^2}}}{U}$
1	19	0.78	4.1
2	31	1.25	4.03
3	45	1.8	4.0
4	87	3.5	4.02
5	101	4.2	4.15
6	117	4.8	4.1

Table 4.1

No.	Investigator	Material	O.D.	Thickness b	K_t† Btu/hr ft^2 ^oF/ft	K*
1	Hughes (27)	Copper	1.992"	0.07"	224	0.951×10^{-3}
2	Hughes	Copper	0.759"	0.042"	224	0.605×10^{-3}
3	Gibson (26)	Stain-less Steel	0.925 cm	0.056 cm	8.08	15.33×10^{-3}
4	Gibson	Stain-less Steel	9.52 cm	0.254 cm	8.08	34.79×10^{-3}
5	Coming, Clapp & Taylor (10)	Copper	1.25"	0.055"	224	0.76×10^{-3}
6	Giedt (8)	Nicrome††	4.04"	0.002"	7.4[x]	2029×10^{-3}

†Ref. Standard Handbook for Mechanical Engineers by Marks, McGraw-Hill, 7th ed., 1967.

††Nicrome ribbon 1" x 0.002" in cross section was wound helically around the center section of the cylinder made from 4" O.D. lucite stock.

[x]Ref. W.H. McAdams, "Heat Transmission," 3rd ed., McGraw-Hill, N.Y., 1954.

TABLE 4.2

TEST TUBE #1 Outside Diameter = 1.016" $K^* = 1.64 \times 10^{-3}$

No.	Angle θ^o	0	15	30	45	60	75	90	105	120	135	150	165	180	t_∞ ^oF	$\bar{q}$ $\frac{Btu}{hr\ ft^2}$	U_∞ ft/sec	$\overline{Nu_f}$	Re_f
1	Δt ^oF	18.62	18.62	18.84	19.06	19.28	19.71	19.93	20.15	20.15	20.37	20.37	20.37	20.37	69.37	266.15	31.53	75.58	15,714
	Nu_f	79.93	79.93	78.99	78.07	77.18	75.44	74.60	73.79	73.79	72.98	72.98	72.98	72.98					
2	Δt ^oF	30.00	30.00	30.43	30.65	31.51	32.15	32.58	32.79	32.79	32.79	32.58	32.58	32.37	69.48	719.99	80.94	125.28	39,745
	Nu_f	132.97	132.97	131.05	130.10	126.47	123.87	122.20	121.38	121.38	121.38	122.20	122.20	123.03					
3	Δt ^oF	27.93	27.93	28.15	28.36	28.79	29.23	29.44	29.44	29.23	29.23	28.79	28.58	28.15	67.45	759.19	108.12	146.87	54,168
	Nu_f	151.37	151.37	150.18	149.01	146.72	144.50	143.42	143.42	144.50	144.50	146.72	147.86	150.18					
4	Δt ^oF	27.54	27.54	27.97	28.19	29.06	29.70	29.92	29.92	29.92	29.70	29.49	29.27	29.27	66.55	904.72	143.66	173.51	69,875
	Nu_f	183.27	183.27	180.36	178.95	173.49	169.61	168.36	168.36	168.36	169.61	170.89	172.18	172.18					

TABLE 4.3

TEST TUBE #2 Outside Diameter = 0.995" $K^* = 7.1 \times 10^{-3}$

No.	Angle θ^o	0	15	30	45	60	75	90	105	120	135	150	165	180	t_∞ ^oF	$\bar{q}$ $\frac{Btu}{hr\ ft^2}$	U_∞ ft/sec	$\overline{Nu_f}$	Re_f
1	Δt ^oF	28.50	28.71	29.36	29.79	30.65	31.29	31.94	32.37	32.58	32.79	32.79	32.37	32.79	69.42	432.79	31.64	75.25	15,296
	Nu_f	82.51	81.88	80.04	78.86	76.59	74.97	73.42	72.43	71.94	71.45	71.45	72.43	71.45					
2	Δt ^oF	20.70	20.70	21.13	21.57	22.22	22.87	23.30	23.52	23.52	23.30	23.10	22.65	22.65	69.91	627.52	111.32	152.79	54,015
	Nu_f	165.66	165.66	162.20	158.87	154.13	149.66	146.82	145.44	145.44	146.82	148.22	151.12	151.12					
3	Δt ^oF	21.83	21.83	22.48	22.92	23.57	24.44	24.66	25.10	24.66	24.44	24.22	24.00	23.79	67.91	756.14	143.83	174.31	70,678
	Nu_f	189.71	189.71	184.10	180.54	175.45	169.10	167.57	164.61	167.57	169.10	170.63	172.21	173.81					

TABLE 4.4

TEST TUBE #3 Outside Diameter = 1.017" $K^* = 9.45 \times 10^{-3}$

No.	Angle θ^o	0	15	30	45	60	75	90	105	120	135	150	165	180	t_∞ ^oF	$\bar{q}$ Btu / hr ft^2	U_∞ ft/sec	$\overline{Nu_f}$	Re_f
1	Δt ^oF	20.67	20.67	21.11	21.76	22.41	23.29	23.72	24.16	24.16	24.37	23.94	23.94	23.72	66.67	312.42	31.12	76.40	15,816
	Nu_f	84.85	84.85	83.07	80.53	78.14	75.16	73.76	72.40	72.40	71.74	73.07	73.07	73.76					
2	Δt ^oF	35.51	35.93	36.79	38.28	39.56	41.69	42.11	42.53	42.53	42.53	41.47	41.05	40.62	68.91	943.31	82.37	129.55	39,874
	Nu_f	146.85	145.05	141.59	135.90	131.38	124.46	123.17	121.89	121.89	121.89	125.12	126.46	127.83					
3	Δt ^oF	33.03	33.46	34.54	36.04	37.55	39.69	40.11	40.76	40.33	39.90	38.40	38.40	37.76	64.30	1046.56	109.89	154.04	54,794
	Nu_f	176.80	174.45	168.86	161.61	154.96	146.34	144.73	142.38	143.94	145.54	151.39	151.39	154.05					
4	Δt ^oF	24.17	24.17	24.81	25.89	26.74	28.03	28.24	28.03	27.60	26.96	26.10	25.46	25.45	75.96	865.73	143.3	180.98	69,106
	Nu_f	197.55	197.55	192.32	184.19	178.17	169.83	168.51	169.83	172.52	176.72	182.65	187.36	187.36					

TABLE 4.5

TEST TUBE 4 — Outside Diameter = 0.999" — $K^* = 19.16 \times 10^{-3}$

No.	Angle θ^o	0	15	30	45	60	75	90	105	120	135	150	165	180	t_∞ ^oF	$\bar{q}$ $\frac{Btu}{hr\ ft^2}$	U_∞ ft/sec	$\overline{Nu_f}$	Re_f
1	Δt ^oF	44.31	44.52	45.38	47.29	50.04	52.58	54.49	55.75	56.17	57.01	56.17	56.17	55.75	65.66	710.9	33.23	74.11	15,725
	Nu_f	87.00	86.58	84.90	81.34	76.69	72.84	70.19	68.53	67.99	66.94	67.99	67.99	68.53					
2	Δt ^oF	27.12	27.34	28.20	29.71	31.65	34.01	34.22	35.08	33.79	33.79	31.86	32.08	31.43	68.91	892.32	113.31	153.74	54,248
	Nu_f	179.83	178.38	172.79	163.82	153.56	142.63	141.72	138.16	143.56	143.56	152.49	151.45	154.63					
3	Δt ^oF	29.28	29.49	29.92	31.64	34.00	36.14	36.56	36.56	35.07	34.64	32.71	32.93	31.86	69.56	1128.95	148.19	184.57	70,621
	Nu_f	210.19	208.62	205.55	194.11	180.31	169.36	167.33	167.33	174.67	176.88	187.59	186.33	192.77					

TABLE 4.6

TEST TUBE #5 Outside Diameter = 0.998" $K^* = 28.9 \times 10^{-3}$

No.	Angle θ^o	0	15	30	45	60	75	90	105	120	135	150	165	180	t_∞ ^oF	$\bar{q}$ Btu/hr ft^2	U_∞ ft/sec	$\overline{Nu_f}$	Re_f
1	Δt ^oF	37.70	38.12	38.34	40.04	41.74	45.14	45.99	47.26	46.84	48.75	47.05	48.75	47.69	68.00	644.86	33.35	79.10	15,741
	Nu_f	92.76	91.69	91.16	87.16	83.49	77.00	75.53	73.42	74.11	71.10	73.76	71.10	72.74					
2	Δt ^oF	33.80	34.23	34.66	36.37	38.29	41.27	41.90	42.33	40.84	40.84	38.72	39.99	39.14	68.90	958.20	81.84	133.86	39,192
	Nu_f	153.96	151.98	150.05	142.80	135.44	125.36	123.39	122.11	126.71	126.71	133.90	129.49	132.40					
3	Δt ^oF	27.90	28.11	28.33	29.83	31.33	33.89	33.89	34.32	32.40	31.54	30.04	30.69	30.47	72.23	946.16	113.82	164.86	54,559
	Nu_f	184.09	182.65	181.24	171.90	163.48	150.81	150.81	148.88	157.95	162.35	170.65	166.99	168.19					
4	Δt ^oF	29.94	30.37	30.37	32.51	34.22	36.57	36.14	35.71	33.79	32.51	31.66	31.23	31.44	71.69	1204.70	148.02	198.19	70,777
	Nu_f	218.23	215.08	215.08	200.57	190.30	177.76	179.92	182.13	192.77	200.57	206.14	209.03	207.57					

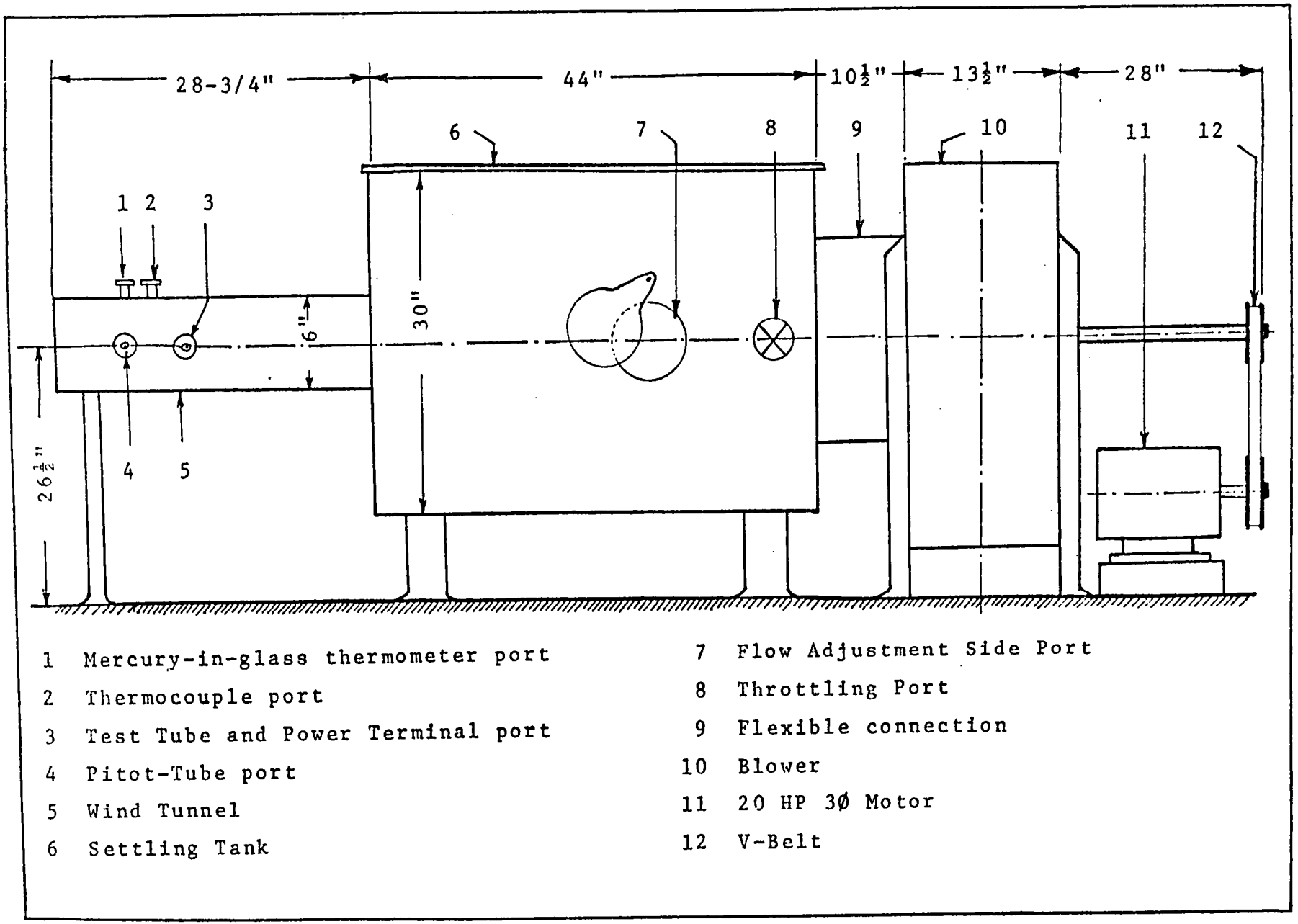

1 Mercury-in-glass thermometer port
2 Thermocouple port
3 Test Tube and Power Terminal port
4 Pitot-Tube port
5 Wind Tunnel
6 Settling Tank
7 Flow Adjustment Side Port
8 Throttling Port
9 Flexible connection
10 Blower
11 20 HP 3Ø Motor
12 V-Belt

FIG. 3 .1 SCHEMATIC DIAGRAM OF APPARATUS

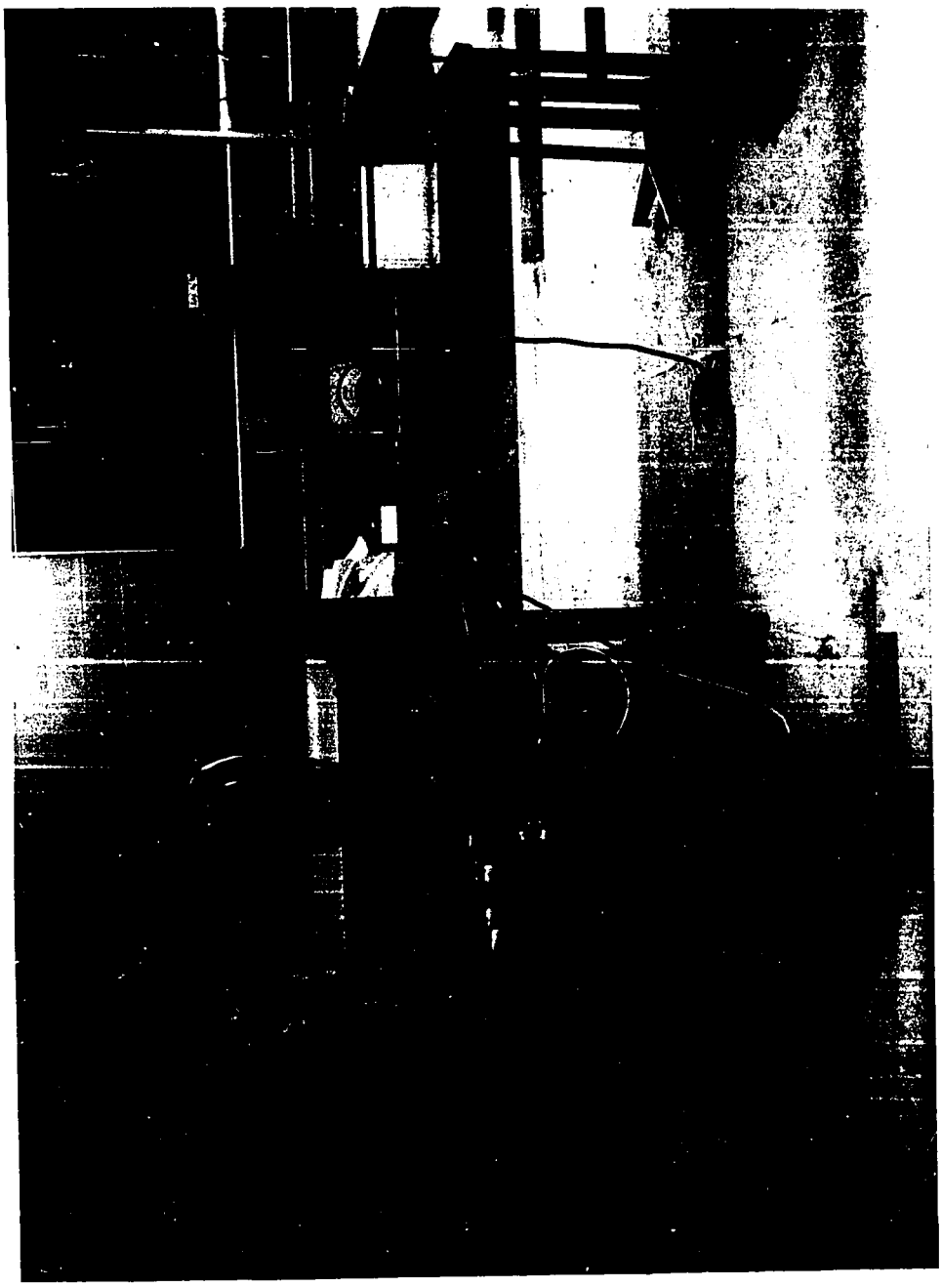

Fig. 3.2 Experimental Set-up, Front View

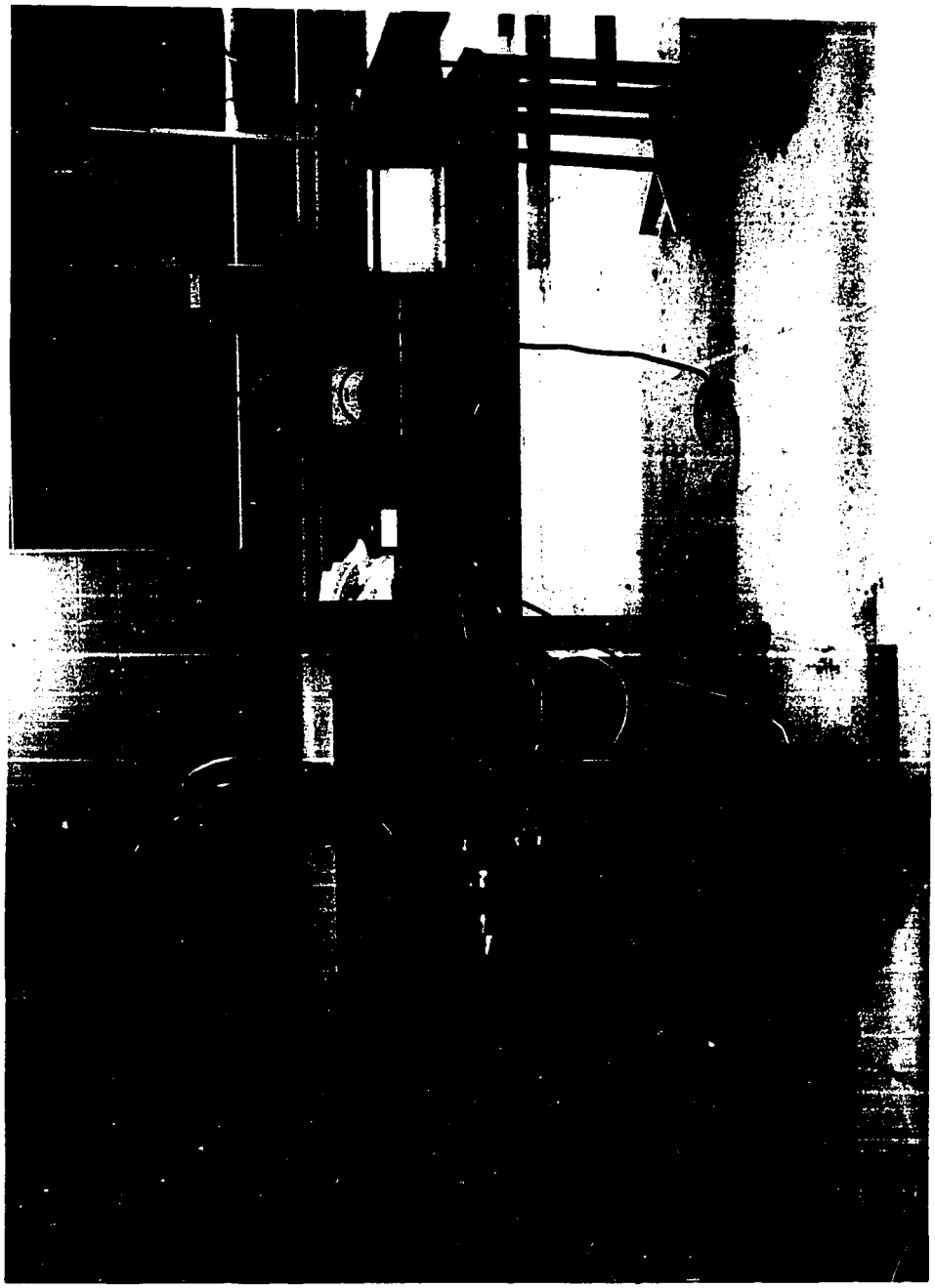

Fig. 3.2 Experimental Set-up, Front View

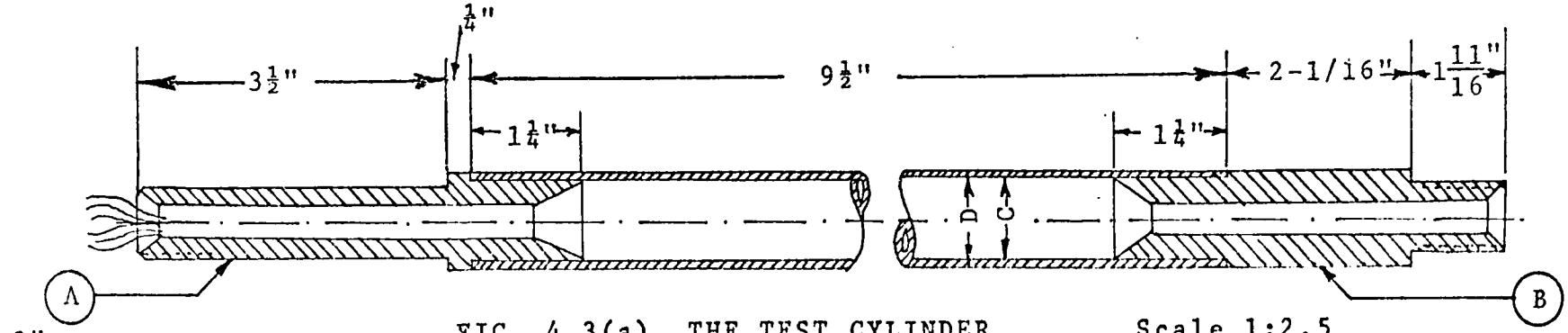

FIG. 4.3(a) THE TEST CYLINDER Scale 1:2.5

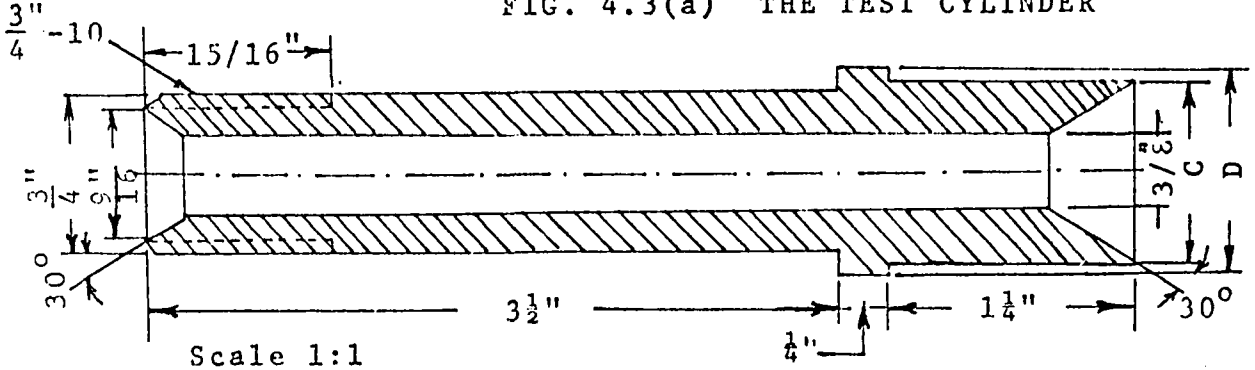

Scale 1:1

Details of (A) Material-copper

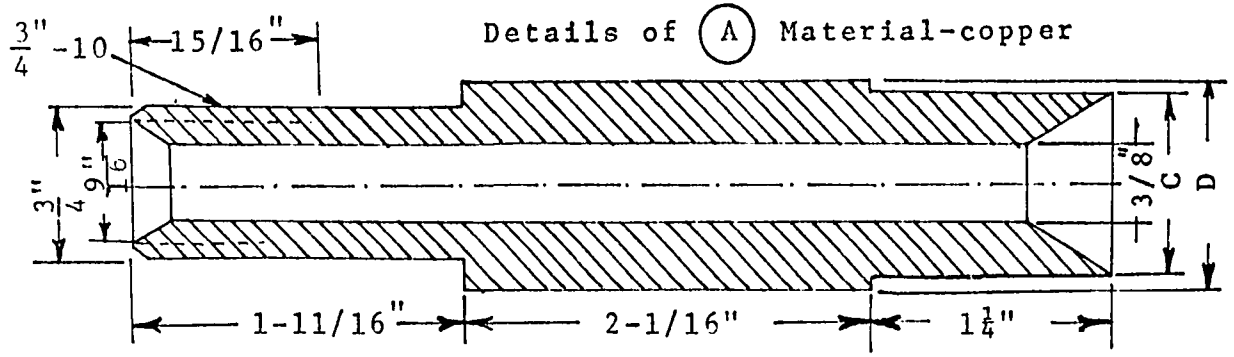

Details of (B) Material-copper

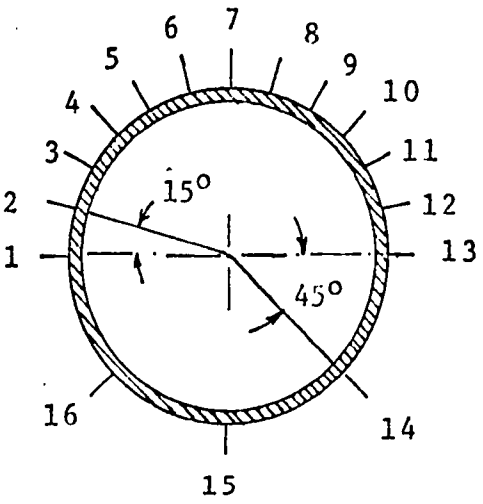

FIG. 4.3(b) WALL TEMPERATURE MEASUREMENT LOCATIONS

FIG. 3.3 DETAILS OF TEST CYLINDER

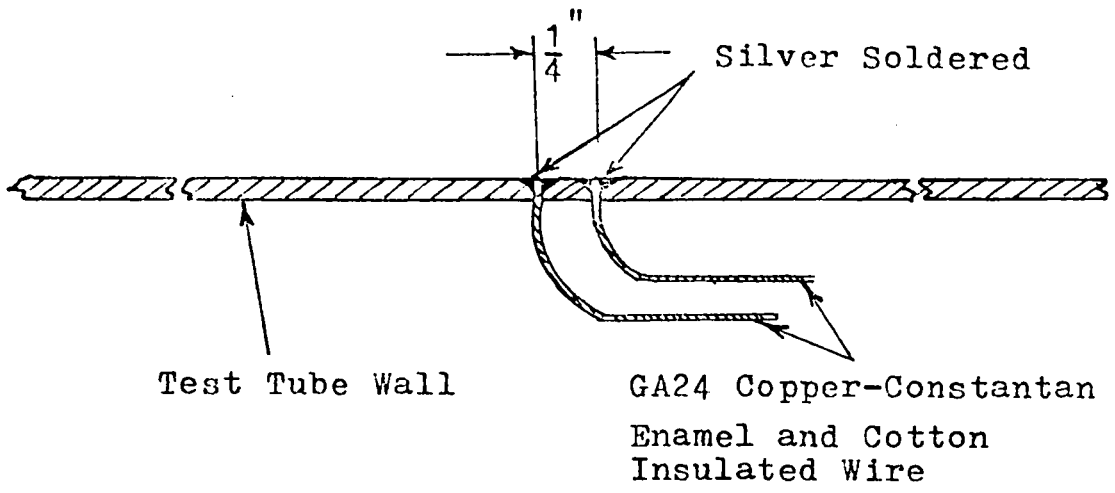

Fig. 3.4(a) Details of Split Hot Junction

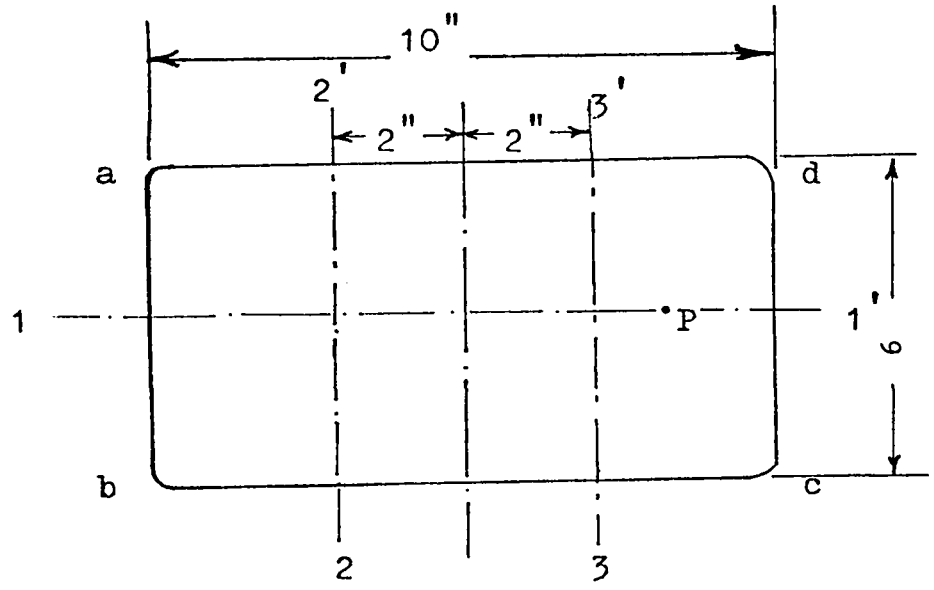

Fig. 3.4(b) Rectangular Channel

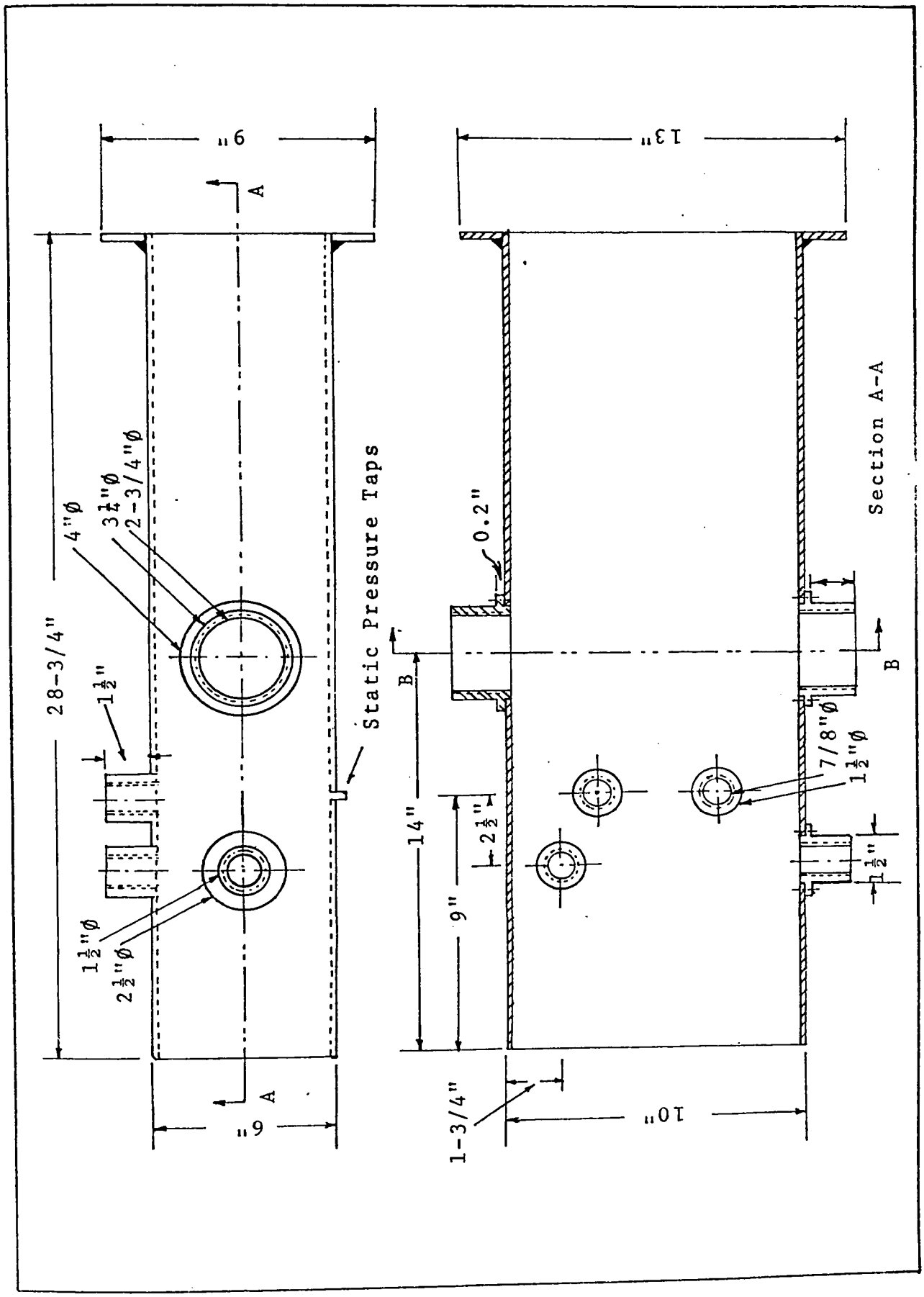

FIG. 3.5(a) DETAILS OF RECTANGULAR CHANNEL

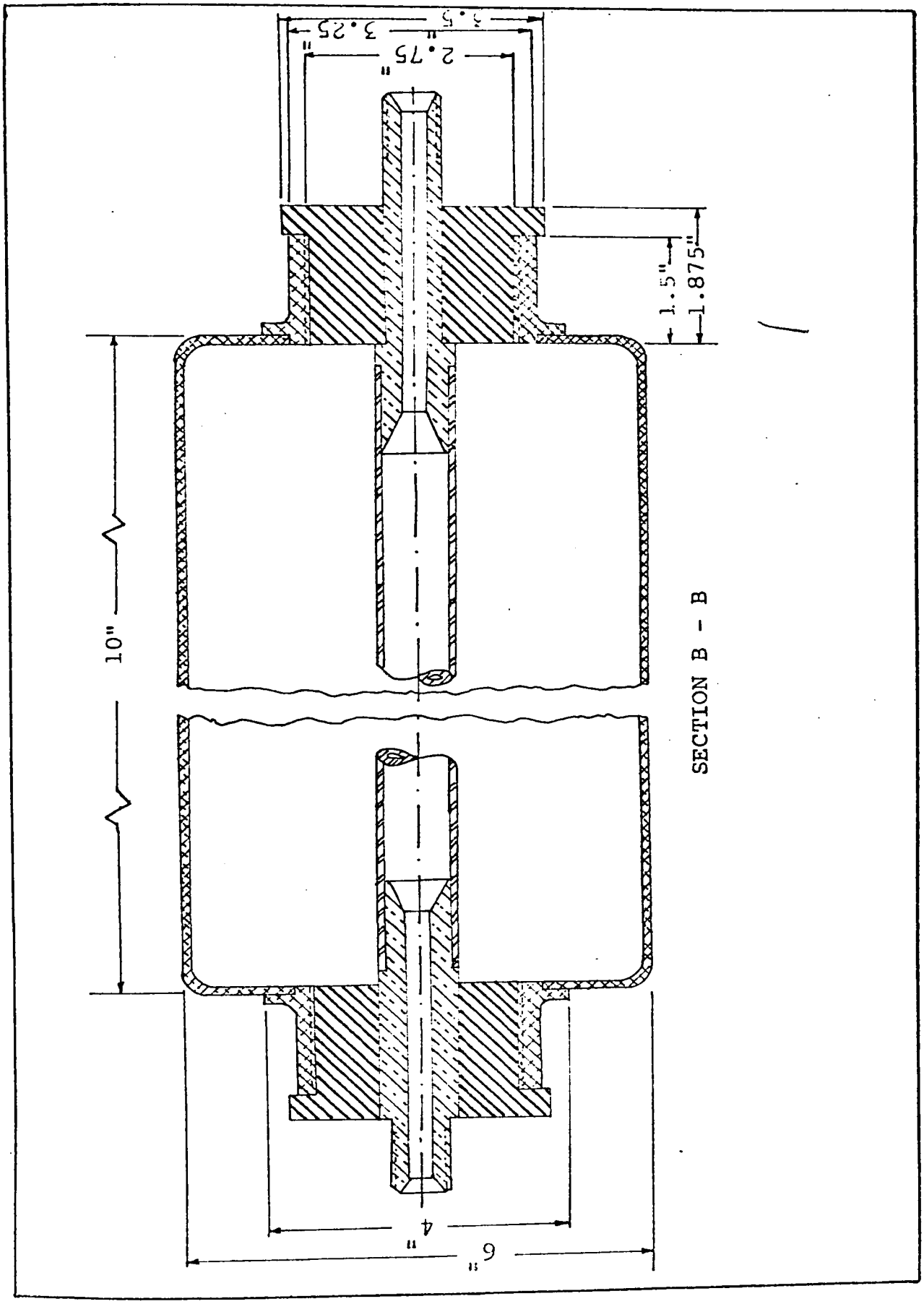

Fig. 3.5(b) Details of Test Tube Support

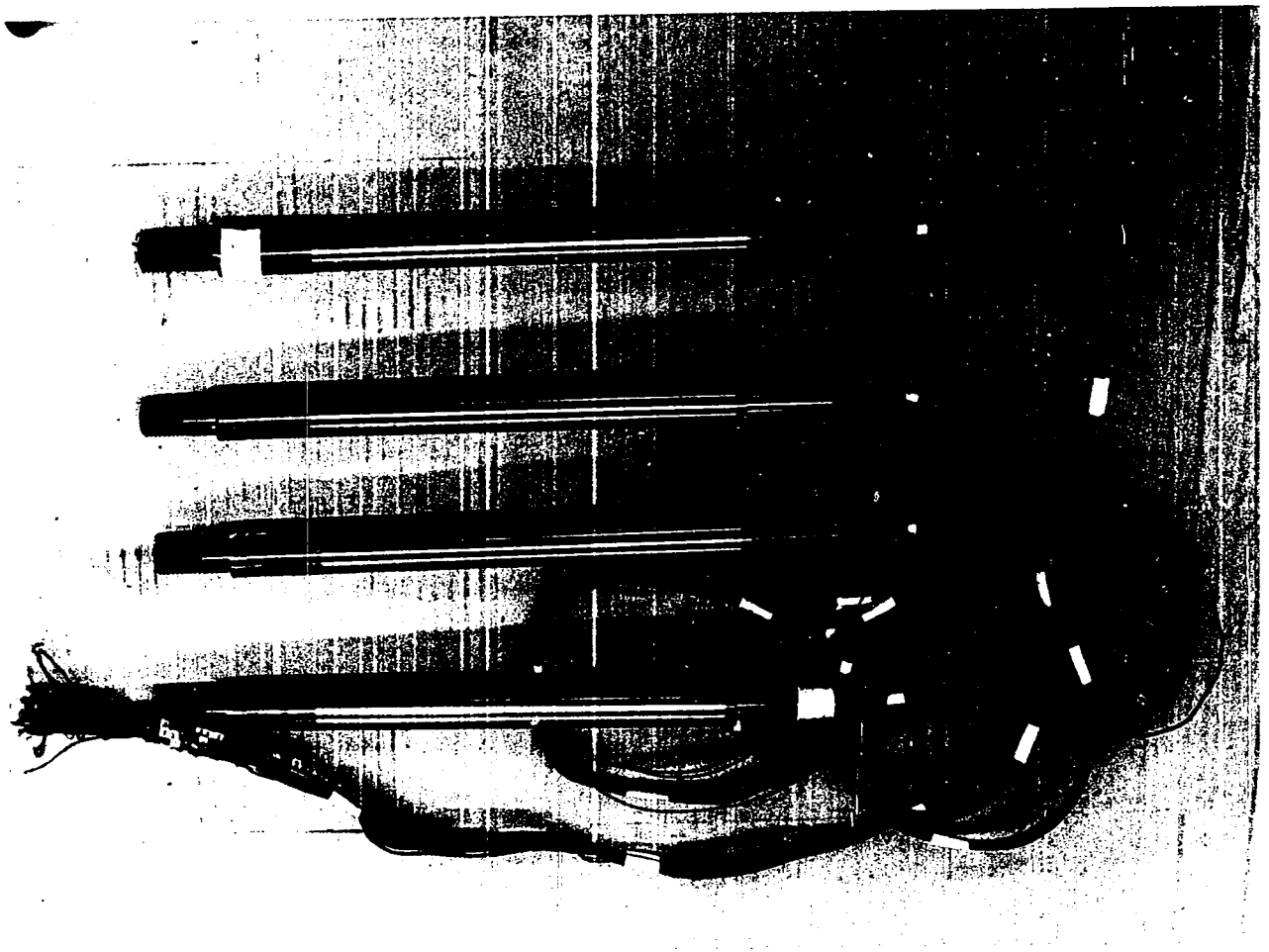

Fig. 3.6 Test Tubes

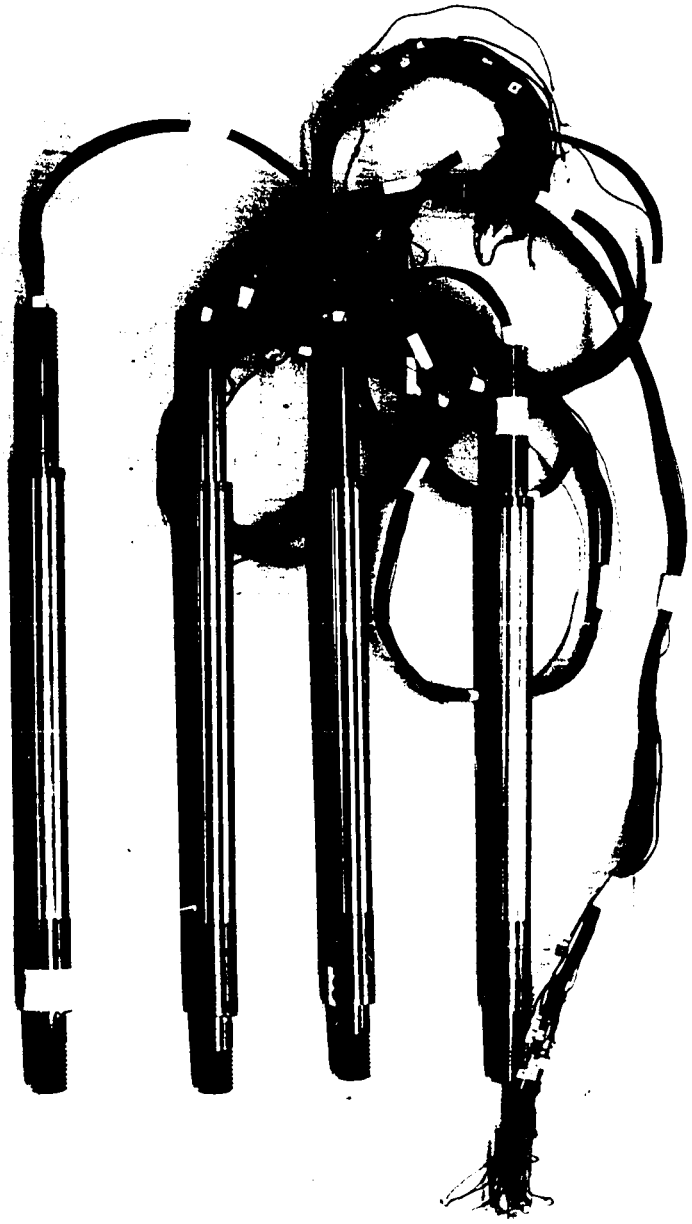

Fig. 3.6 Test Tubes

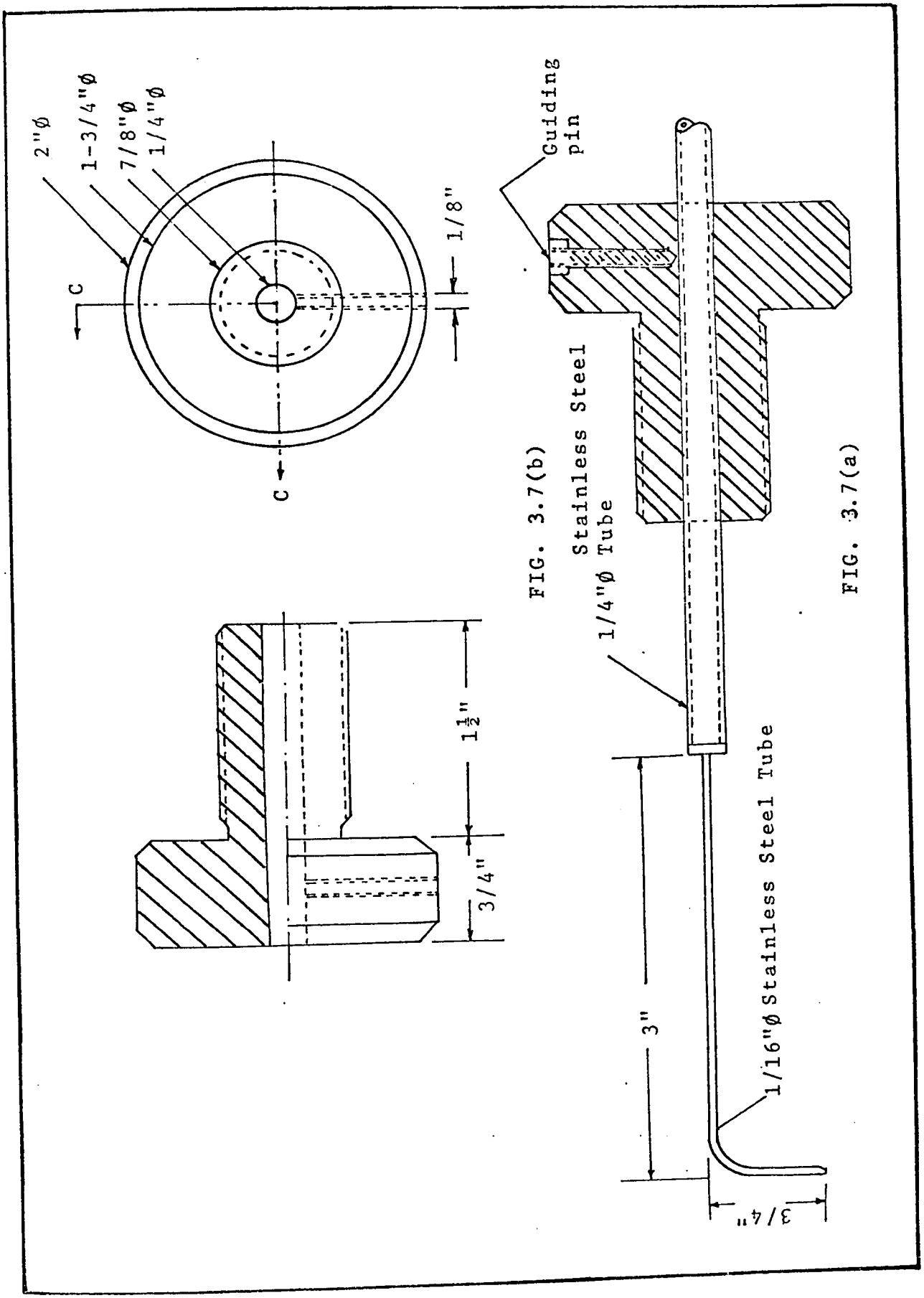

FIG. 3.7 DETAILS OF PITOT-TUBE

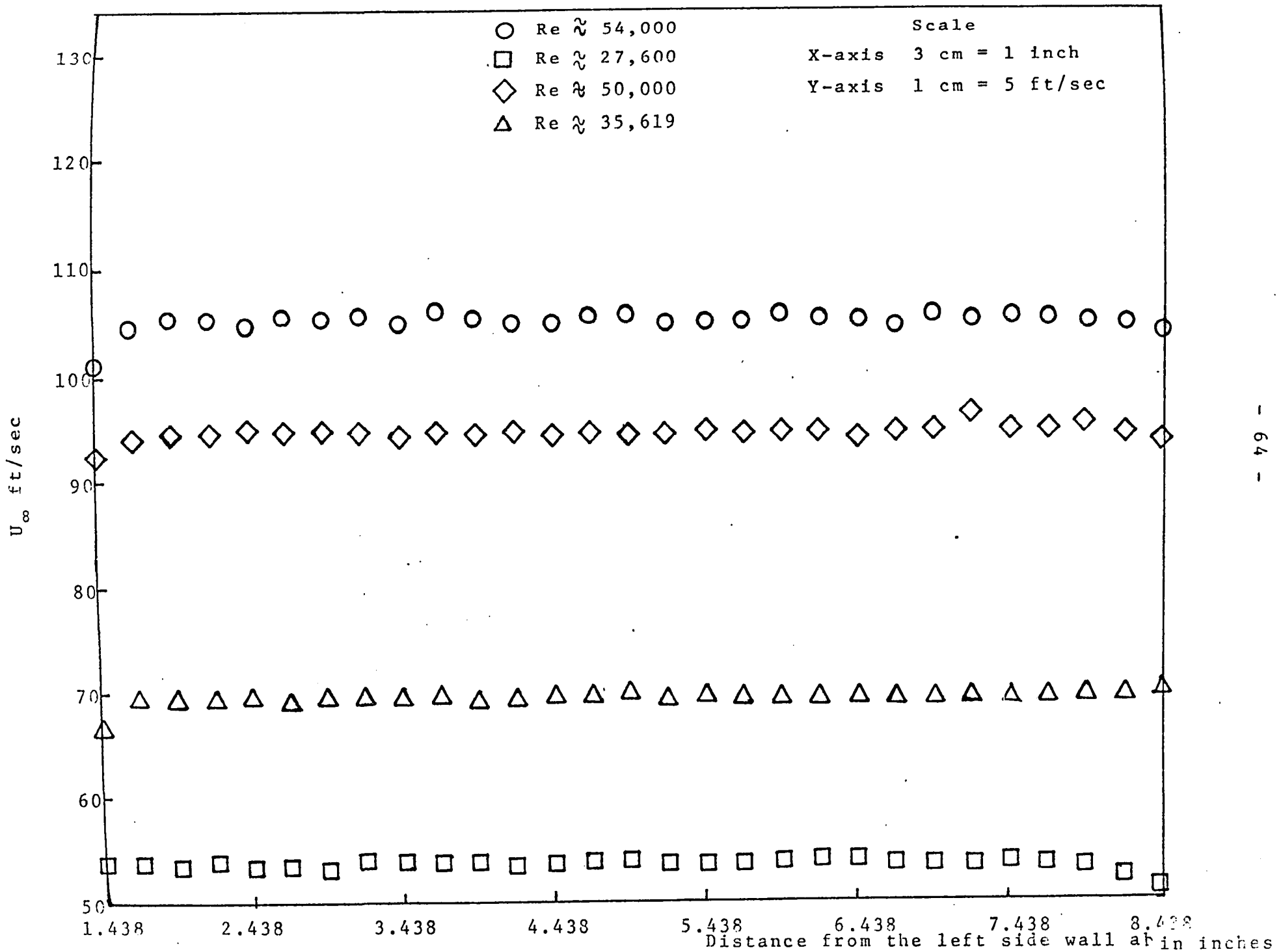

FIG. 3.8 TYPICAL VELOCITY MEASUREMENT

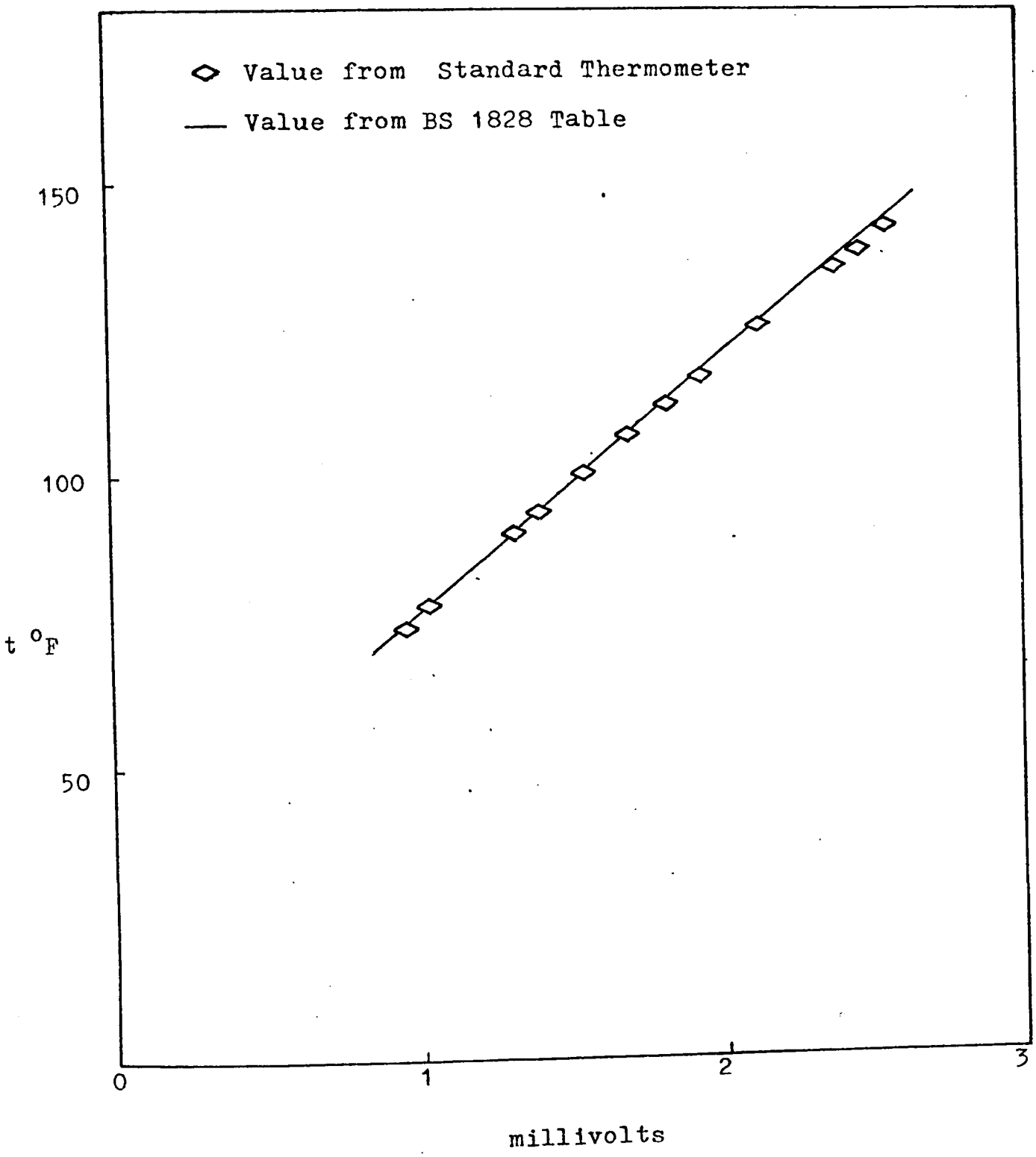

Fig. 3.9 The Thermocouple Calibration Curve

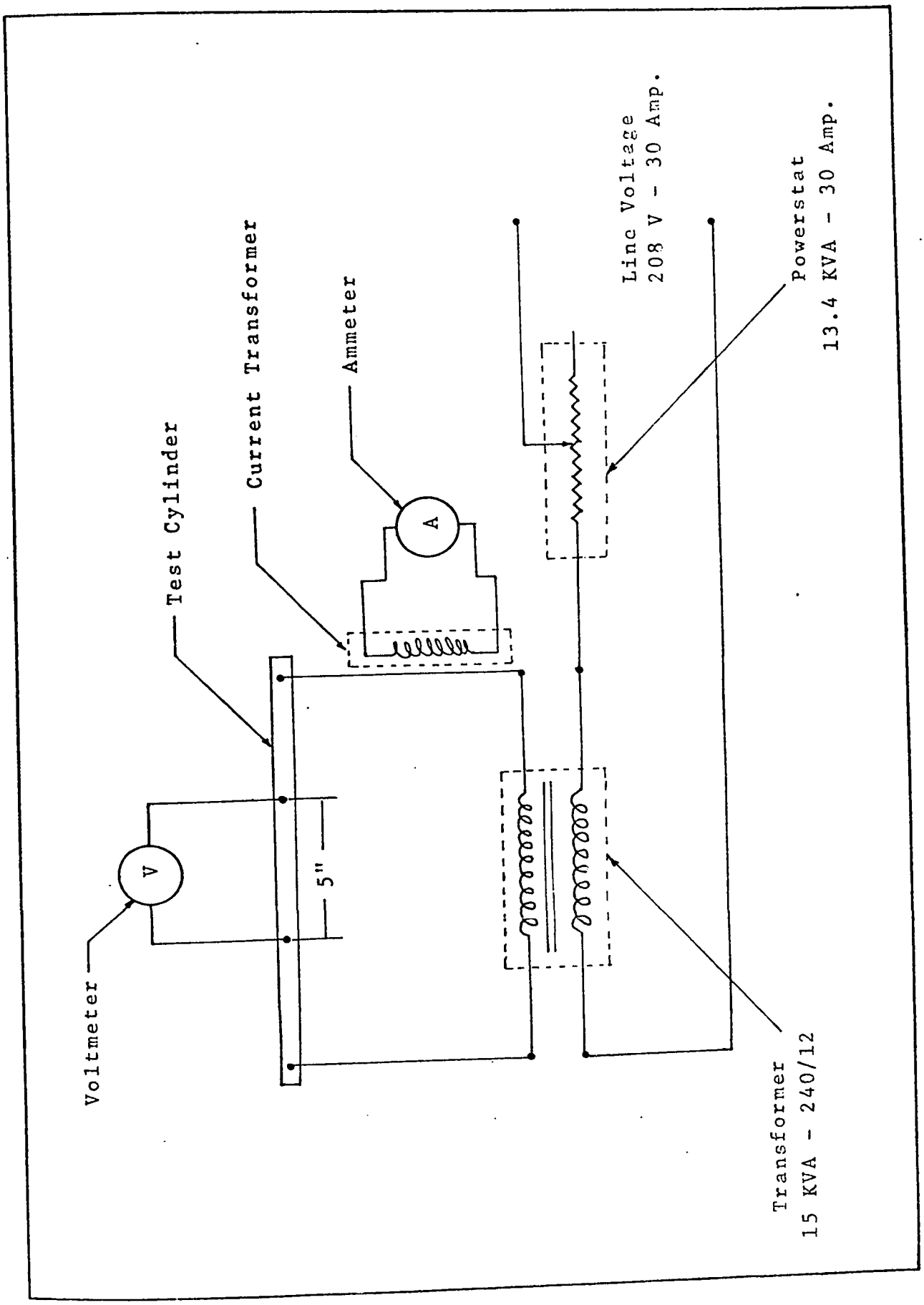

FIG. 3.10 POWER SUPPLY AND INSTRUMENTATION CIRCUIT

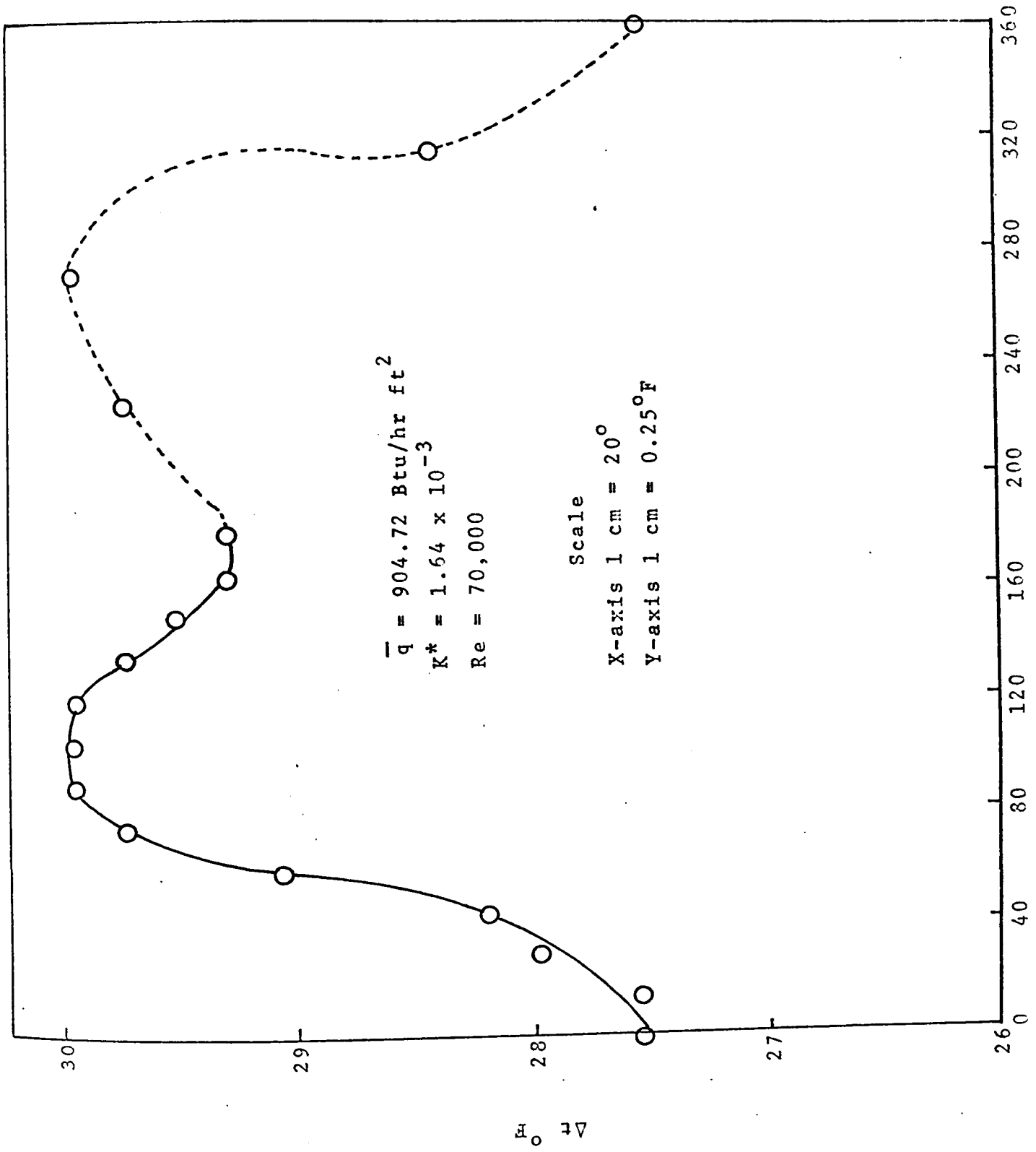

FIG. 3.11 A REPRESENTATIVE TEMPERATURE DISTRIBUTION CURVE

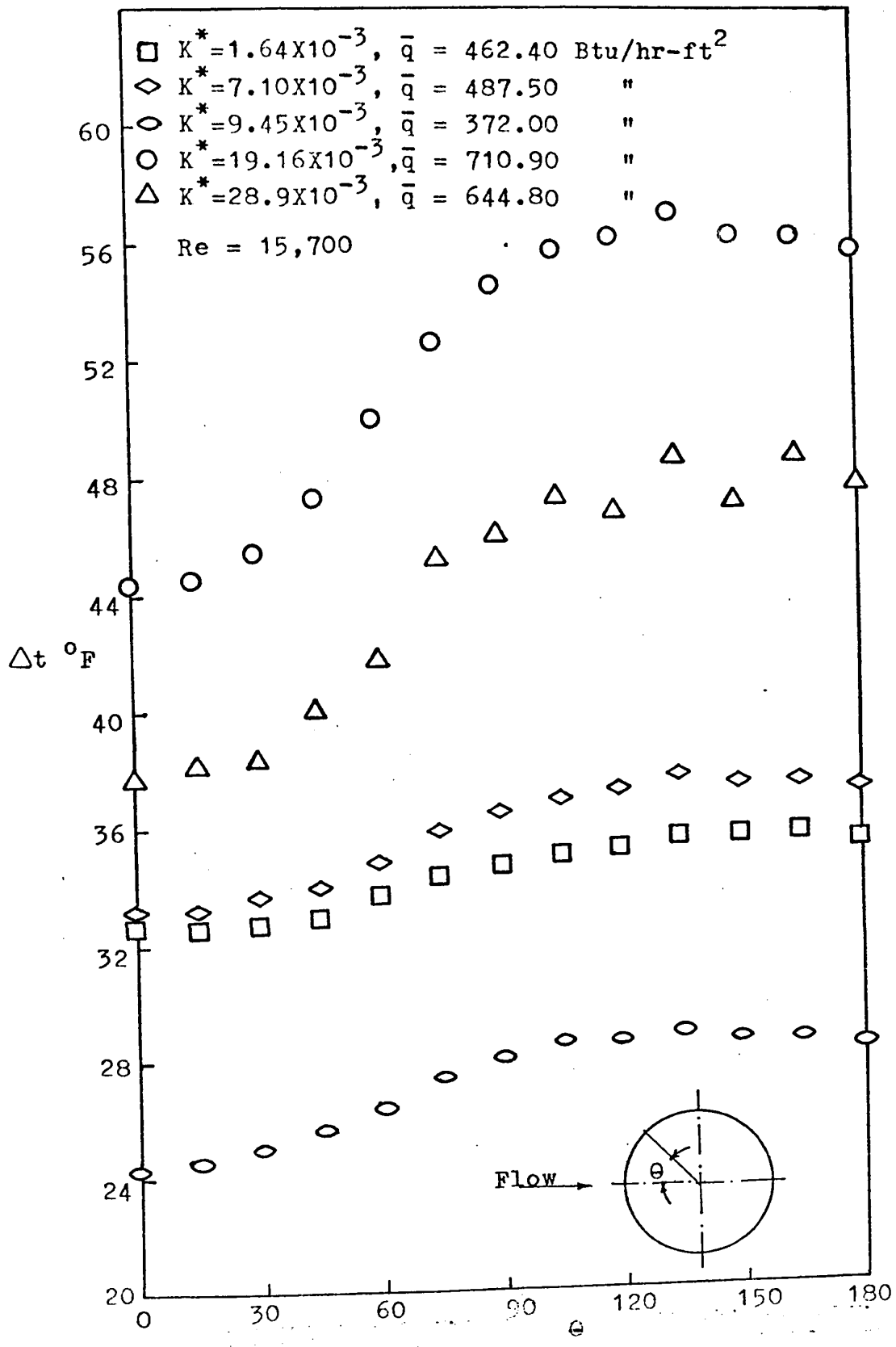

Fig. 4.1 Wall Temperature Distribution

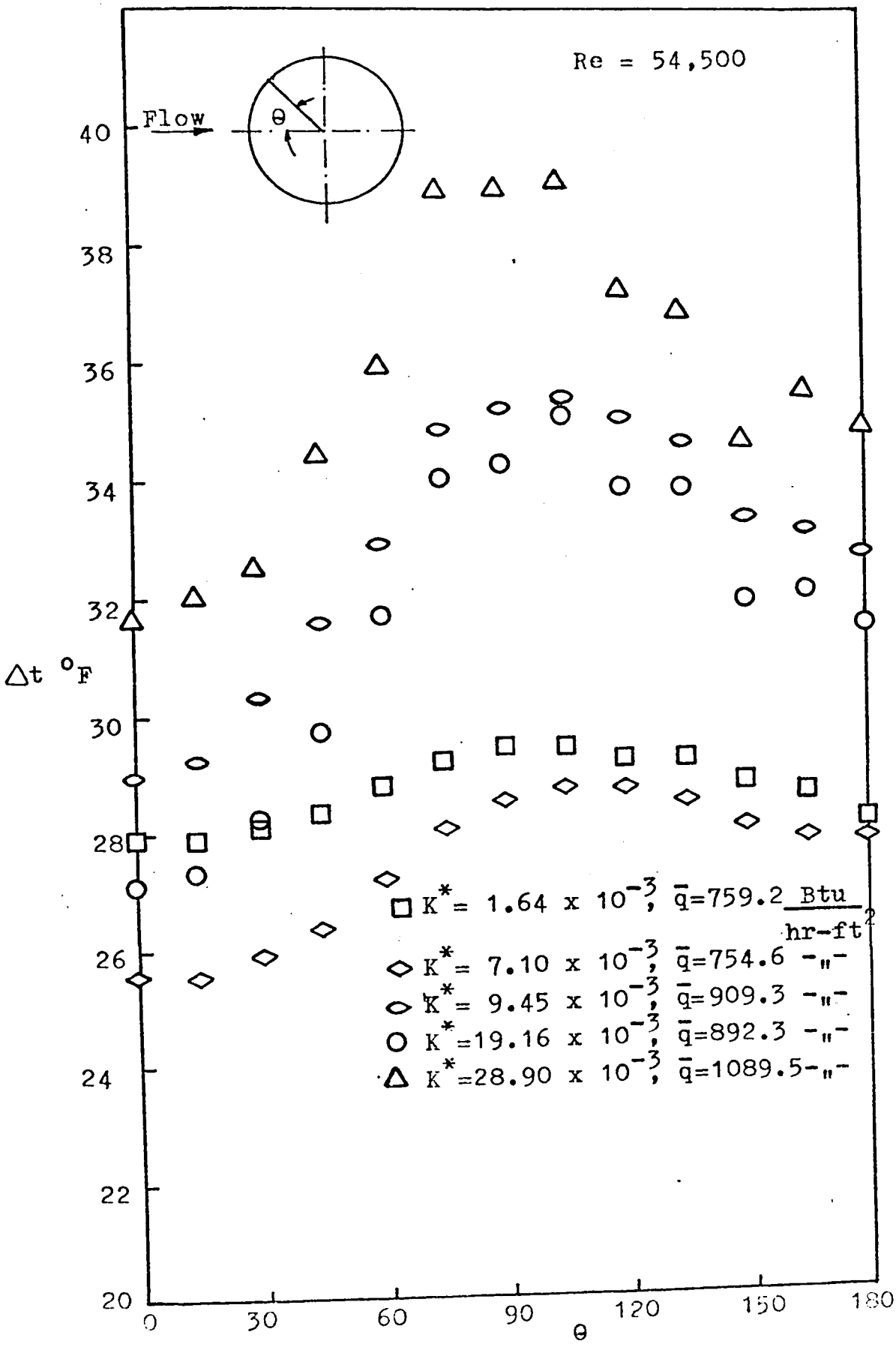

Fig. 4.2 Wall Temperature Distribution

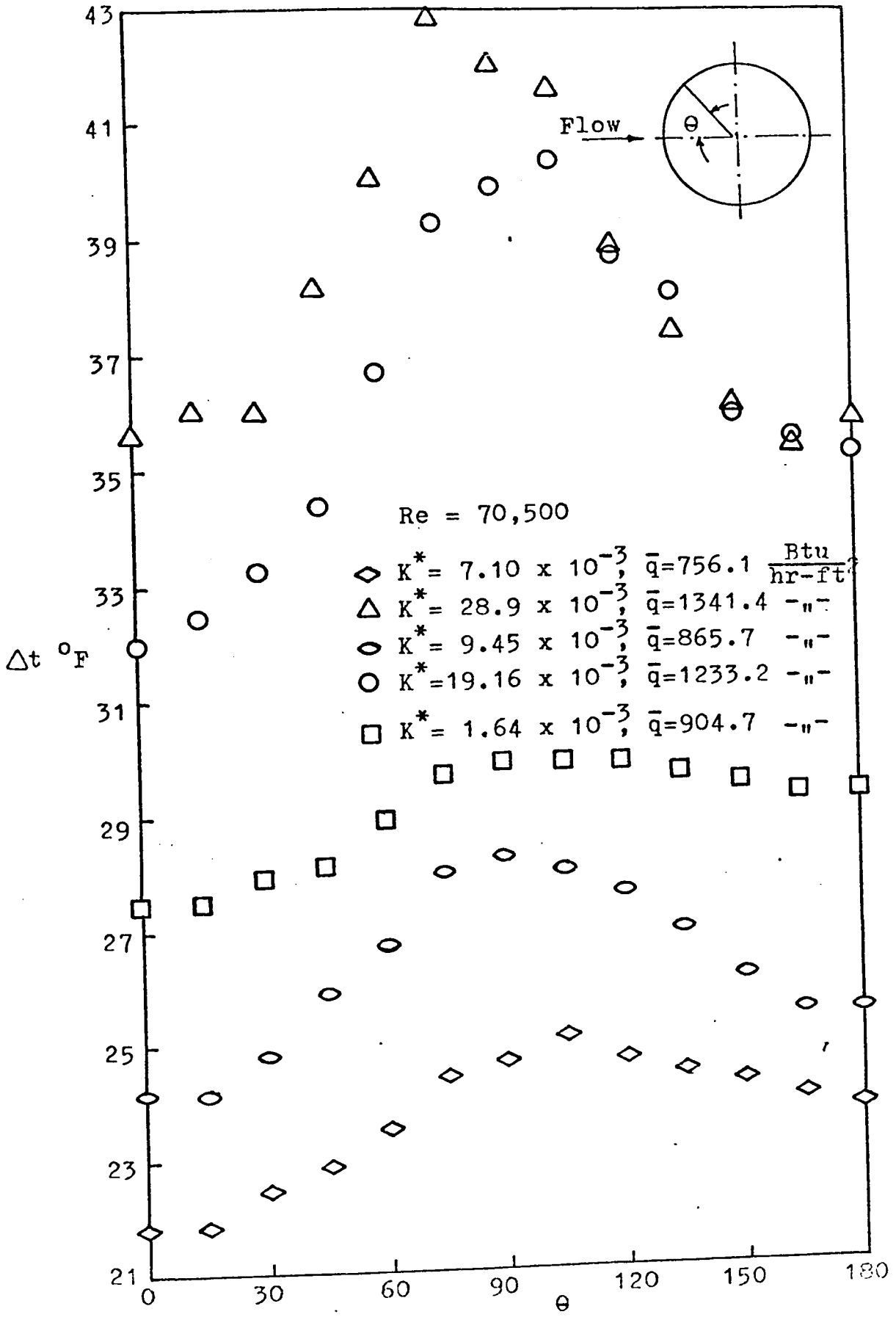

Fig. 4.3 Wall Temperature Distribution

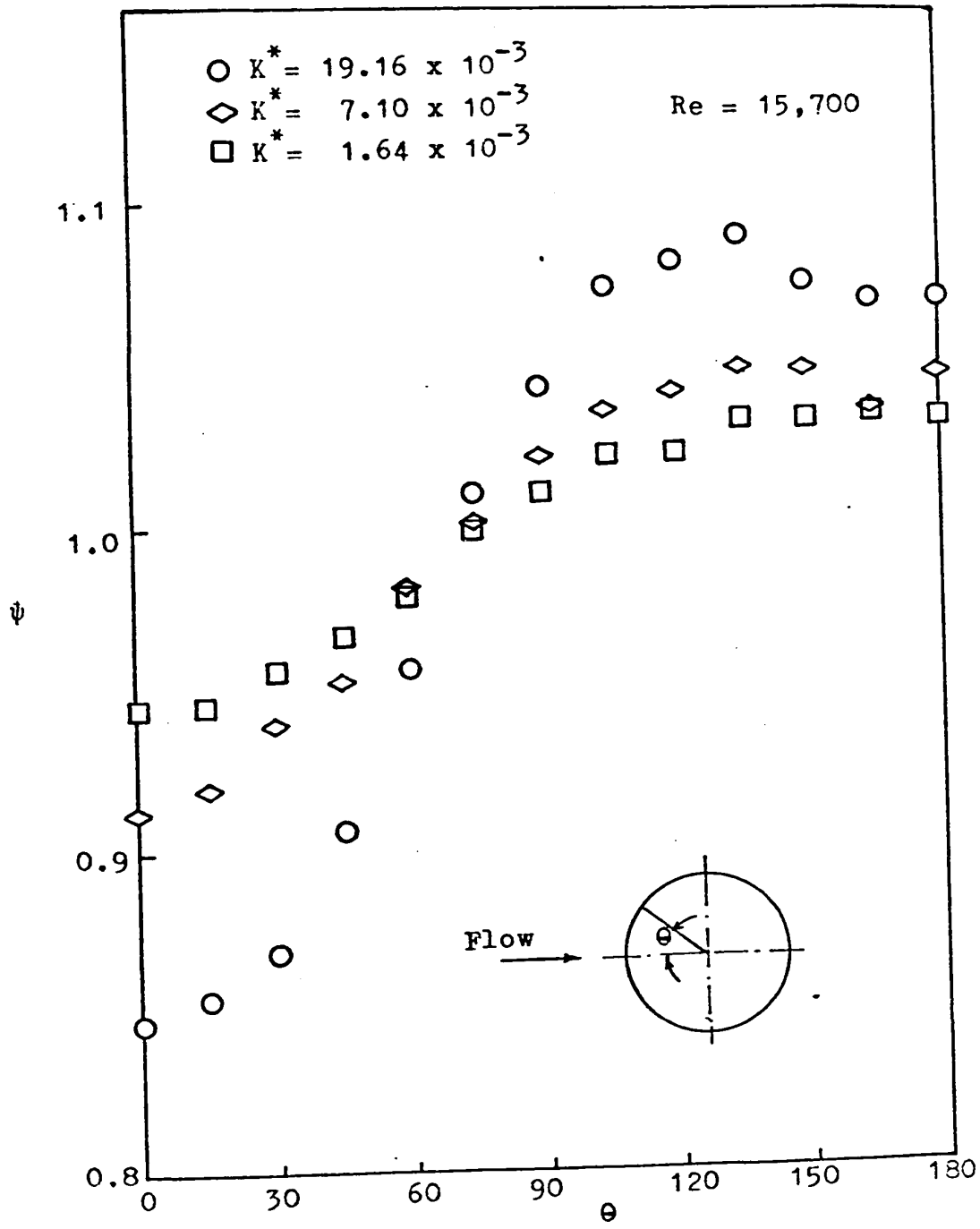

Fig. 4.4 (a) Non-Dimensional Wall Temperature Distribution

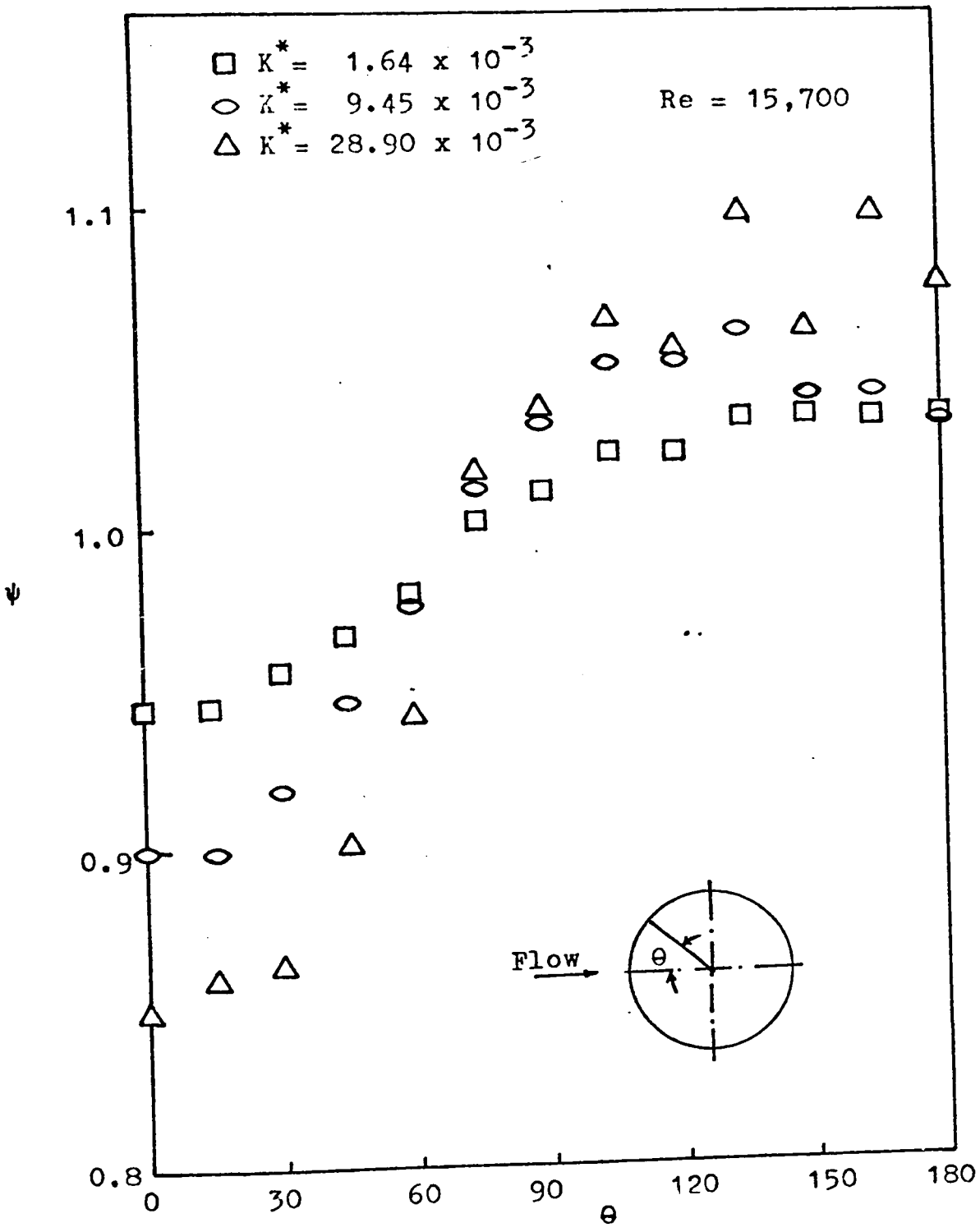

Fig. 4.4 (b) Non-Dimensional Wall Temperature Distribution

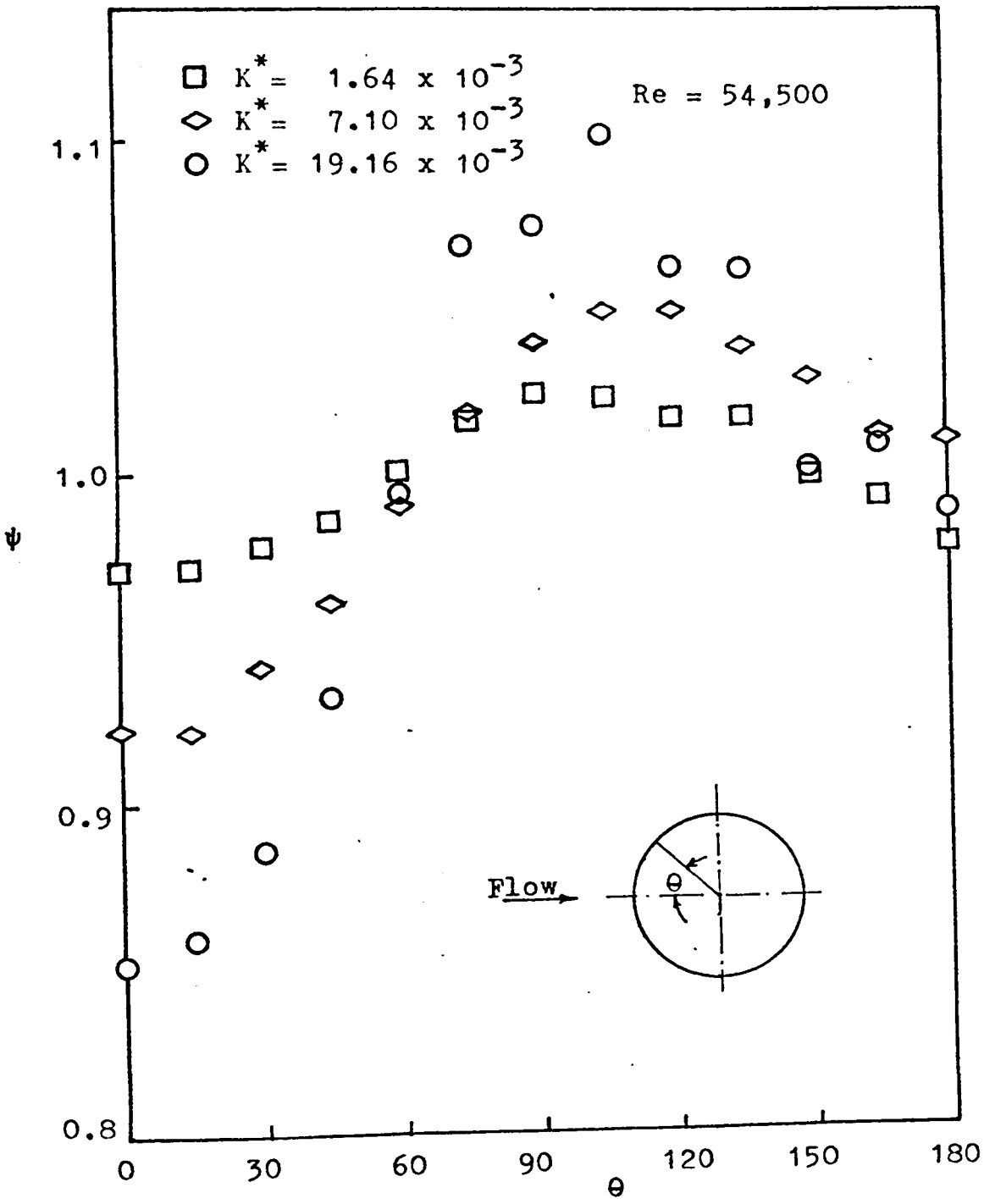

Fig. 4.5(a) Non-Dimensional Wall Temperature Distribution

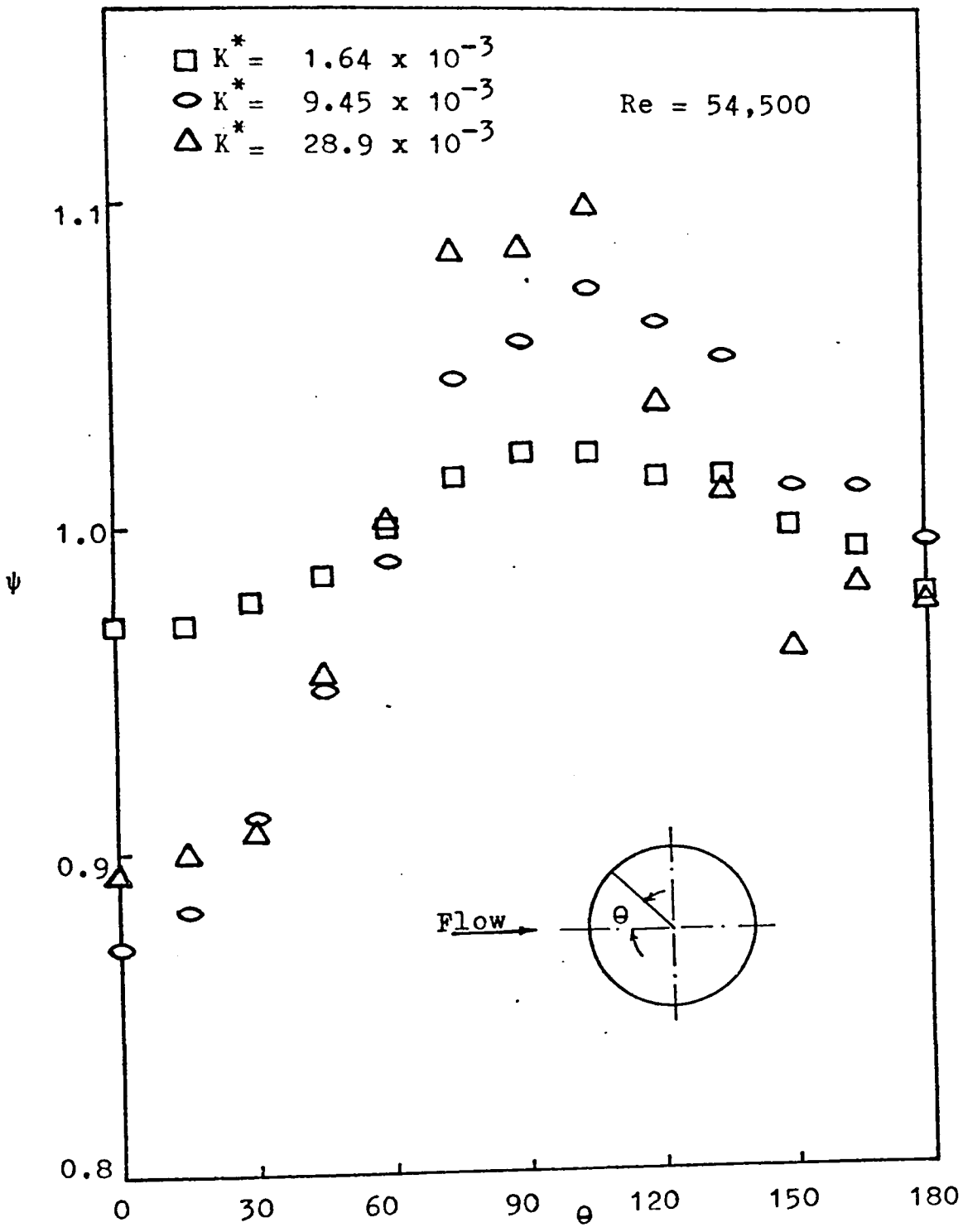

Fig. 4.5 (b) Non-Dimensional Wall Temperature Distribution

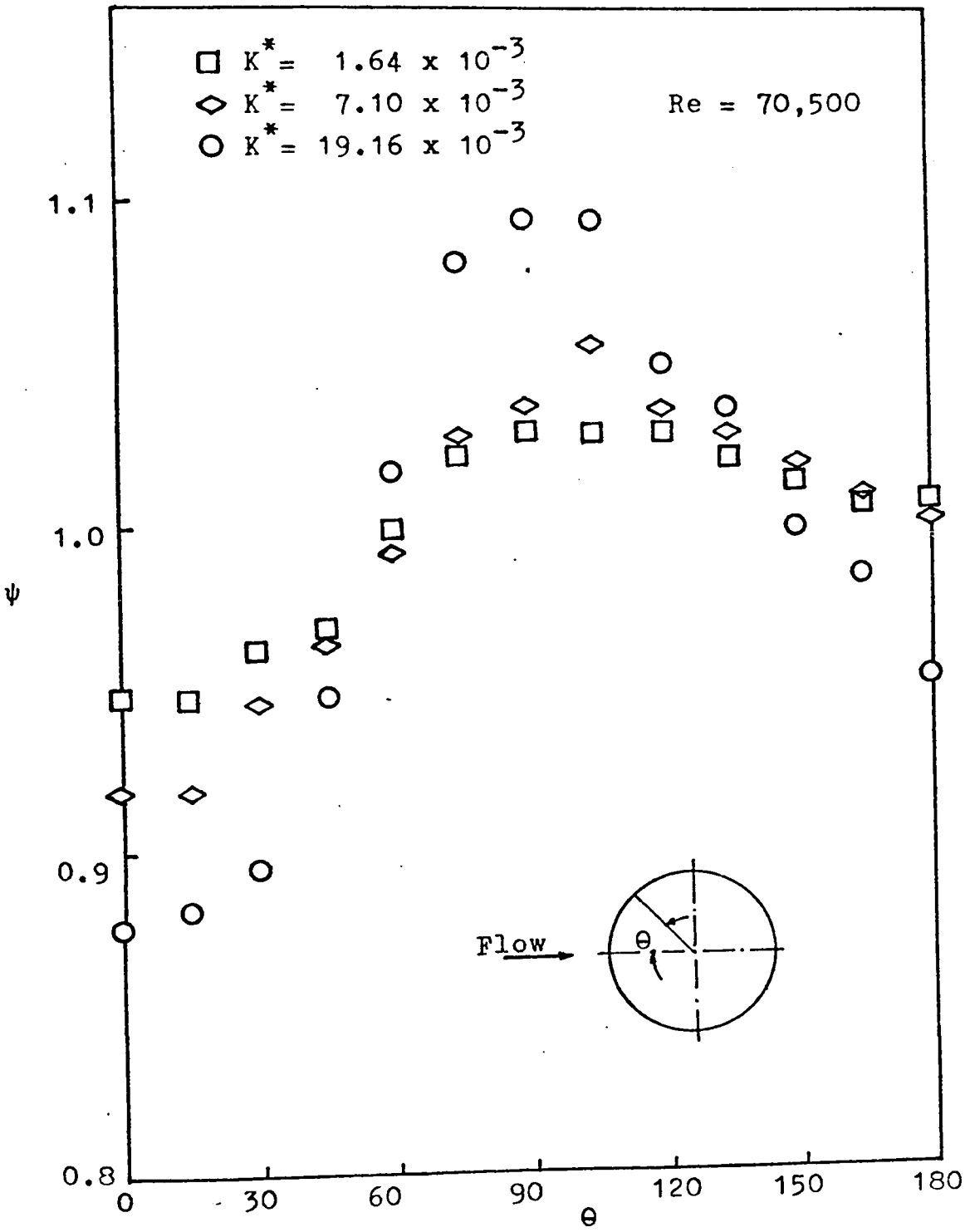

Fig. 4.6 (a) Non-Dimensional Wall Temperature Distribution

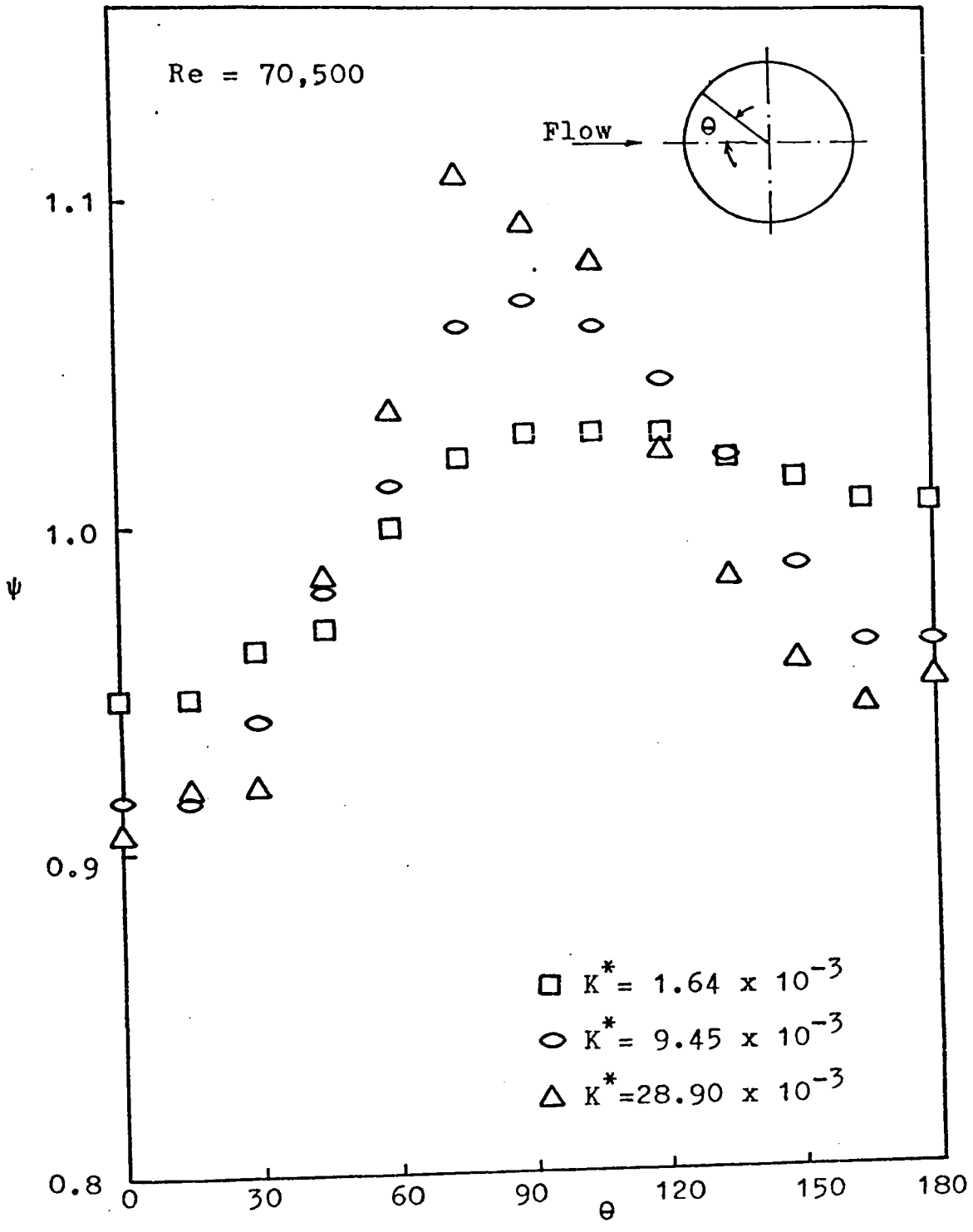

Fig. 4.6 (b) Non-Dimensional Wall Temperature Distribution

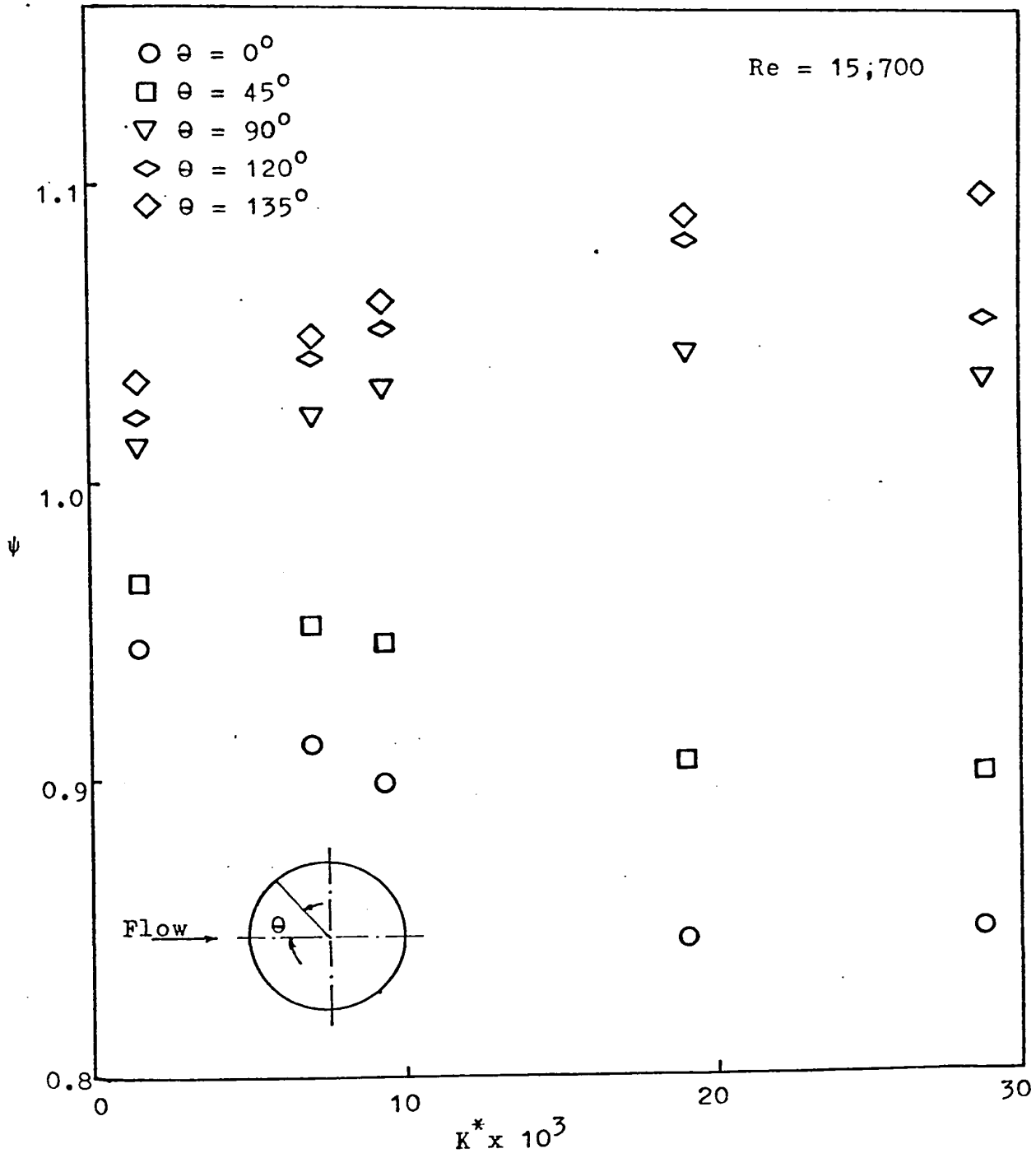

Fig. 4.7 Variation of Wall Temperature with K^*

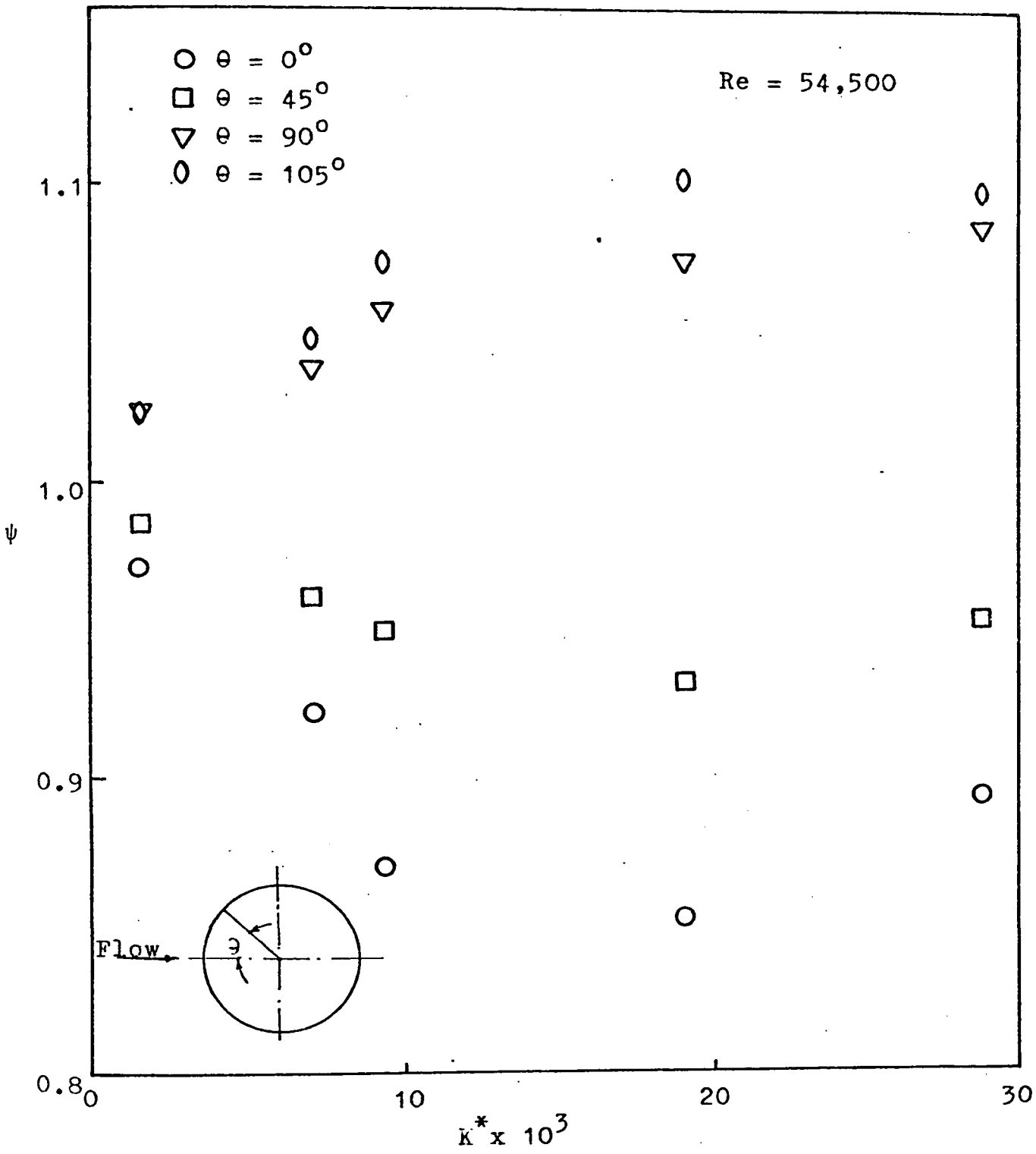

Fig. 4.8 Variation of Wall Temperature with K^*

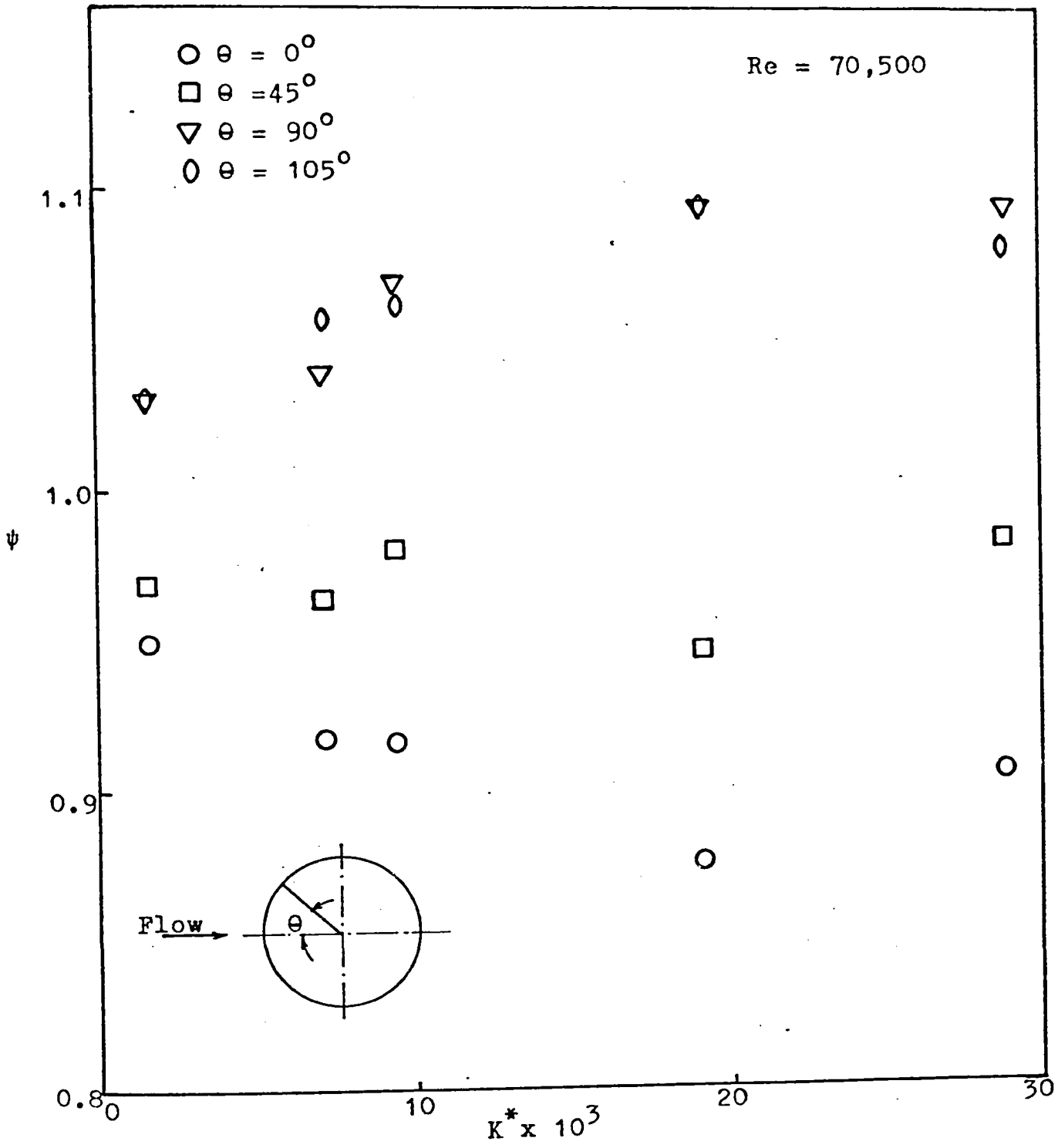

Fig. 4.9 Variation of Wall Temperature with K^*

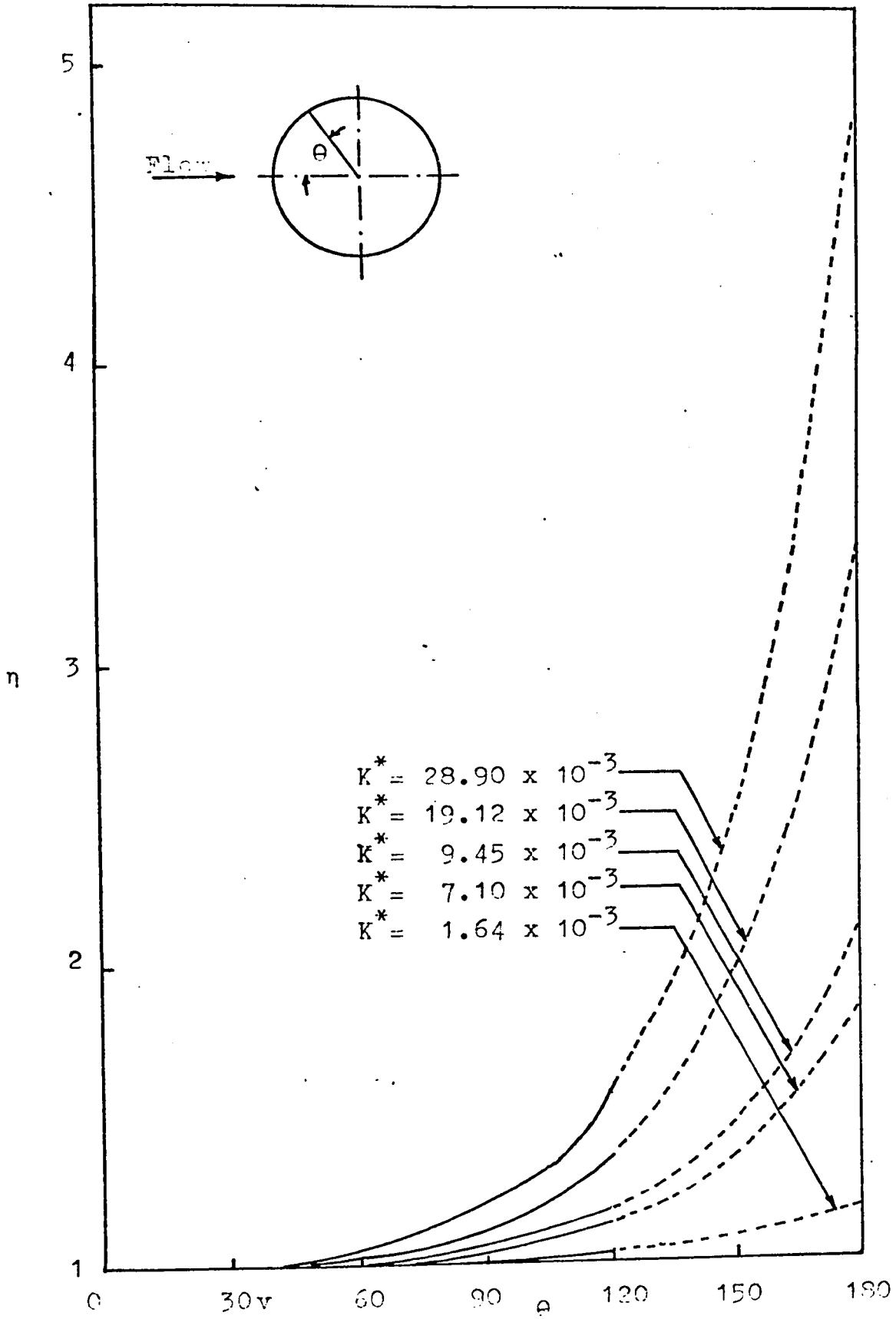

Fig.4.10 Predicted Variation of Wall Temperature for various values of K^* with θ

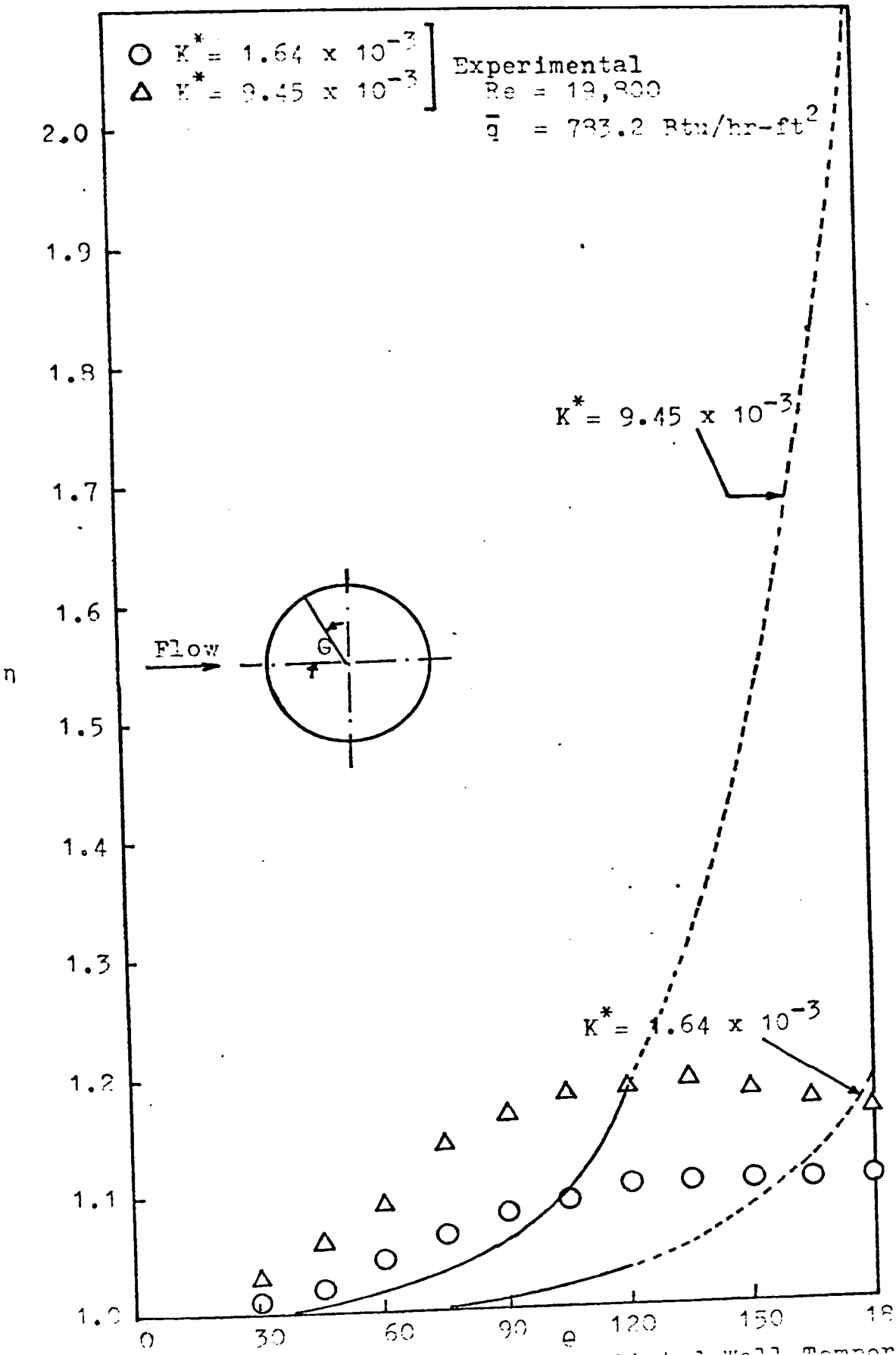

Fig. 4.11 Comparison of Predicted Wall Temperature Distribution with the Experimental Data

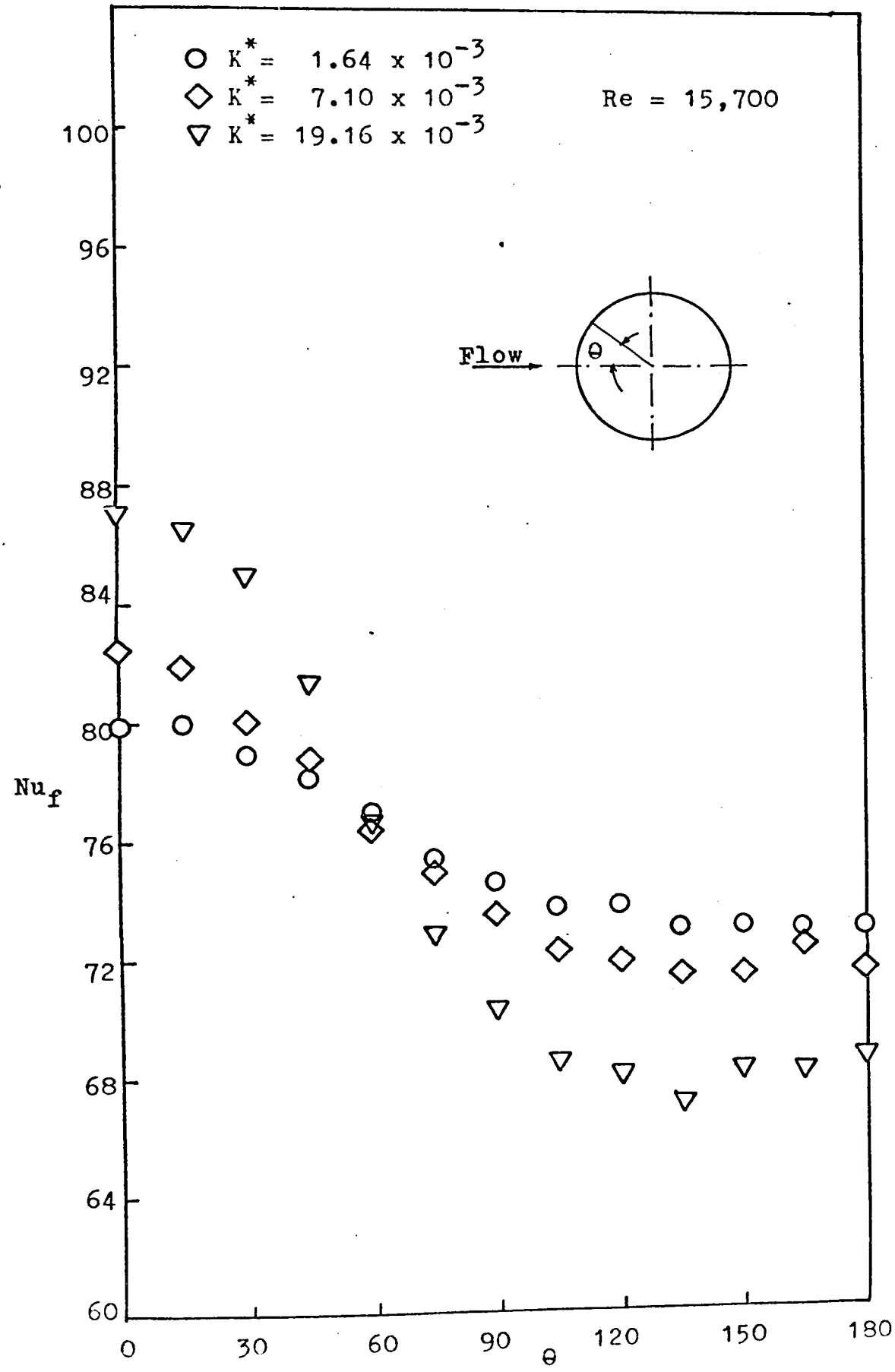

Fig. 4.12 (a) Heat Transfer Coefficient

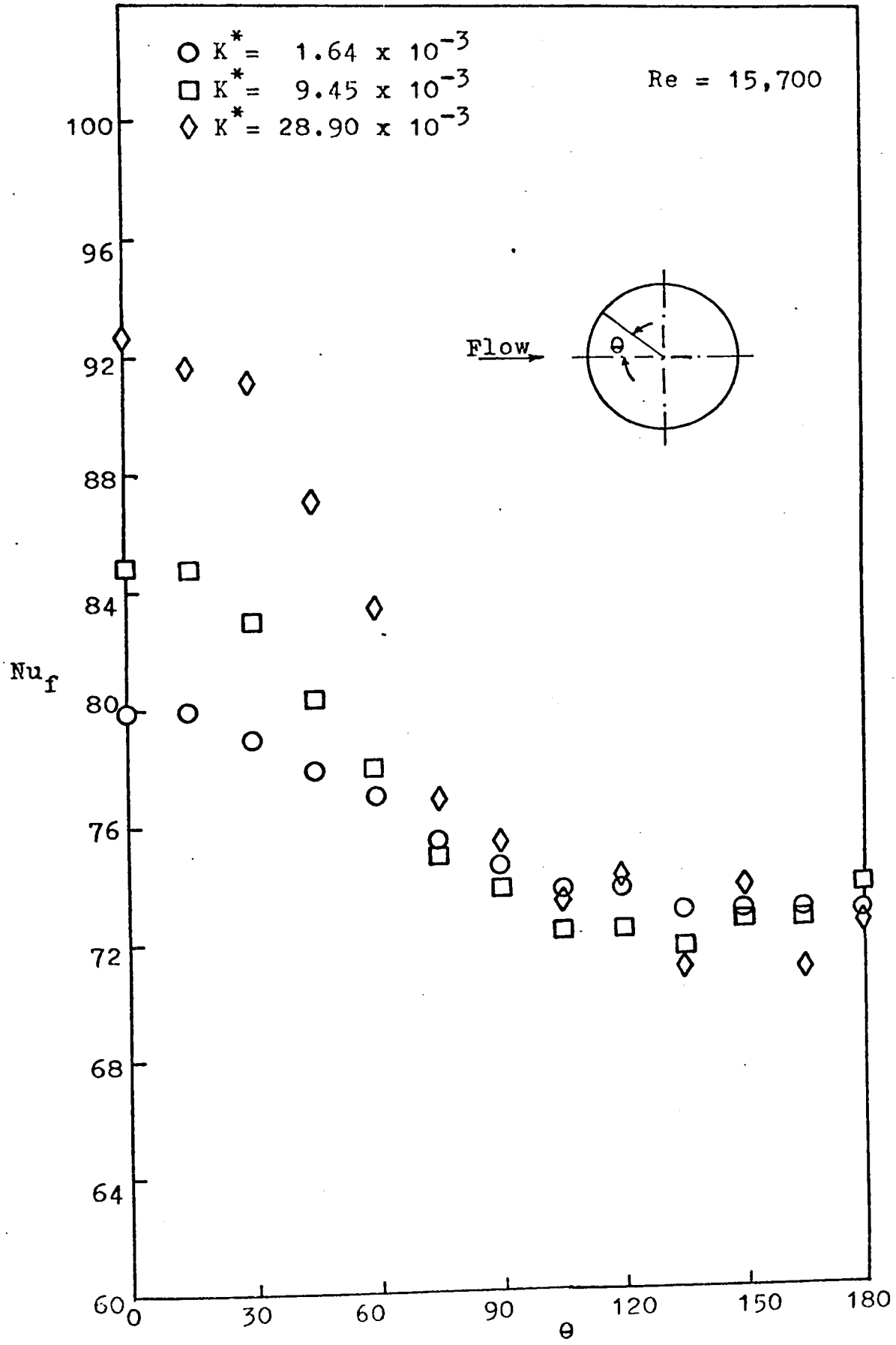

Fig. 4.12 (b) Heat Transfer Coefficient

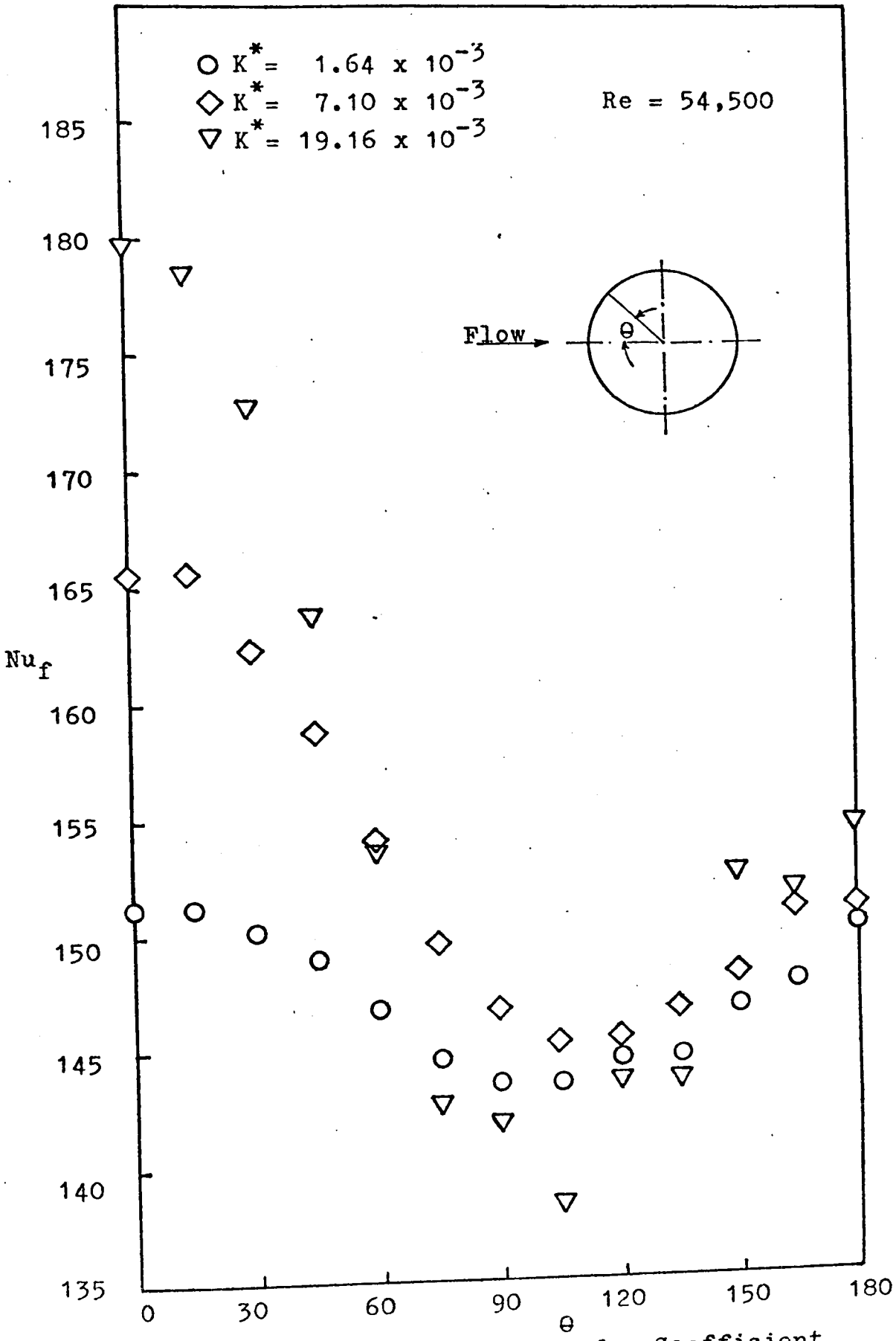

Fig. 4.13 (a) Heat Transfer Coefficient

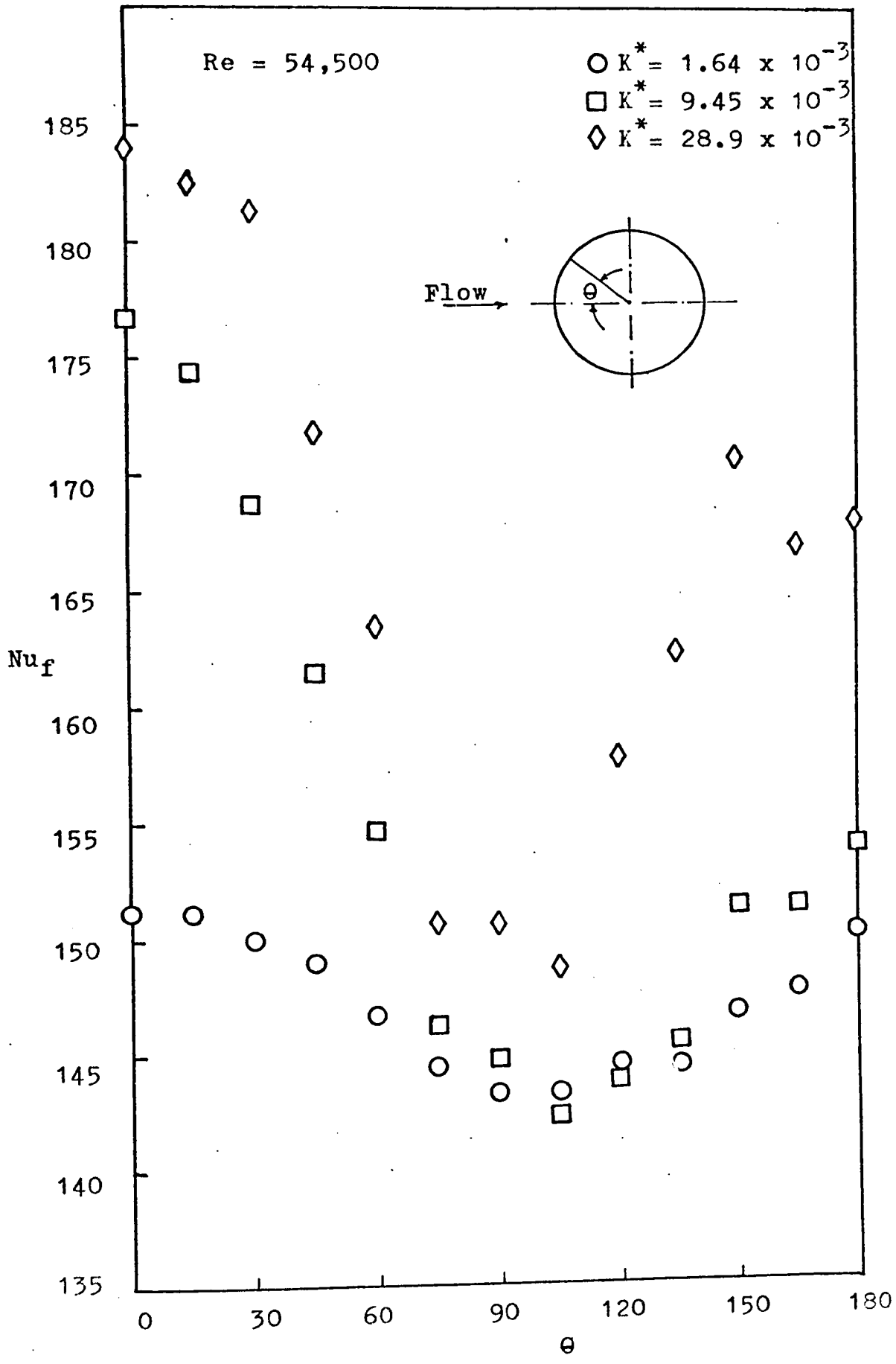

Fig. 4.13 (b) Heat Transfer Coefficient

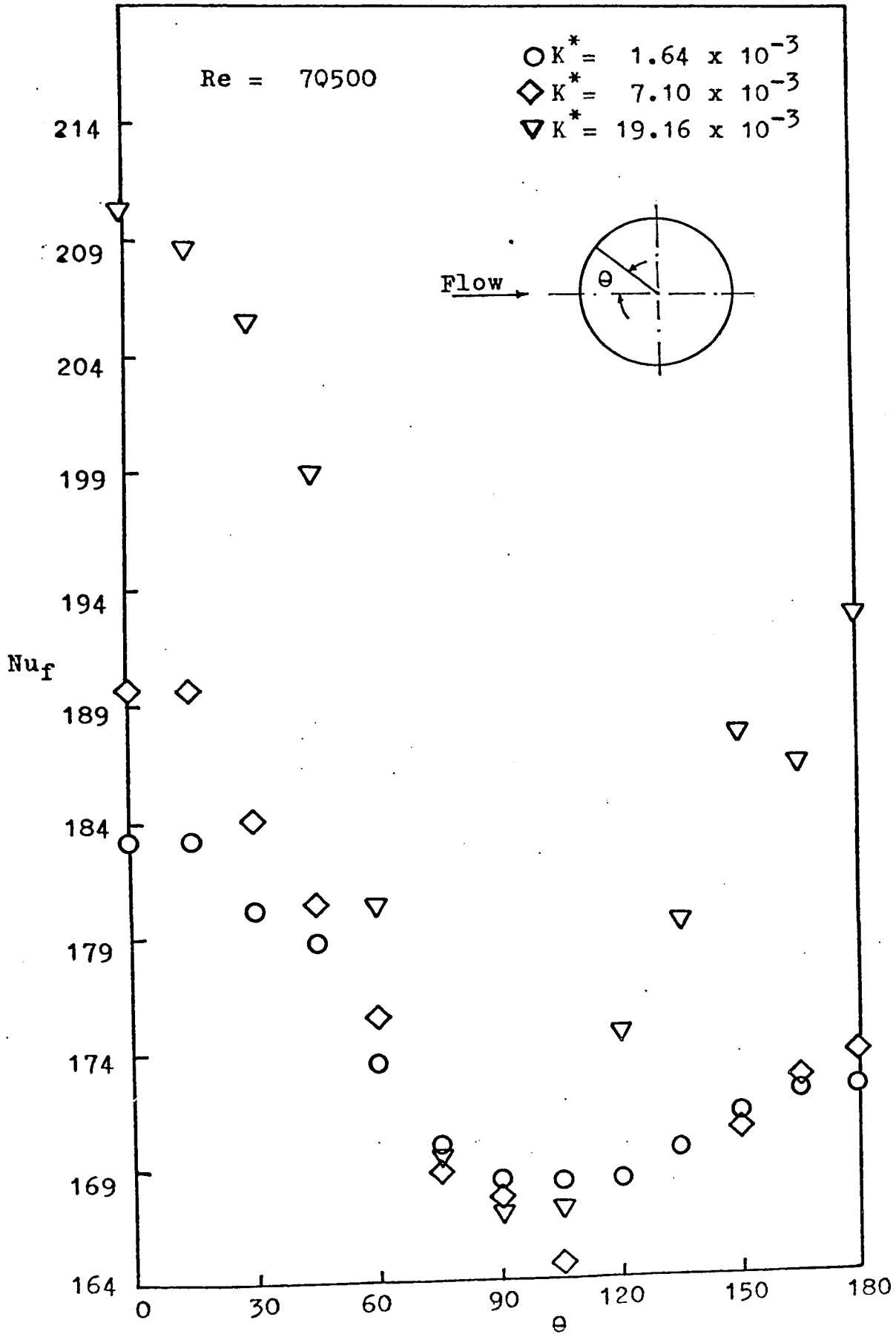

Fig.4.14 (a) Heat Transfer Coefficient

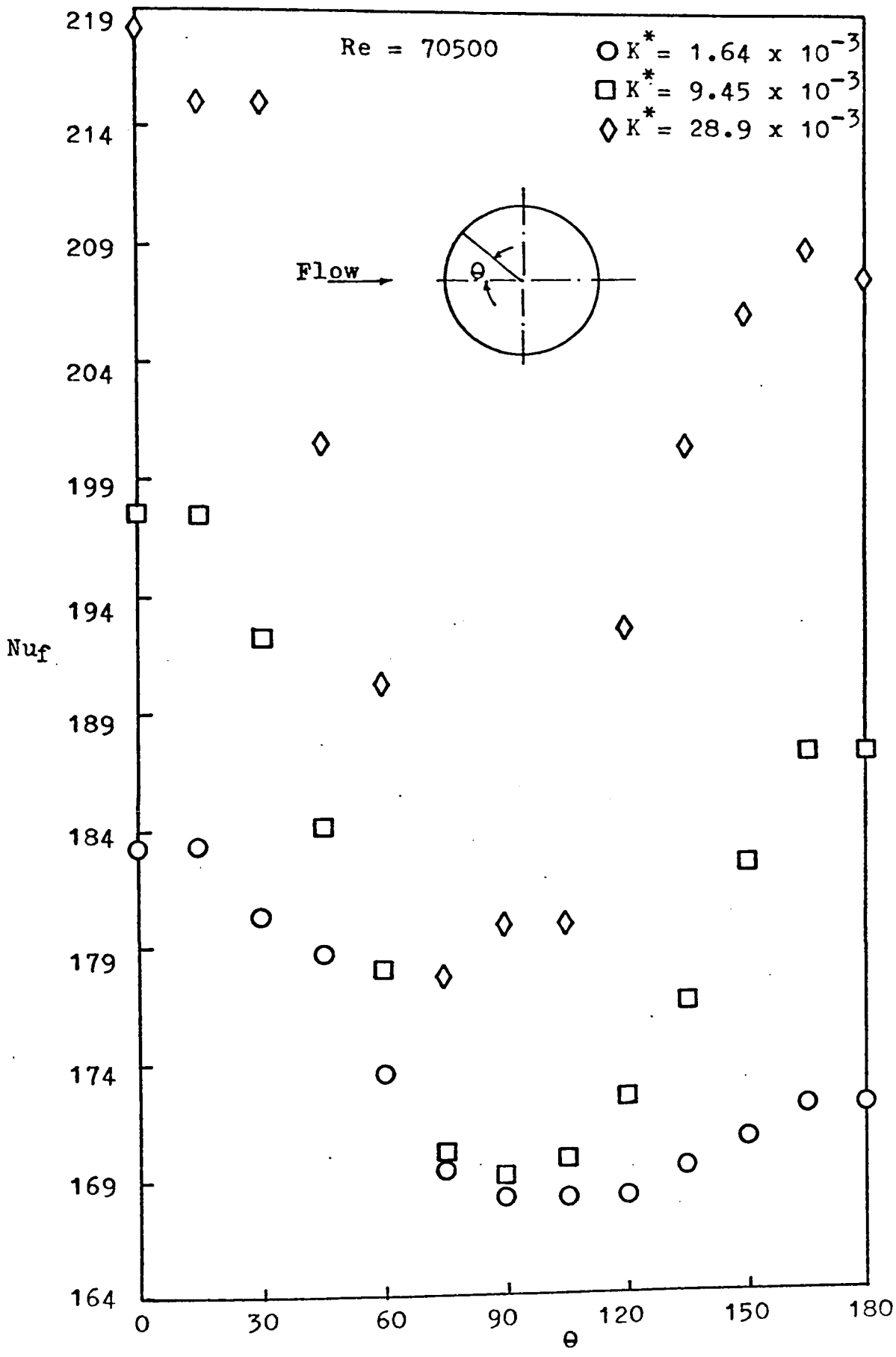

Fig. 4.14 (b) Heat Transfer Coefficient

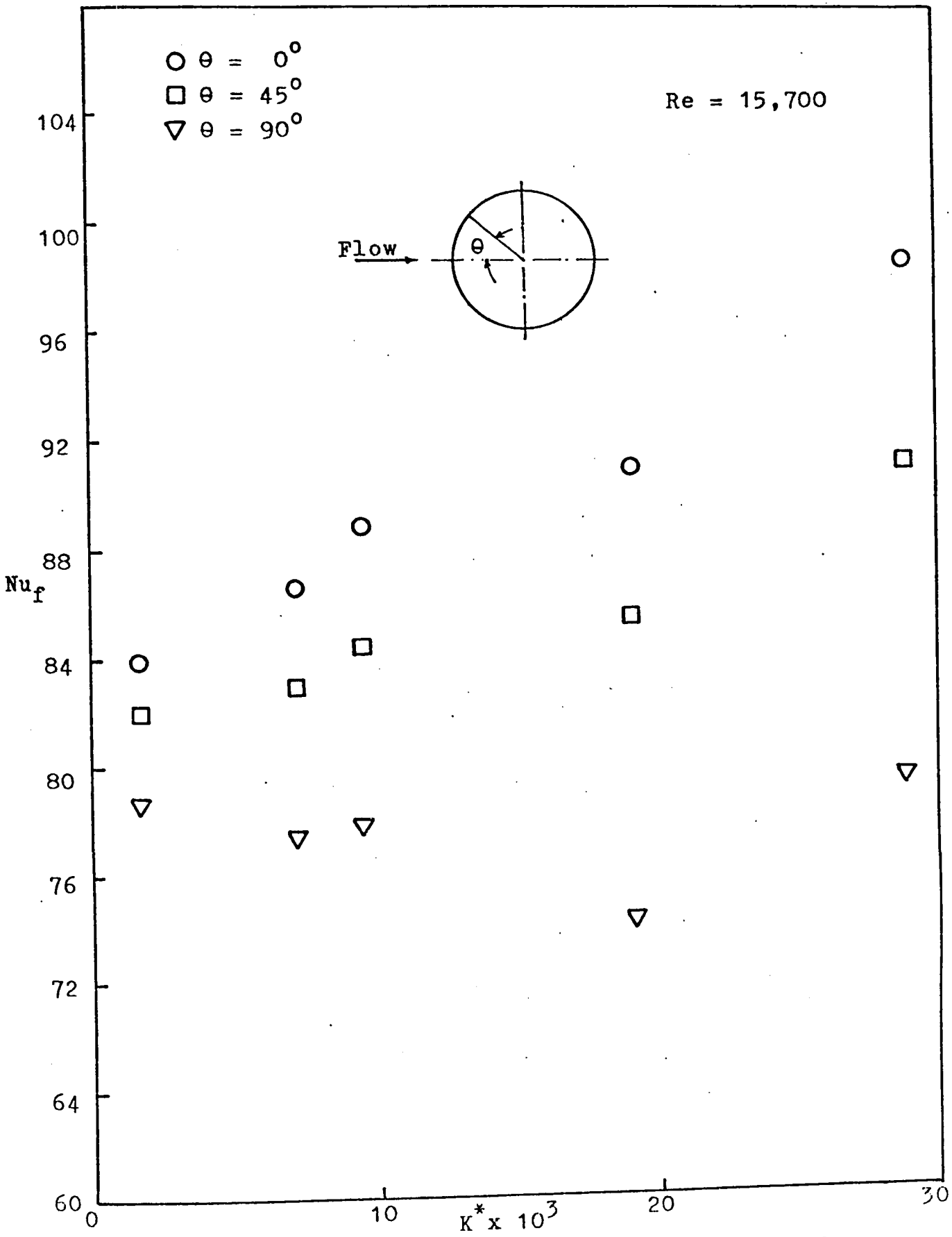

Fig. 4.15 (a) Variation of Local Heat Transfer Coefficient with K^*

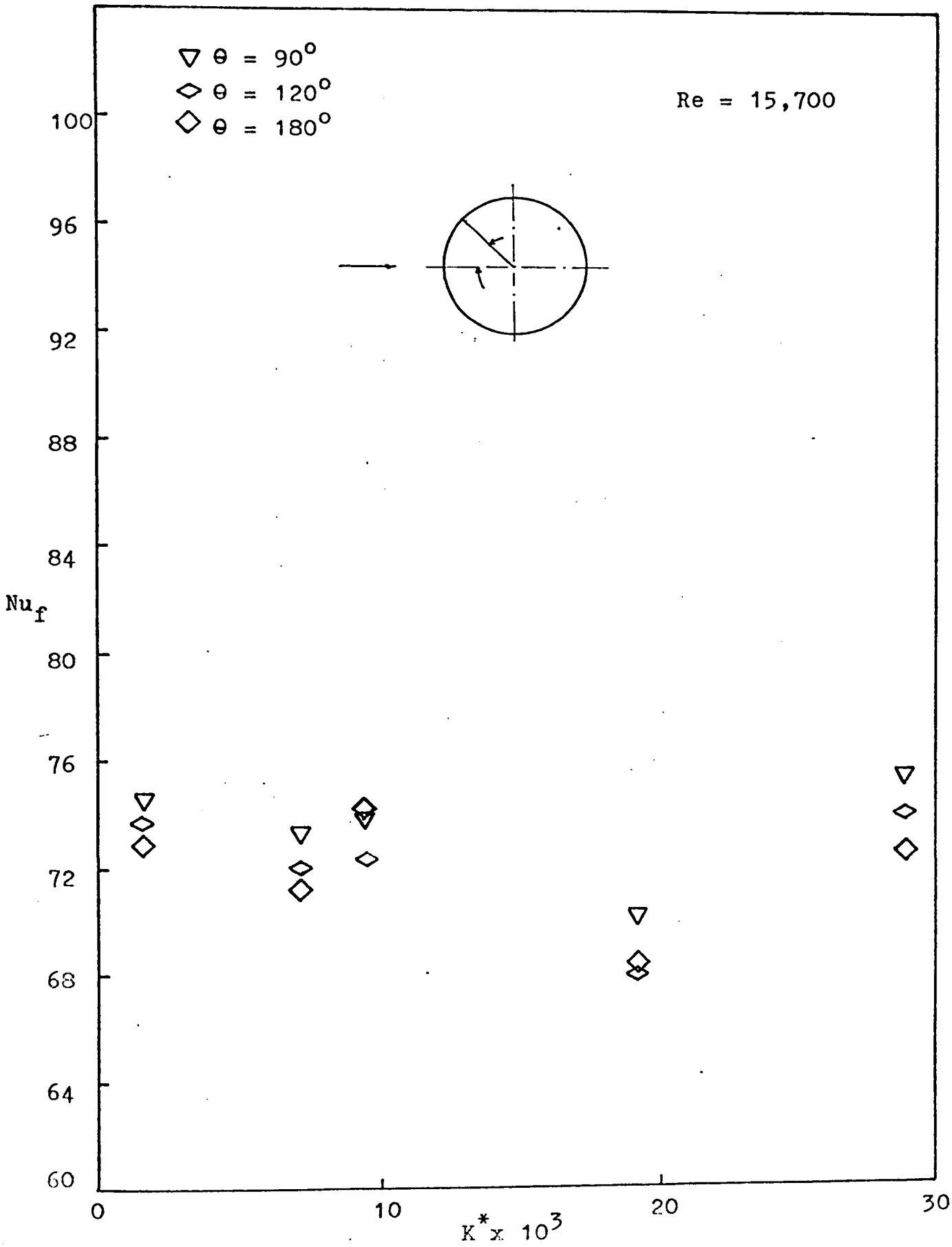

Fig. 4.15 (b) Variation of Local Heat Transfer Coefficient with K^*

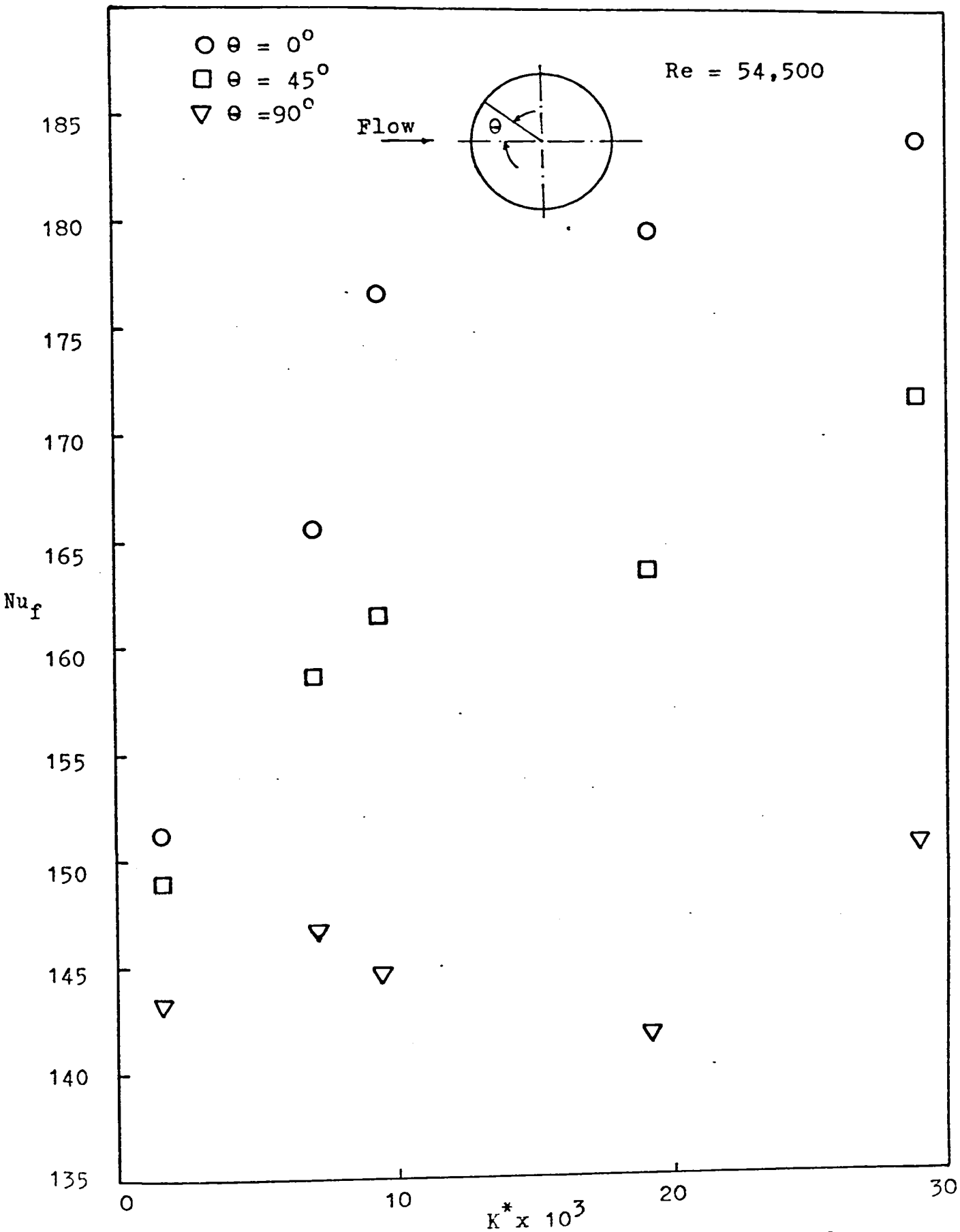

Fig. 4.16 (a) Variation of Local Heat Transfer Coefficient with K^*

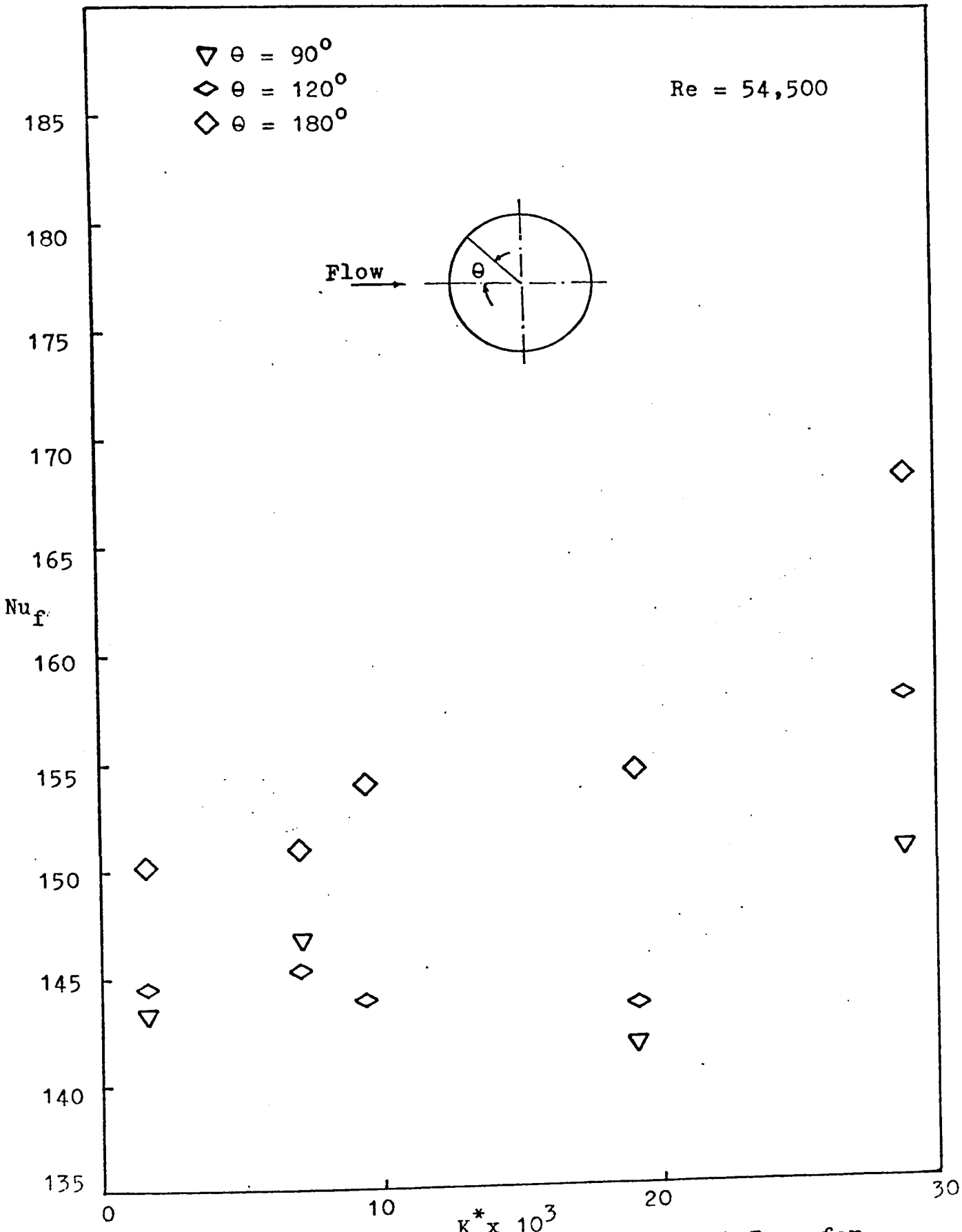

Fig. 4.16 (b) Variation of Local Heat Transfer Coefficient with K^*

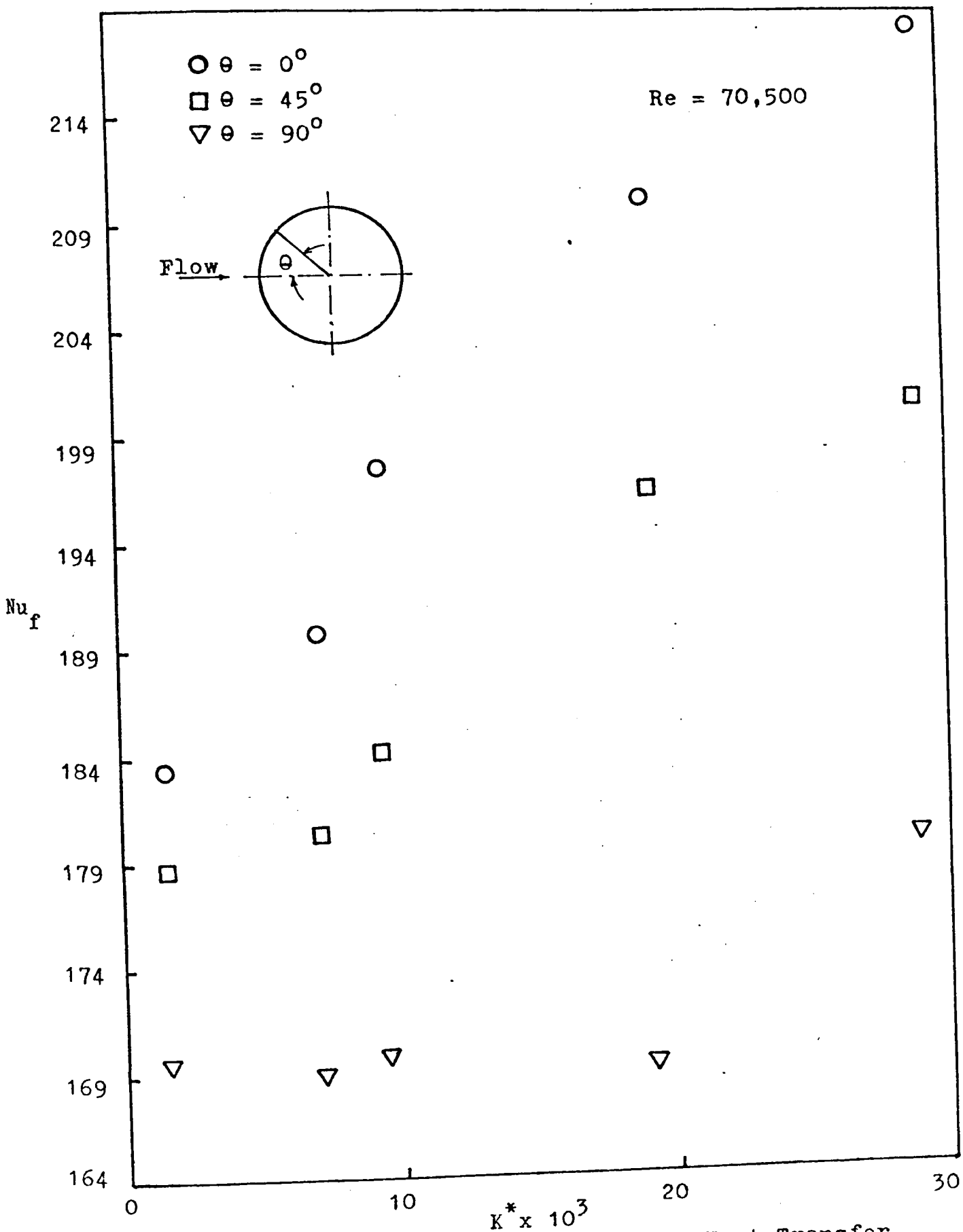

Fig. 4.17 (a) Variation of Local Heat Transfer Coefficient with K^*

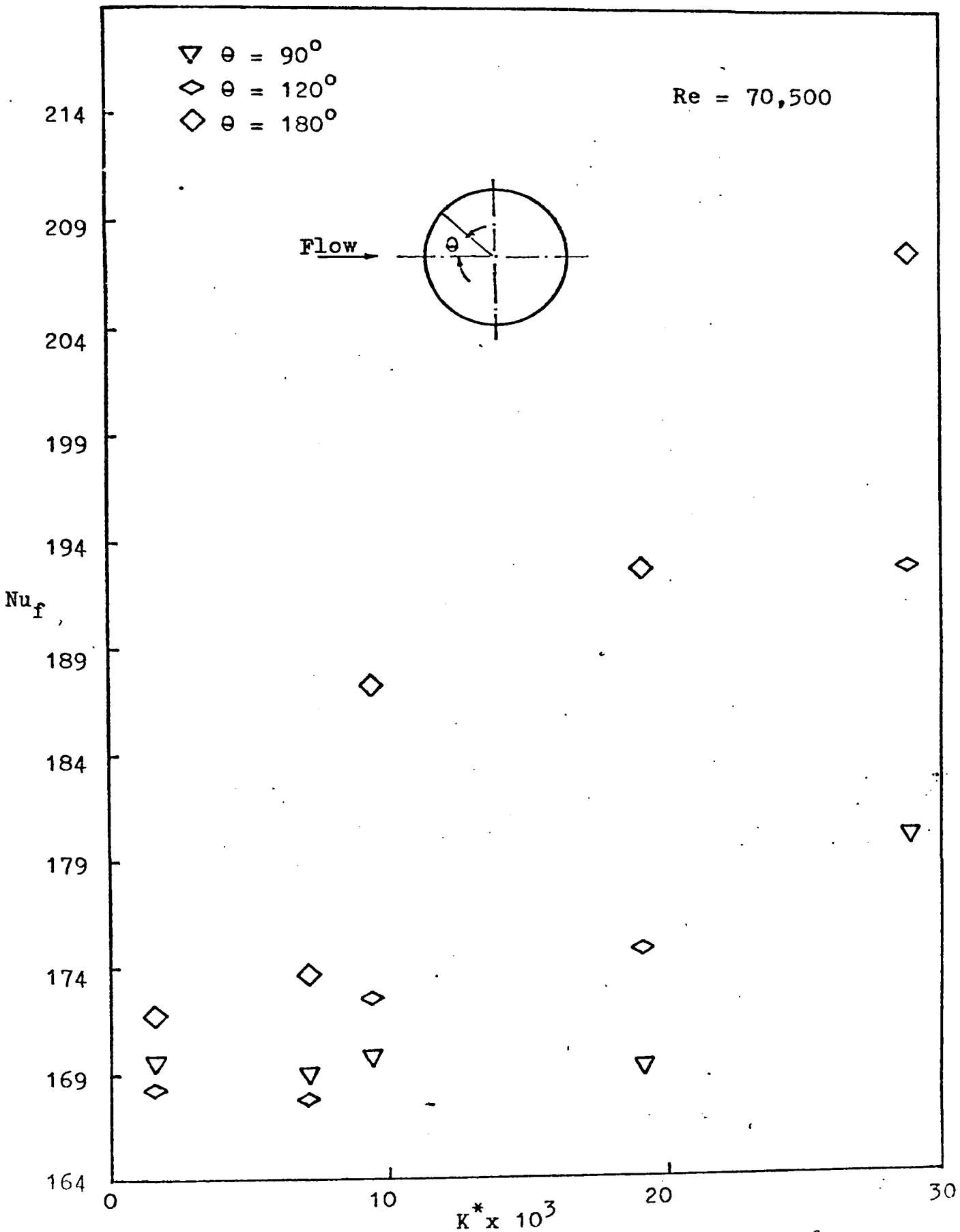

Fig. 4.17(b) Variation of Local Heat Transfer Coefficient with K^*

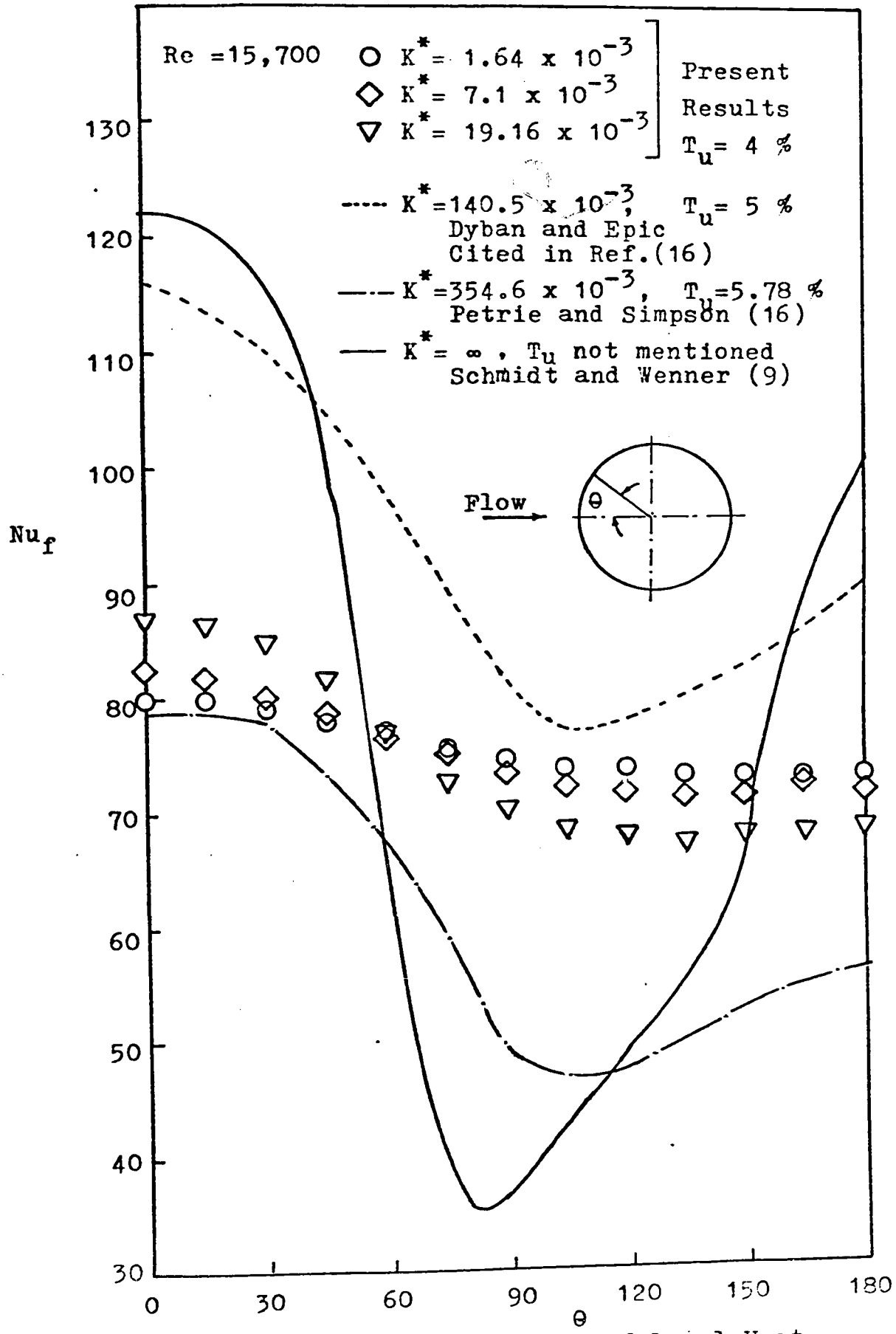

Fig. 4.18 Distribution of Local Heat Transfer Coefficient

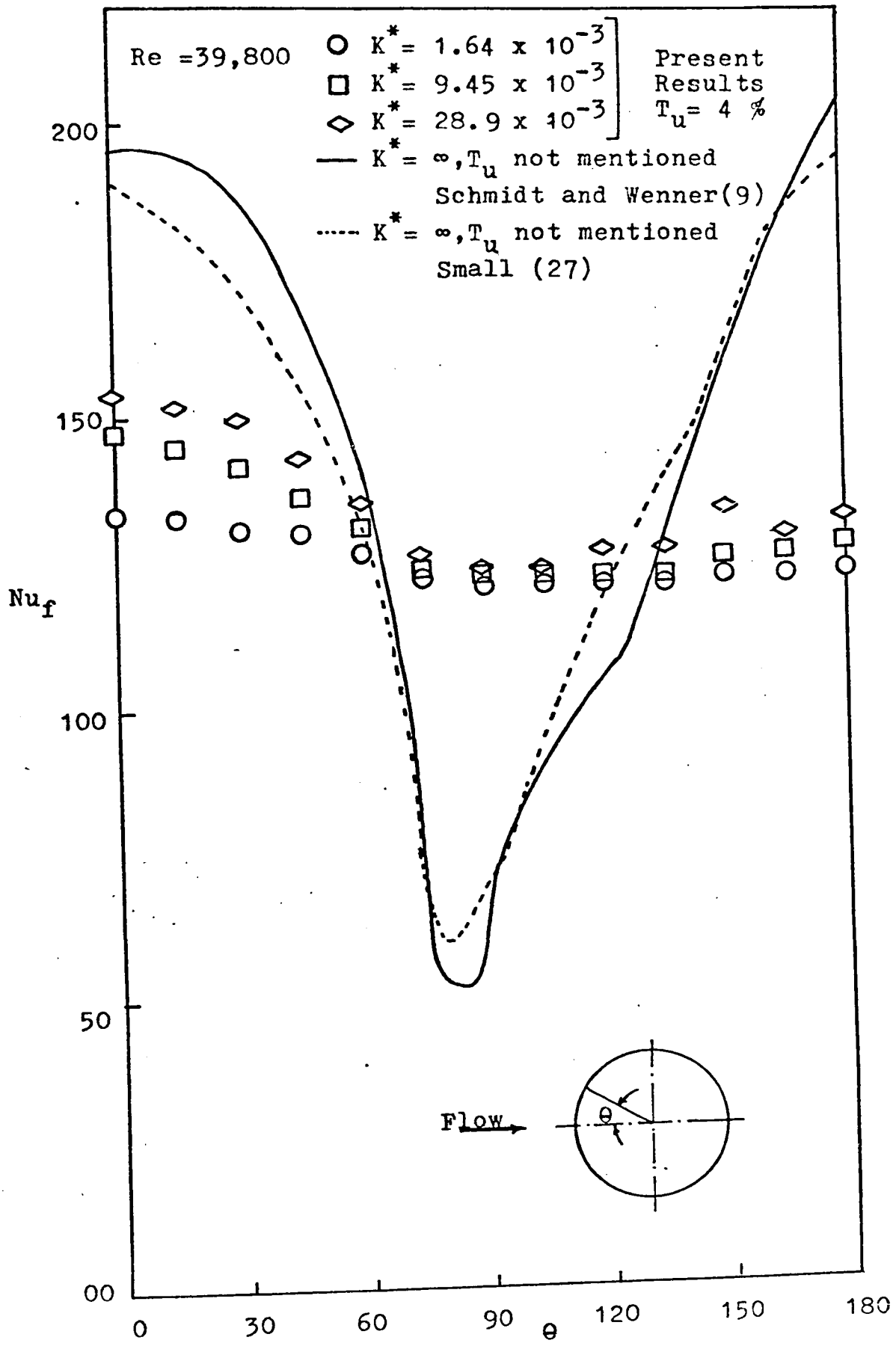

Fig. 4.19 Distribution of Local Heat Transfer Coefficient

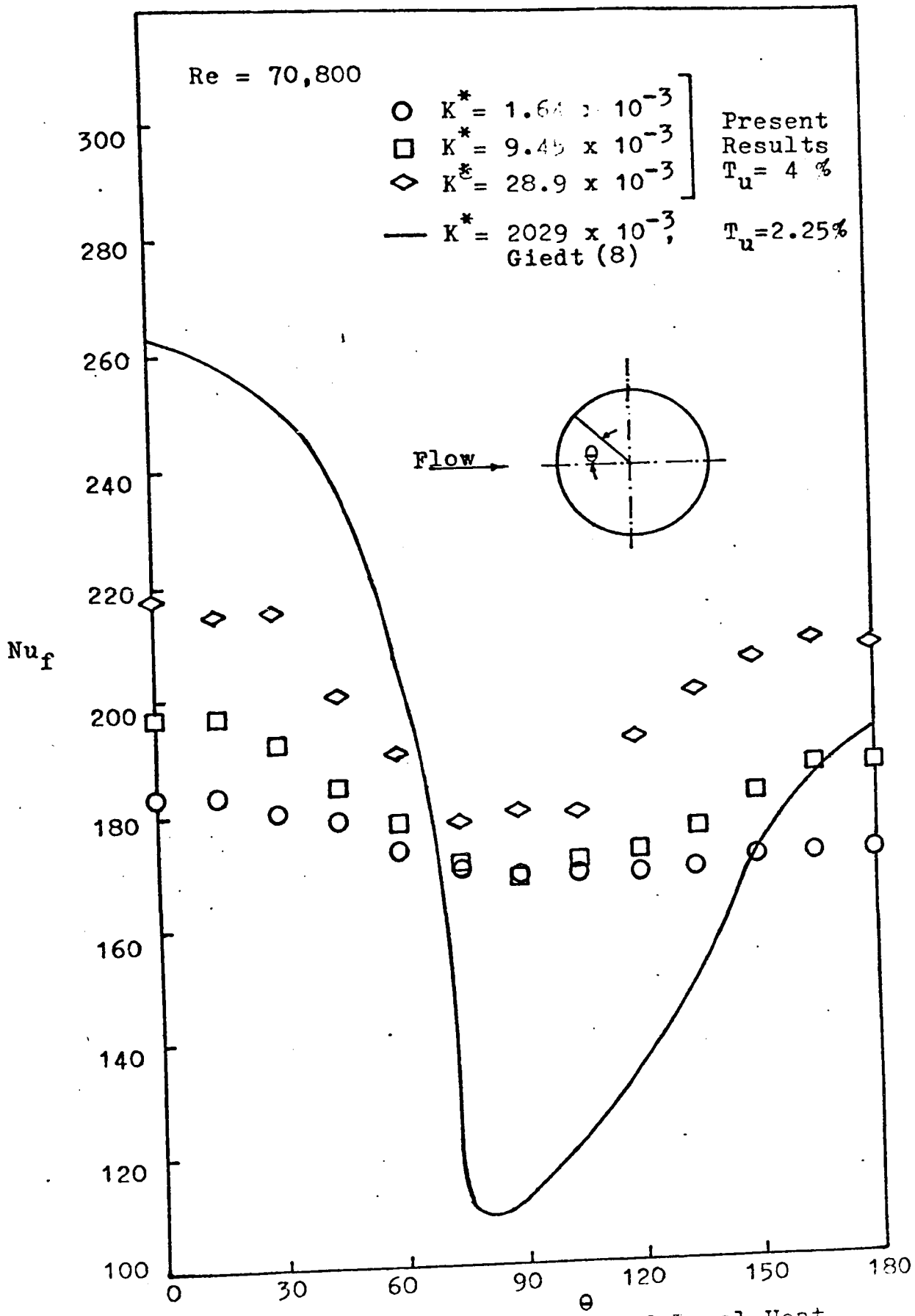

Fig. 4.20 Distribution of Local Heat Transfer Coefficient

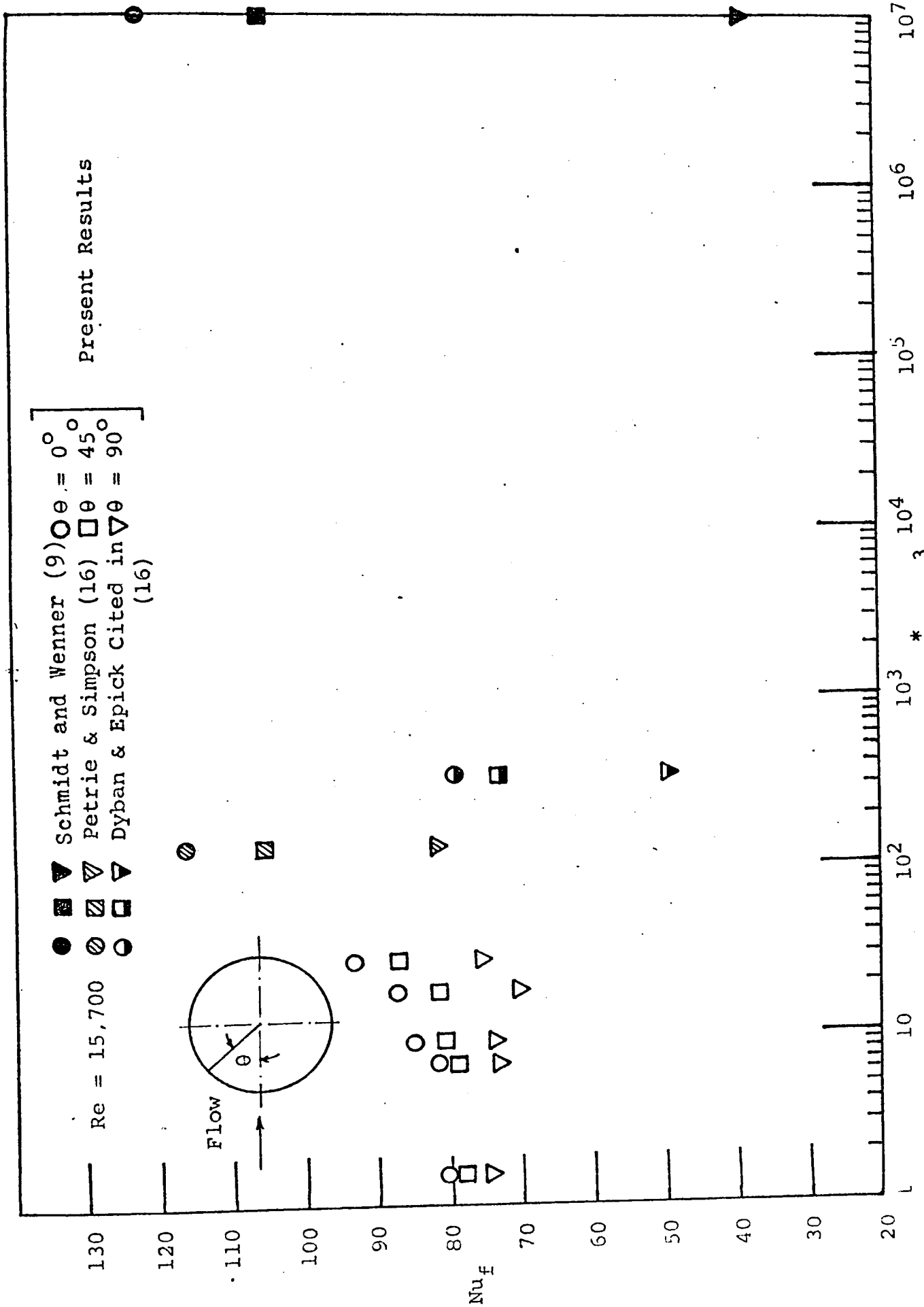

Fig. 4.21 Variation of Local Heat Transfer Coefficient with K^*

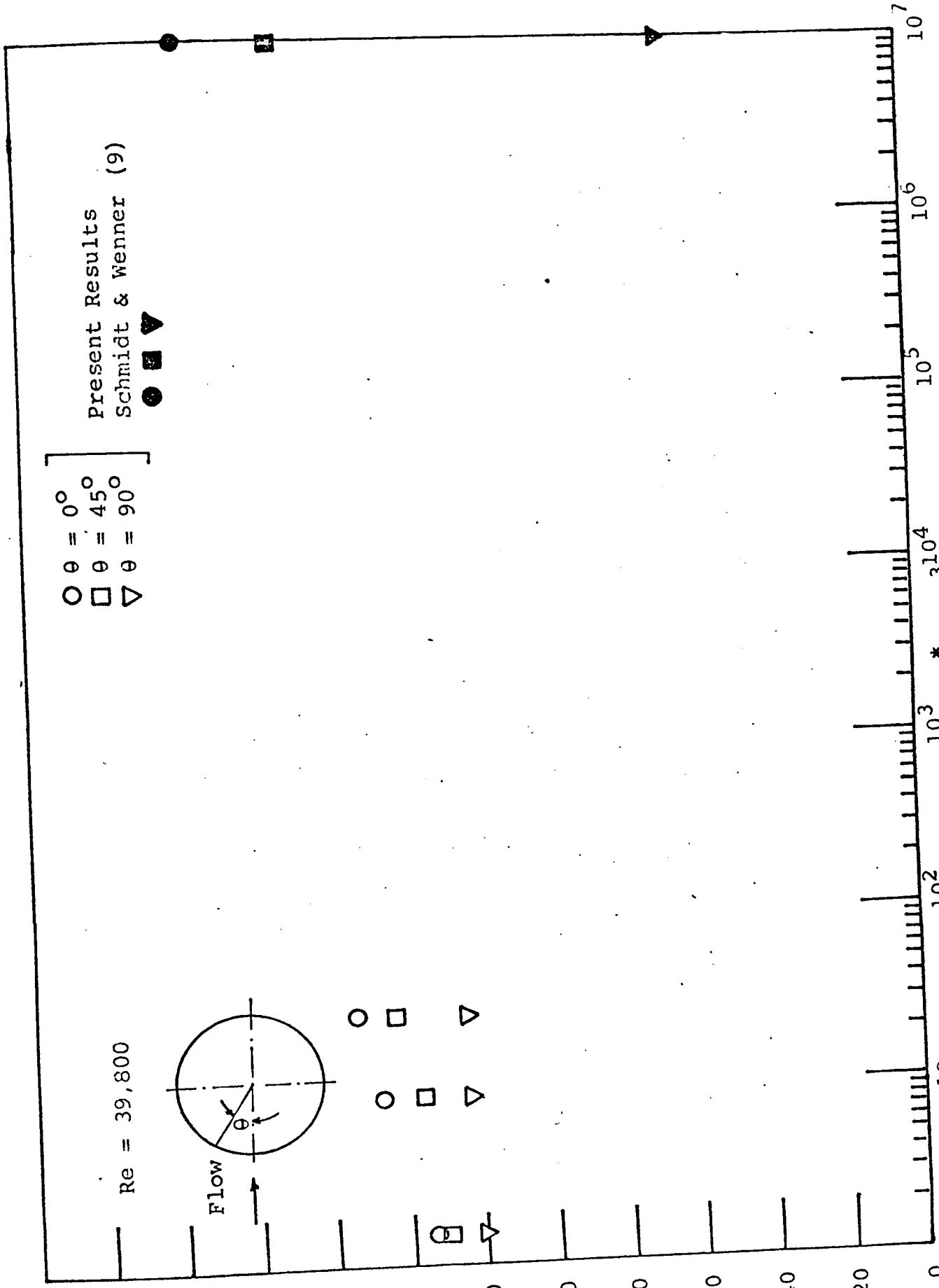

Fig. 4.22 Variation of Local Heat Transfer Coefficient with K^*

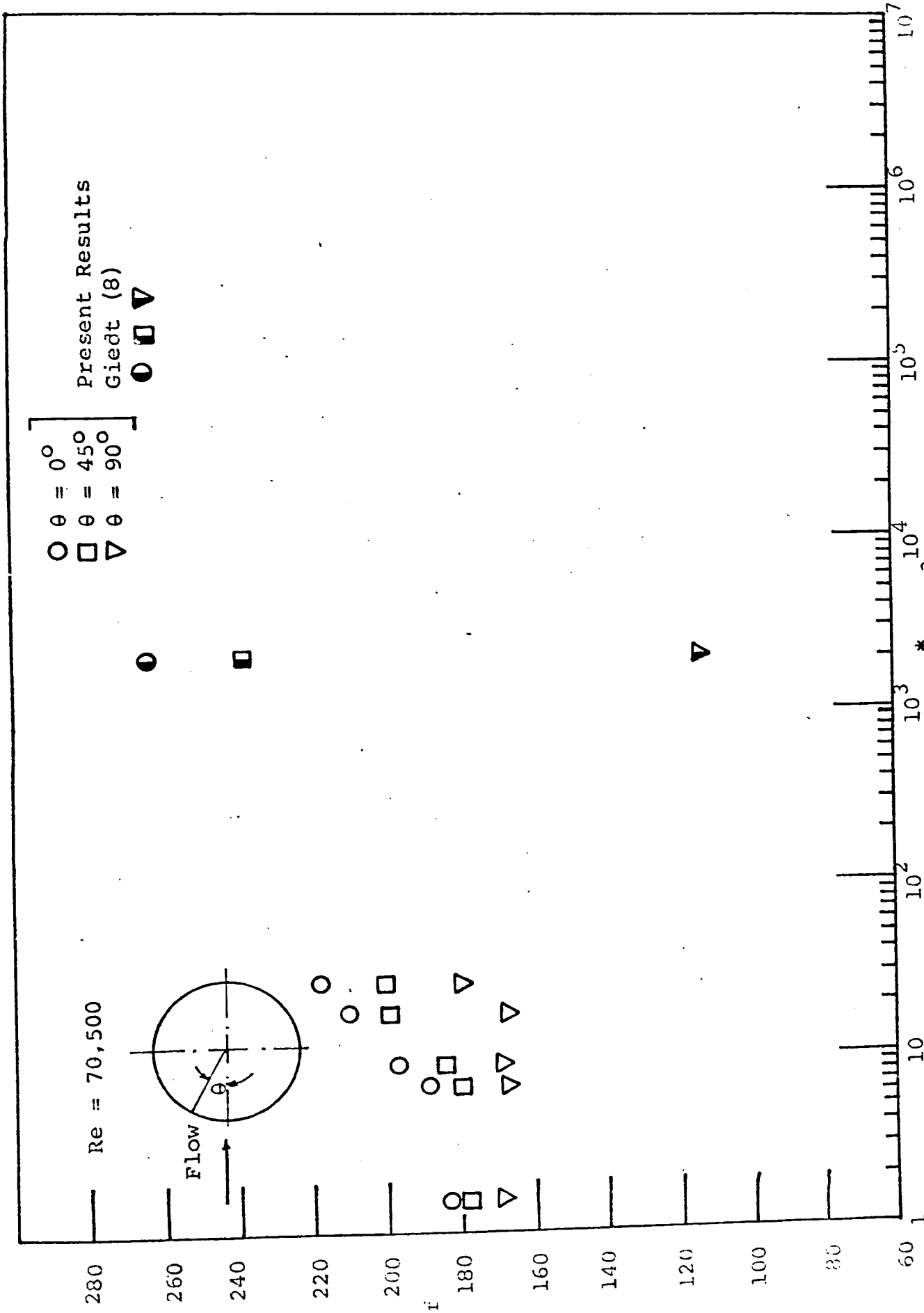

Fig. 4.23 Variation of Local Heat Transfer Coefficient with K^*

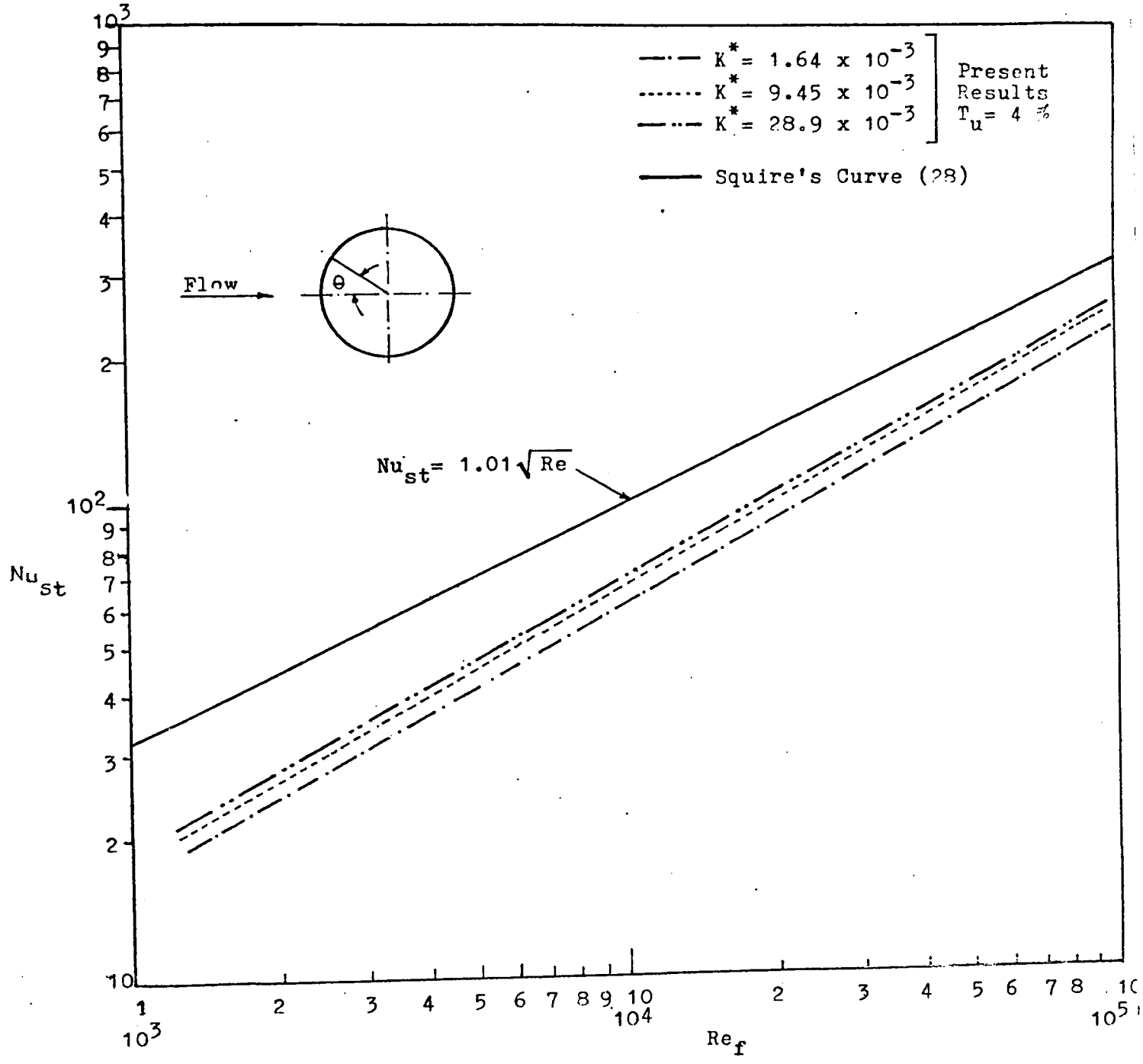

Fig. 4.24 Nusselt number at the forward stagnation point of cylinder compared with Sqoire's equation

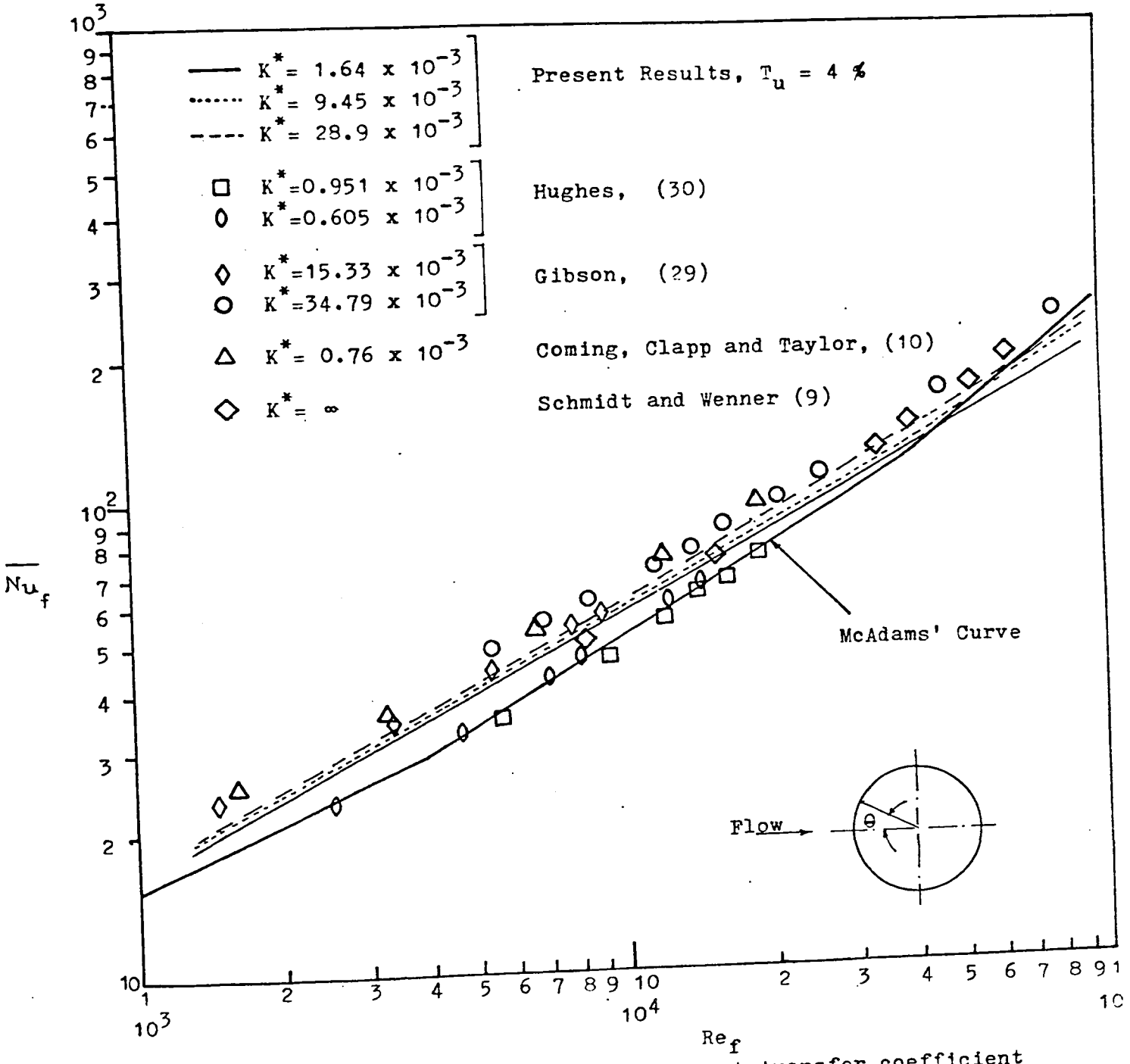

Fig. 4.25 Comparison of the average heat transfer coefficient with those of other observers

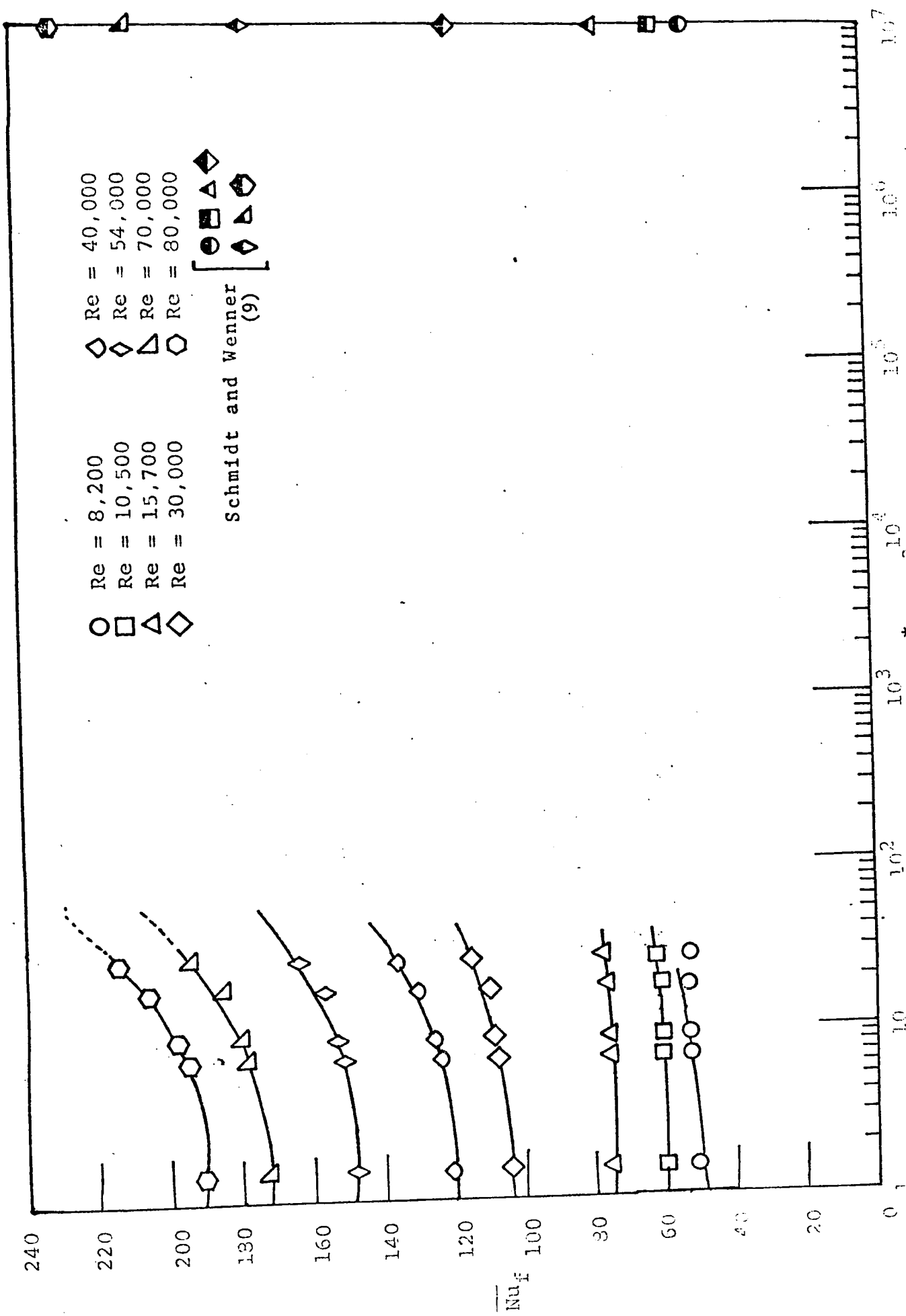

Fig. 4.26 Variation of Average Heat Transfer Coefficient with K^*

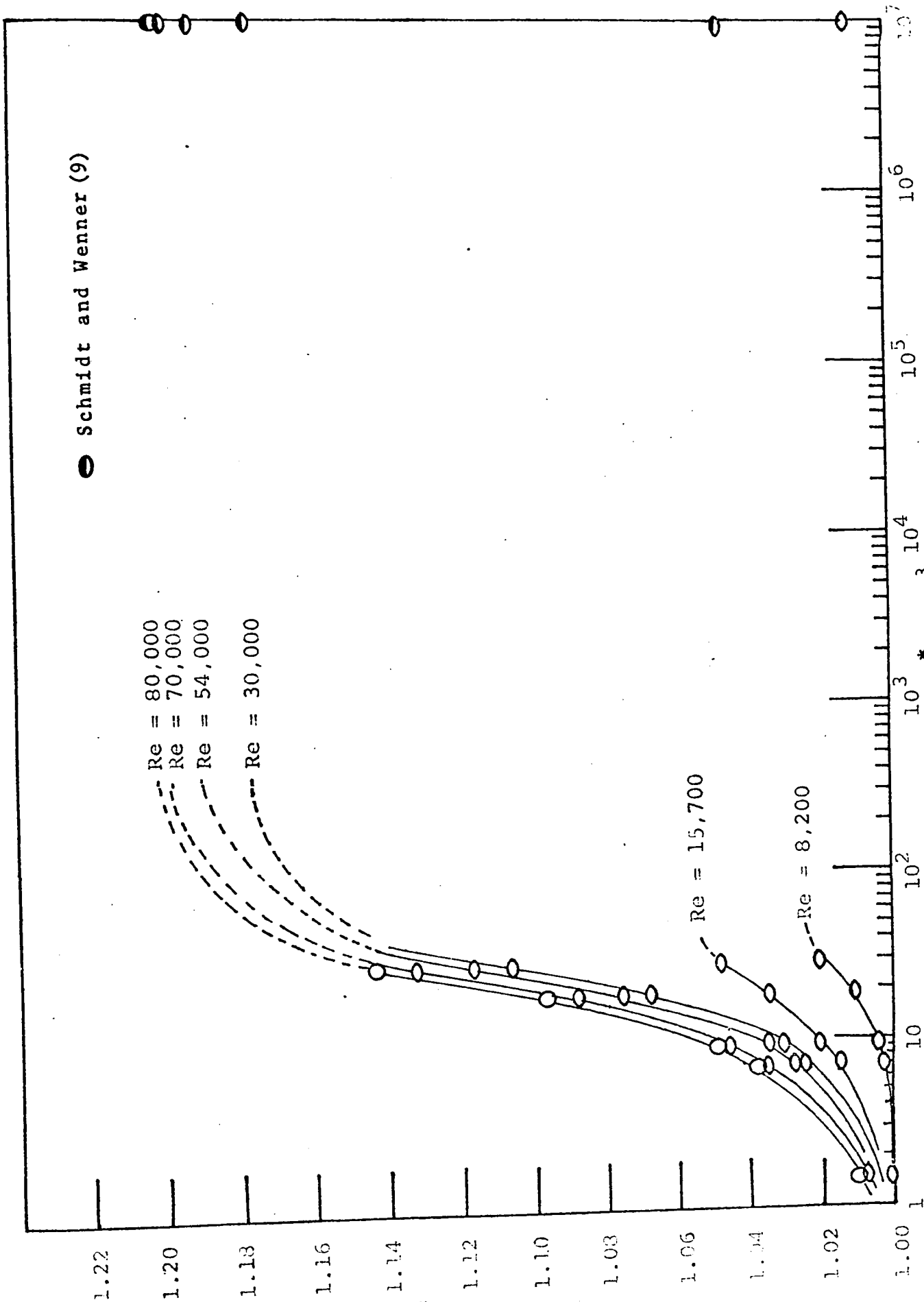

Fig. 4.27 Effect of K* on the Average Heat Transfer Coefficient